Physicochemical Properties of Atmospheric Aerosol Particles over Suburban and Remote Locations and Development of Techniques for the Improvement of their Determination Methods

A dissertation submitted to the

University of the Aegean

presented by

Bezantakos Spyridon

Status: Draft

Acknowledgments

In our dualistic way of thinking there are certain periods of our lives which we think as bad or as good. After losing a "good" job, due to the "economical crisis" i found myself studying in the Aegean University, initially as a Master student. For me, back in 2010, that was a rational decision for obtaining more knowledge and thus better job opportunities. There i met with G. Biskos, who is passionate about atmospheric sciences (especially those involving aerosols) and got interested in a different field than the one i used to be before. Before starting as a PhD candidate i found myself in a dilemma of using what i already knew and search for a new job or following my curiosity and try to obtain knowledge in something i was less familiar with. Exploring the properties of nano-scale particles opened new ways in my mind and revealed a rather unknown world for me. At the same time it was the everyday interaction and relationships with my supervisor, colleagues and members of other scientific groups that made the last 4 years an outstanding experience for me and led to this result. So, except G. Biskos, i would like to thank prof. K. Eleftheriadis and the group of *Institute of Nuclear Technology and Radiation Protection*, N.S.C.R. Demokritos , prof. N. Mihalopoulos and the group of *Department of Chemistry, University of Crete*, prof. S. Pandis and the group of *Institute of Chemical Engineering, ICE-HT, Patras*, prof. A. Nenes and Dr. A. Bougiatioti, prof. A. Schmidt-Ott and the group of *Faculty of Applied Sciences, Delft University of Technology*. Last but not least, i would like to thank my beloved friends and family for their continuous support and encouragement.

This research has been co-financed by the European Union (European Social Fund – ESF) and Greek national funds through the Operational Program "Education and Lifelong Learning" of the National Strategic Reference Framework (NSRF) - Research Funding Program: THALES. Investing in knowledge society through the European Social Fund: "Sources and physicochemical properties of fine and ultrafine aerosol particles that affect the regional climate of Greece".

Contents

Summary

Aerosol particles affect the Earth's climate directly by absorbing or scattering solar radiation and indirectly by acting as cloud condensation nuclei. The contribution of the aerosol effects on the global climate depends on their size and chemical composition which in turn defines their hygroscopicity (i.e. the ability to take up water). Despite that thermodynamic models can be used to accurately predict the hygroscopic behavior of particles consisting of inorganic matter, existing knowledge leads to inaccurate predictions in cases of particles consisting purely of organic or mixtures of inorganic and organic matter. The use of the hygroscopic parameter κ allows more accurate approximation of the hygroscopic behavior of mixed particles when the hygroscopicity and the volume fraction of each species composing the particle are known. However, the estimation of atmospheric aerosols hygroscopicity poses difficulties due to their complex and diverse chemical composition which varies spatially and temporally. Thus, high temporal resolution, direct observations of particles hygroscopicity and/or chemical composition in different regions are needed in order to reduce the uncertainties of their impact on the climate.

In part I of this work we provide direct observations on the hygroscopic behavior of atmospheric aerosols over remote and suburban regions, located in Greece. Measured particle hygroscopic properties are directly compared to their estimated hygroscopicity, which is derived by their chemical composition. Measurements were conducted at the remote site of Vigla, located on the island of Lemnos in the Aegean sea and at two suburban sites, located near Patras and Athens.

Particles measured at the remote site of Vigla exhibited moderate hygroscopicity, which is indicative of particles consisting of a mixture of inorganic and organic matter, which was corroborated by measurements of their chemical composition. The later were conducted using an airborne platform with an array of instruments for studying particles physicochemical properties, which during that time was flying over the wider region of the Aegean Sea. The good closure between the particles chemical composition derived hygroscopicity (airborne platform) and the measurements (ground station) allowed for the further estimation of particles hygroscopicity in the wider Aegean Sea region. The spatial variation of the estimated aerosol hygroscopicities was attributed to the different origins

and paths of the air masses reaching the region, which in turn had a major effect in particles chemical composition.

Particles measured at the suburban sites of Patras and Athens showed differences in their hygroscopic properties. Particles sampled at Patras exhibited moderate hygroscopic behavior, more or less similar to other rural regions of continental Europe, while in contrast, those sampled in Athens exhibited significant temporal variation, ranging from moderate to highly hygroscopic. Particles estimated hygroscopicity (derived by chemical composition measurements conducted on both sites) gave better closure with the measurements at Patras suburban site than the one located near Athens. Responsible for the latter differences could be either the existence of refractory, highly hygroscopic matter, which cannot be chemically detected with the methods used, or the presence of certain organic species which are more hygroscopic than the common found organics in the atmosphere.

The second part of the thesis provides means and methods of improving the techniques used in determining particles physicochemical properties. The motivation in trying to improve or find new methods/equipment is directly linked with the importance of their study and serves the scope of providing measurements of higher spatial/temporal resolution which could be achieved by:

- Reducing the time needed for each measurement, thus increasing the temporal resolution of the measurements.
- Reducing the size/weight of the measuring equipment, thus improving its mobility, allowing easier and faster transport, leading to higher spatial resolution.
- Reducing the cost allowing the development of a more extended network for monitoring aerosol physicochemical properties.

In this part we studied the performance of a cost effective and highly portable, simple cylindrical geometry particle segregator, made by electrostatic dissipative materials (EDMs). Apart from characterizing its performance we provided a semi-empirical equation for estimating particle size, based on particles penetration through the EDM-segregator and the main physical principles behind its operation. This work revealed the possibility of substituting parts of the equipment, which is mostly used in

nowadays for the determination of size dependent particle physicochemical properties (e.g. hygroscopicity or volatility), thus reducing their cost and increasing their portability.

Περίληψη

Τα αιωρούμενα σωματίδια επηρεάζουν το κλίμα της γης άμεσα απορροφώντας ή σκεδάζοντας την ηλιακή ακτινοβολία και έμμεσα ενεργώντας ως πυρήνες συμπύκνωσης συννέφων. Η συνεισφορά αυτών των επιδράσεων των αιωρούμενων σωματιδίων στο παγκόσμιο κλίμα εξαρτάται από το μέγεθος και την χημική τους σύσταση, η οποία με την σειρά της καθορίζει την υγροσκοπικότητά τους (δηλ. την ικανότητά τους να απορροφούν νερό). Παρότι θερμοδυναμικά μοντέλα μπορούν να χρησιμοποιηθούν για να προβλέψουν επακριβώς την υγροσκοπική συμπεριφορά σωματιδίων που αποτελούνται από ανόργανη ύλη, η υπάρχουσα γνώση οδηγεί σε μη ακριβείς προβλέψεις σε περιπτώσεις που τα σωματίδια αποτελούνται καθαρά από οργανική ή από μίγματα ανόργανης και οργανικής, ύλης. Η χρήση της υγροσκοπικής παραμέτρου *κ* επιτρέπει την ακριβέστερη προσέγγιση της υγροσκοπικής συμπεριφοράς των ανάμικτων σωματιδίων, όταν η υγροσκοπικότητα και το κλάσμα όγκου του κάθε χημικού είδους που αποτελεί το σωματίδιο, είναι γνωστά. Παρόλα αυτά, η εκτίμηση της υγροσκοπικότητας των ατμοσφαιρικών σωματιδίων ενέχει δυσκολίες, λόγω της περίπλοκης και διαφορετικής χημικής τους σύστασης, η οποία ποικίλη χωρικά και χρονικά. Για αυτό χρειάζονται, υψηλής χρονικής ανάλυσης, απ' ευθείας παρατηρήσεις της υγροσκοπικότητας των σωματιδίων και/ή της χημικής τους σύστασης σε διαφορετικές περιοχές, με σκοπό να μειωθούν οι αβεβαιότητες των επιδράσεών τους στο κλίμα.

Στο πρώτο μέρος αυτής της εργασίας παρέχονται απ' ευθείας παρατηρήσεις της υγροσκοπικής συμπεριφοράς των ατμοσφαιρικών αιωρούμενων σωματιδίων σε απομακρυσμένες και περιαστικές περιοχές της Ελλάδας. Οι μετρούμενες υγροσκοπικές ιδιότητες των σωματιδίων συγκρίνονται ευθέως με την εκτιμώμενη υγροσκοπικότητά τους, η οποία προκύπτει από την χημική τους σύσταση. Οι μετρήσεις διεξήχθησαν στον απομακρυσμένο σταθμό της Βίγλας, ο οποίος βρίσκεται στο νησί της Λήμνου, στο Αιγαίο Πέλαγος και σε δύο περιαστικούς σταθμούς, που βρίσκονται πλησίον της Πάτρας και της Αθήνας.

Τα σωματίδια που μετρήθηκαν στον απομακρυσμένο σταθμό της Βίγλας επέδειξαν μέτρια υγροσκοπικότητα, ενδεικτική για σωματίδια που αποτελούνται από μείγμα ανόργανης και οργανικής ύλης, κάτι το οποίο επιβεβαιώθηκε από τις μετρήσεις της χημικής τους σύστασης. Οι τελευταίες διεξήχθησαν χρησιμοποιώντας μια εναέρια

πλατφόρμα (αεροσκάφος) που έφερε πλήθος οργάνων για την μελέτη των φυσικοχημικών ιδιοτήτων των αιωρούμενων σωματιδίων και η οποία κατά την ίδια χρονική περίοδο πετούσε πάνω από την ευρύτερη περιοχή του Αιγαίου Πελάγους. Η καλή συμφωνία μεταξύ της υγροσκοπικότητας που υπολογίστηκε από την χημική σύσταση των σωματιδίων (αεροσκάφος) και των μετρήσεων (σταθμός εδάφους) επέτρεψε την περαιτέρω εκτίμηση της υγροσκοπικότητας των αιωρούμενων σωματιδίων για ολόκληρη την ευρύτερη περιοχή του Αιγαίου. Η χωρική ποικιλομορφία των εκτιμώμενων υγροσκοπικοτήτων των αιωρούμενων σωματιδίων αποδόθηκε στις διαφορετικές αφετηρίες και διαδρομές των αέριων μαζών που έφταναν στην περιοχή, οι οποίες με την σειρά τους επηρέαζαν έντονα την χημική σύσταση των σωματιδίων.

Τα σωματίδια που μετρήθηκαν στους περιαστικούς σταθμούς της Πάτρας και της Αθήνας έδειξαν διαφορές ως προς τις υγροσκοπικές τους ιδιότητες. Τα σωματίδια που μετρήθηκαν στην Πάτρα επέδειξαν μέτρια υγροσκοπικότητα, παρόμοια λίγο πολύ με αυτήν που παρατηρείται σε ημιαστικές/αγροτικές περιοχές της ηπειρωτικής Ευρώπης, ενώ αντίθετα αυτά που μετρήθηκαν στην Αθήνα επέδειξαν σημαντική χρονική μεταβολή, κυμαινόμενα από μετρίως ως υψηλά υγροσκοπικά. Η εκτιμώμενη (βάση των μετρήσεων της χημικής τους σύστασης που διεξήχθη και στους δύο σταθμούς) υγροσκοπικότητα συσχετίστηκε καλλίτερα με τις μετρήσεις στον περιαστικό σταθμό της Πάτρας από ότι σε αυτόν που βρίσκονταν κοντά στην Αθήνα. Υπεύθυνες για τις τελευταίες διαφορές θα μπορούσαν να είναι είτε η ύπαρξη πυρίμαχης, υψηλής υγροσκοπικότητας ύλης, η οποία είναι αδύνατον να ανιχνευτεί χημικά με τις μεθόδους που χρησιμοποιήθηκαν, είτε η παρουσία συγκεκριμένων οργανικών ενώσεων, οι οποίες είναι πολύ περισσότερο υγροσκοπικές από ότι οι οργανικές ενώσεις που βρίσκονται συνήθως στην ατμόσφαιρα.

Στο δεύτερο μέρος αυτής της διατριβής παρέχονται τρόποι και μέθοδοι για την βελτίωση των τεχνικών που χρησιμοποιούνται για τον καθορισμό των φυσικοχημικών ιδιοτήτων των αιωρούμενων σωματιδίων. Το κίνητρο στην προσπάθεια βελτίωσης ή ανεύρεσης νέων μεθόδων/εξοπλισμού συνδέεται άμεσα με την σημαντικότητα της μελέτης τους και εξυπηρετεί τον σκοπό του να παρέχει μετρήσεις με υψηλότερη χωρική/χρονική ανάλυση, κάτι που μπορεί να επιτευχθεί με:

- Την μείωση του αναγκαίου χρόνου για κάθε μέτρηση, αυξάνοντας έτσι την χρονική ανάλυση των μετρήσεων.

- Την μείωση του βάρους/μεγέθους του μετρητικού εξοπλισμού, βελτιώνοντας την κινητικότητα του, επιτρέποντας ευκολότερη και ταχύτερη μεταφορά, οδηγώντας έτσι σε υψηλότερη χωρική ανάλυση.
- Την μείωση του κόστους, επιτρέποντας την ανάπτυξη ενός πιο εκτεταμένου δικτύου για την παρακολούθηση των φυσικοχημικών ιδιοτήτων των αερολυμάτων.

Σε αυτό το μέρος μελετήθηκε η απόδοση ενός φτηνού και φορητού, απλής κυλινδρικής γεωμετρίας ταξινομητή σωματιδίων, ο οποίος φτιάχτηκε από υλικά διάχυσης στατικού ηλεκτρισμού (electrostatic dissipative materials; EDMs). Εκτός από τον χαρακτηρισμό της απόδοσης, παρέχεται και μια ημι-εμπειρική εξίσωση για την εκτίμηση του μεγέθους των σωματιδίων, βασιζόμενη στην διείσδυση τους μέσω του ταξινομητή EDM, καθώς και οι βασικές φυσικές αρχές πίσω από την λειτουργία του. Αυτή η εργασία ανέδειξε την πιθανότητα της αντικατάστασης τμημάτων εξοπλισμού, που χρησιμοποιείται κυρίως στις μέρες μας για τον προσδιορισμό φυσικοχημικών ιδιοτήτων των σωματιδίων, οι οποίες εξαρτώνται από το μέγεθός τους (π.χ. υγροσκοπικότητα ή πτητικότητα), μειώνοντας έτσι το κόστος τους και αυξάνοντας την φορητότητά τους.

A. Introduction

1 Atmospheric aerosol particles

The term aerosol is used to define suspended solid or liquid particles in a gas, having sizes that vary from a few nanometers to a few hundreds of micrometers (Hinds et al., 1999). Aerosol particles may directly emitted (primary aerosols) in the atmosphere or result as the products of physicochemical processes converting gases to particles (secondary aerosols; Seinfeld and Pandis, 2006). While their origin is both natural and anthropogenic, the contribution of the later is constantly increasing since the beginning of the industrial revolution primarily due to the increased usage of fossil fuels for supporting the modern way of living (Raes et al., 2000).

Aerosols affect earth's climate directly by absorbing or scattering incoming solar radiation (Haywood and Boucher, 2000) and indirectly by acting as Cloud Condensation Nuclei (i.e., indirect effect; Ogren and Charlson, 1992). Both these effects depend on particles size and chemical composition, which both vary spatially and temporarily as a result of the large diversity of their sources and the different physicochemical processes they are involved in during their lifetime (Hallquist et al., 2009). Particles chemical composition also defines their ability to take up water (i.e. hygroscopicity), which in turn affects their size, optical properties and their ability to act as CCN.

2 Aerosols hygroscopic growth

Particles that take up water (i.e. hygroscopic) exhibit an increase in their size when exposed to increased relative humidity (RH) environment. Therefore the term hygroscopic growth factor (g) is often used to quantify particles growth due to water uptake and is expressed as:

$$g(\mathrm{RH})=\frac{d(\mathrm{RH})}{d_{dry}}, \quad (1)$$

where d(RH) and d_{dry} are diameters of the sampled particles at the hydrated and at the dry state, respectively.

Most common, atmospheric relevant, inorganic species will spontaneously transform from solid particles to droplets if they are exposed to RH above a certain threshold, namely the deliquescence RH (DRH; Seinfeld and Pandis, 2006). However,

the same particles while in the liquid state will reform into solids at lower RH than the DRH, exhibiting a hysteresis effect. The RH threshold at which particles in the droplet state will reform into solids is called the efflorescence RH (ERH; Seinfeld and Pandis, 2006). Both DRH and ERH depend on particles chemical composition. Particles hygroscopic growth after the DRH or if in droplet state before ERH, can be predicted by the Köhler theory (Köhler, 1936):

$$S_R = a_{w,s}\ exp\left(\frac{4\sigma_{\mathrm{aq}} M_{\mathrm{w}}}{\rho_{\mathrm{w}} RT d(\mathrm{RH})}\right) \quad (2)$$

where S_{R} stands for the water saturation (RH/100), $\alpha_{\mathrm{w,s}}$ is the water activity for the specific solution, σ_{aq} is the surface tension of the solution droplet, M_{w} and ρ_{w} are respectively the density and molar weight of water, R is the universal gas constant and T the absolute temperature. The exponential term (kelvin term) accounts for the increase in relative vapor pressure, compared to the one over a flat surface, caused by particles curved surface. Kelvin term provides a correction in the hygroscopic behavior of particles smaller than ca. 100 nm.

While basic thermodynamic models (e.g. Clegg et al., 1998) are used to accurately predict the hygroscopic behavior of pure or mixed inorganic species, the complexity of the atmospheric particles which mainly consist of mixtures of inorganic and organic species limits their usage. To overcome these complexities involved in associating the chemical composition of atmospheric particles with their hygroscopic behaviour Petters and Kreidenweis (2007) proposed the use of a single hygroscopic parameter κ. Particles hygroscopic growth factor can be then expressed as:

$$g\,(\mathrm{RH}) = \left(1 + \kappa\left(\frac{a_w}{1-a_w}\right)\right)^{1/3}, \quad (3)$$

with

$$a_{\mathrm{w}} \approx \frac{\mathrm{RH}}{100}\ \left(exp\left(\frac{4\sigma_{s/\alpha}\ M_w}{RT\rho_w d(RH)}\right)\right)^{-1}. \quad (4)$$

Here $\sigma_{\mathrm{s/a}}$ denotes the surface tension of pure water, equal to 0.072 J m^{-2}.

In this way, a κ value of zero is assigned to hydrophobic (i.e. completely insoluble but wettable) particles while most typical atmospheric soluble-salt particles have higher values (e.g. 0.53 and 1.12 for ammonium sulfate and sodium chloride, respectively) and most secondary organic aerosols (SOAs) lay in the range between zero and 0.3 (Petters and Kreidenweis 2007). In the case that aerosol particles are consisted by a mixture of different species their hygroscopic parameter κ can be calculated by their chemical composition as follows:

$$\kappa = \sum_i \varepsilon_i \kappa_i , \quad (5)$$

where $\varepsilon_i = V_{si}/V_s$ and κ_i are the volume fraction and the hygroscopic parameter of the *i*th chemical species comprising the particles, with V_{si} being the volume occupied by that species and V_s the volume of the dry particle.

3 Measurement techniques of aerosols hygroscopicity

A variety of experimental methods has been employed for measuring particles hygroscopic behavior by measuring the changes in particle properties due to water absorption. More specifically, these methods involve changes in particle mass (e.g. Electrodynamic balance EBDs; Peng and Chan, 2001), changing in particles optical properties(e.g. wet/dry nephelometry; McInnes et al., 1998) and in particles electrical mobility diameter (e.g. Hygroscopic Tandem Differential Mobility Analyzer; HTDMA; Rader and McMurry, 1986). The later offers high precision, near real-time measurements of changes in particles electrical mobility diameter after exposing them to elevated RH conditions and is considered the method of choice for sub micrometer particles. It mainly consists of two Differential Mobility Analyzers (DMAs; Knutson and Whitby, 1975), and a Condensation Particle Counter (CPC, TSI Model 3772; Stolzenburg and McMurry, 1991). Figure 1.1 depicts the operating principle of the HTDMA. In brief, the particles in the sample flow are initially dried and passed through a bipolar charger before entering the first DMA (DMA-1) that produces a monodisperse aerosol flow. The monodisperse particles downstream DMA-1 are then exposed to elevated RH conditions inside the humidifier before their size is measured by the second DMA (DMA-2) and the CPC.

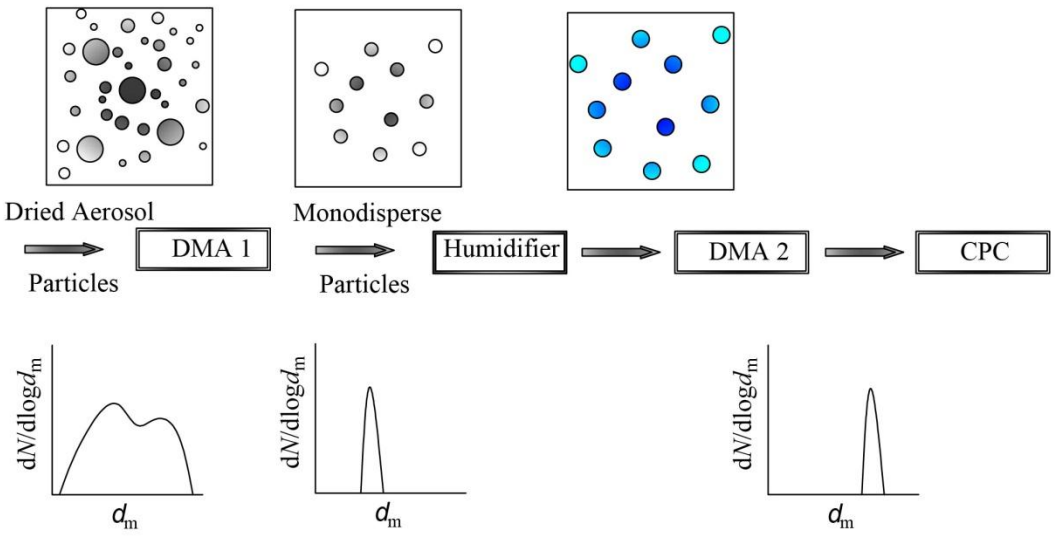

Figure 1.1: Schematic illustration of the HTDMA measuring principle.

While all of the above methods are used for measuring particle hygroscopic properties at sub-saturation conditions (i.e. RH<100%) a CCN counter (CCNC) is able to provide information on particle hygroscopicity at the super-saturation regime, by directly counting particles that are CCN active. In order to achieve super-saturated conditions a CCNC exposes particles which are surrounded by a saturated (i.e. RH=100%) sheath flow inside a wet ceramic column. A temperature gradient is maintained within the column resulting in water vapour supersaturation. According to their size in dry conditions and chemical composition, aerosols will become CCN active above a certain supersaturation, namely critical supersaturation (S_c). CCN active particles are then optically counted downstream of the growth chamber by an Optical Particle Counter (OPC).

3.1 Development of a custom-made HTDMA

A custom made HTDMA was developed as part of this work incorporating commercially available and custom made parts. The first DMA (DMA-1, TSI 3080) includes a ^{85}Kr aerosol neutralizer and a closed-loop system for recirculating the sheath flow. The second DMA (DMA-2) employs a custom-made system for the sheath flow

recirculation (cf. Biskos et al., 2006). The system also uses two nafion-tube humidity exchangers (Perma Pure Model MD-110), three humidity/temperature sensors (two Rotronic Model SC-05 and one Rotronic Model HC2-C05), two multi input-output cards (Multifunction Data Acquisition cards; National Instruments models NI USB 6211 and 6008), two Mass Flow Controllers (Sierra Mass-Trak 810), one air pump and one laptop computer. The voltage on DMA-1 was adjusted to select dry aerosol particles of a specific mobility diameter. Automatic, time scheduled voltage selection on DMA-1 was also used to provide the ability of sampling more than one particle sizes in regular time circles during field measurements. The quasi monodisperse particles downstream were conditioned inside a nafion humidity exchanger to a constant RH value (usually between 85 and 87%), before the measurement of their size distribution by DMA-2 and the CPC. The RH of sheath flow in DMA-2 was maintained at the same level with the one of the aerosol flow after passing through the second nafion humidity exchanger.

Responsible for maintaining both the sheath and aerosol RHs upstream DMA-2 at the desired level, was a closed loop automatic control system. In brief the RHs upstream DMA-2 were constantly monitored using two RH/T sensors. The flows of two parallel streams of very high RH (ca. 100%) on the outer annuluses of the two nafion-tube humidity exchangers were properly adjusted, using the two mass flow controllers, in order to reduce the difference between the measured and desired RH. For optimal performance two software proportional-integral-derivative (PID) controllers were incorporated for this purpose.

Parts of the HTDMA and the system as a whole were tested in laboratory conditions after its assembly and before each field application. In particular the classification accuracy of both DMAs of the HTDMA system was tested with Polystyrene latex spheres (PSLs) and found to be within 1% accuracy in respect of classification size. The automatic humidification/control system was able to control both the sheath and aerosol RH within a ±2% accuracy. Hygroscopic growth factors at RHs ranging from 20 to 94% (i.e. humidogramms) of sodium chloride and ammonium sulfate particles were measured and compared with the theory to verify the overall performance of the system.

3.2 Measurements of particle hygroscopicity at both sub and super saturation regimes

In part of this work a Continuous Flow Streamwise Thermal Gradient CCN Chamber (CFSTGC; Roberts and Nenes, 2005; CCNC from now on for simplicity reasons) was employed downstream DMA-1 of the HTDMA system (c.f. Fig. 1.2). With this setup we were able to simultaneously provide size resolved hygroscopicity measurements at both sub- and super-saturated conditions. The instrument was operated in "Scanning Flow CCN Analysis" (SFCA) mode, in which the flow rate in the growth chamber changes over time, while a constant streamwise temperature difference is maintained. This causes supersaturation to change continuously, allowing the rapid and continuous measurement of supersaturation spectra with high temporal resolution (~60-120 seconds and potentially even less) without being affected by shifts in activation kinetics and aerosol composition (Moore and Nenes, 2009). The flow rate during measurements was increased linearly between a minimum flow rate (Q_{min} ~ 300ccm) and a maximum flow rate (Q_{max} ~ 1000ccm) over a ramp time of 60 seconds. The flow was maintained at Q_{max} for 10 seconds and then linearly decreased to Q_{min} over the same ramp time. Finally, the flow rate was held constant at Q_{min} for 10 more seconds and the scan cycle is repeated. Droplet concentrations and size distributions at the OPC are continuously measured during this scan with a 1 s integration time.

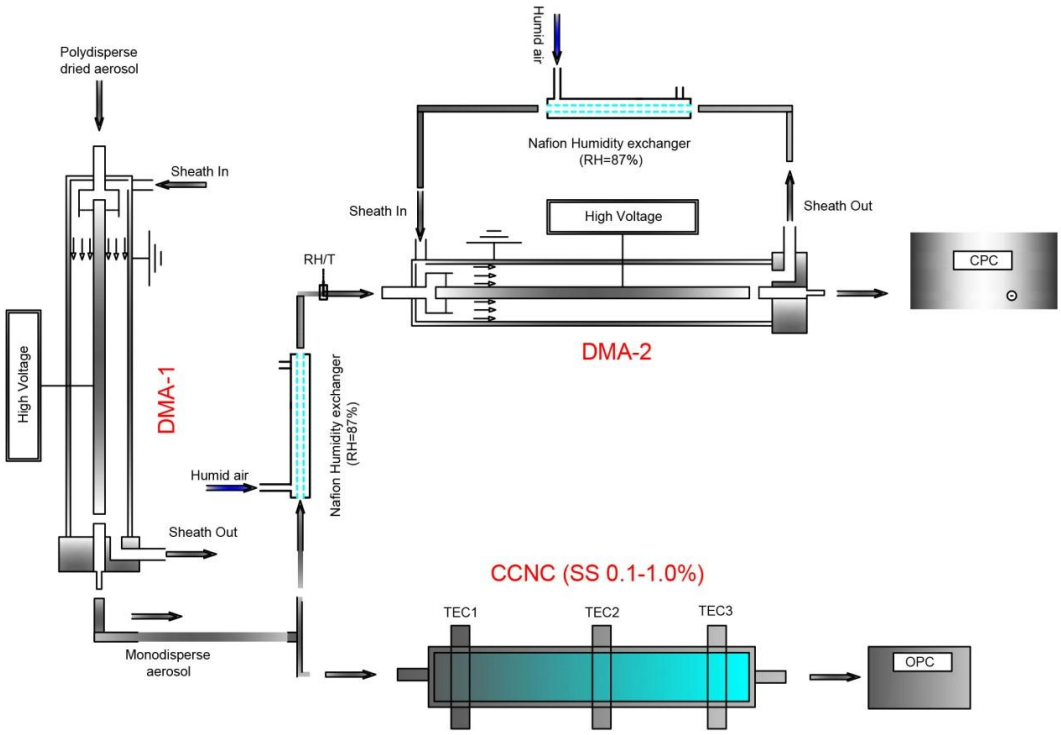

Fig 1.2. Experimental setup of HTDMA-CCNC combo. In brief, dried aerosols were sampled, neutralized by a ^{85}Kr neutralizer and size selected inside DMA-1. Part of the monodisperse flow downstream DMA-1 was passed through a nafion humidifier, where its RH was increased to 87 ±2%, before measured by DMA-2 and the CPC. The rest of the monodisperse flow was directed through the CCNC, where it was super-saturated from 0.1 to 1.0% with water vapors. Particles that activated as Cloud Condensation Nuclei were detected downstream by an Optical Particle Counter.

The super-saturated conditions within the CCNC were calibrated in terms of the temperature difference between the inlet and the outlet (ΔT = 5 °C), the instantaneous flow rate and the overall flow rate range. The relationship between super-saturation and instantaneous flow rate was determined by the procedure described by Moore and Nenes (2009). According to that, size-classified ammonium sulfate particles from DMA-1 were introduced into the CCNC whose flow and thus the range of super-saturated conditions, was scanned. For each particle size, the critical super-saturation value $S_{c,}$ above which particles act as CCN was obtained from Köhler theory (Moore et al., 2012a). The calibration measurements were fitted with sigmoidal curves where the inflection point,

corresponding to the S_c of the selected ammonium sulfate particles, was used to determine the critical activation flow rate Q_{50}. The absolute uncertainty of the calibrated CCNC super-saturation is estimated to be ±0.04% (Moore et al., 2012a; 2012b).

The CCN activity of the particles is characterized by the activation ratio given by:

$$R_a \equiv \frac{CCN}{CN} = a_0 + \frac{a_1 - a_0}{1 + (Q/Q_{50})^{-a_2}}, \qquad (6)$$

where CCN and CN are the activated and total particle concentrations, while a_0, a_1, a_2 and Q_{50} are constants that describe the minimum, maximum, slope and inflection point of the sigmoidal, respectively, while Q is the instantaneous volumetric flow rate. Ideally, a_0 is zero and a_1 is expected to be unity; however, values for a_1 varied throughout the measurement period depending on the selected aerosol particle size and the mixing state. The inflection point (i.e. Q_{50} or "critical flow rate"), corresponds to the instantaneous flow rate, that produces a level of super-saturation within the CCNC, required to activate the measured monodisperse aerosol. An example of a CCN activity spectrum with the sigmoidal fit and its defined parameters is depicted in Fig. 1.3.

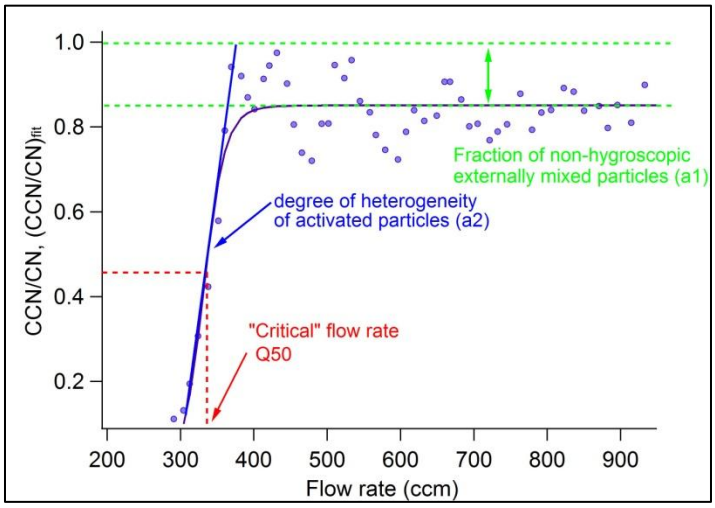

Fig. 1.3: Example of an ambient CCN activity spectrum (at constant ΔT) with sigmoidal fit and its defined parameters.

4 Motivation

The earth's climate is changing more rapidly than in other geological periods due to human intervention in the planet's "thermostat", which in simple terms is the energy

balance between the radiation that the planet is exposed to (i.e. incoming solar energy) and the amount that returns back to space either by reflection or by secondary radiative reemission (i.e. infrared radiation due to earth's temperature). The main mechanisms behind this balancing act involve the reflection of incoming solar radiation (albedo), its absorption by earth's surface and the absorption of reemitted infrared radiation by the atmosphere. The latter is known as the "greenhouse" effect. During the last few decades a large attempt is made in order to better understand the ways that the modern human civilization affects the planet's climate and predict the consequences of our actions. During this short, in terms of historical time, period we have already concluded that the release of certain gases ("greenhouse gases") in the atmosphere causes an increase in its potential to absorb more infrared radiation and thus an increase in the temperature of the planet. Climate models have been employed to study the complex interactions involved in the planet's energy balance and predict the evolution of what we use to call "climate change". Atmospheric aerosols play a key role in earth's climate and therefore the study of their effects in climate is intense.

Although the uncertainties regarding the effects of aerosols in the global climate have been reduced during the last few years, these uncertainties remain relatively high in contrast to other sources of climate change (IPCC, 2014). Climate models are largely affected by inaccurate particle hygroscopic properties, leading to uncertain estimation of the aerosol indirect effect on a global scale (Lohmann and Ferrachat, 2010). For this reason monitoring of their properties in different locations and with high temporal resolution is important for reducing these uncertainties. Part I of this work is dedicated in studying aerosols hygroscopicity, in remote and sub-urban locations of Greece. Part II provides the means of improving the methods/techniques of determining their properties in order to improve spatial and temporal resolution of these measurements.

4.1 Aerosols hygroscopic properties at a remote location and over the Aegean Sea

Particles observed in remote areas are typically suspended in the atmosphere long enough to reach an internally mixed state through coagulation and condensation of gaseous species (Heintzenberg 1989). This is typically the case for the wider area of

Eastern Mediterranean, and particularly the region over the Aegean Sea, during July and August when the prevailing northern winds (i.e., the Etesians) carry polluted air masses from central Europe, the Balkans (including Greece), and the Black Sea (Mihalopoulos et al., 1997; Lelieveld et al., 2002). The polluted air masses blend with natural primary and secondary particles, resulting in increased particle concentrations commonly observed in the region (Salisbury et al, 2003).

Although information about the size, the concentration, and the integrated chemical composition of particles found over the southern Aegean region has been extensively reported in the literature (Koulouri et al., 2008; Kalivitis et al., 2008), high temporal resolution measurements of their hygroscopicity and/or chemical composition has been rather scarce (Pikridas et al., 2010).

In this work we report high temporal resolution chemical composition and hygroscopicity measurements of particles in the atmosphere over the Aegean Sea. Chemical composition measurements of non-refractory fine aerosol particles were conducted using an airborne compact time-of-flight aerosol mass spectrometer (cToF-AMS). Particle hygroscopicity measurements were performed by an HTDMA system located in the northern region of the Aegean Sea. Good closure between cToF-AMS and HTDMA measurements (agreement within ±5% uncertainty) was achieved when the aircraft flew in the vicinity of the ground station. Using the parameterisation from the closure study, we employ the cToF-AMS measurements to determine vertical profiles of the hygroscopic parameter κ of the particles in the region.

4.2 . Hygroscopic Properties and Mixing State of Ultrafine Aerosol Particles in Urban Background Sites

In contrast to remote, urban areas are affected by long range transported particles and by the ones that are produced by local sources. The large variability of their composition combined with the insufficient suspension time of the latter (i.e. new formed particles) could result in particles that are externally mixed (Alfarra et al., 2004). This is typically the case for most of the suburban areas of major cities, where wind direction could significantly affect the observable particles. The suburban areas of Patras and Athens were selected as measuring sites, due to their proximity in large cities, forests, sea

and rural areas. To the best of our knowledge , the only data available for suburban environments in the broader region of Southeastern Europe and especially for the mainland of Greece are those reported by Petäjä et al. (2007), which measured the hygroscopicity of sub 50 nm particles in a suburban site close to Athens.

In this work we report and compare, hygroscopicity, mixing state, and CCN activity measurements of particles in the atmosphere over the two suburban areas of Patras and Athens. Hygroscopicity measurements below saturation were conducted using one HTDMA while particles CCN activity was measured at various super-saturation ratios by a CCNC. The HTDMA and the CCNC were combined in order to measure the hygroscopic properties of the same dry mobility diameter particles in different saturation conditions. The mixing state of the particles, obtained by appropriate analysis of the HTDMA measurements, was corroborated by wind back-trajectories calculations. High resolution, near real time, chemical composition measurements of non-refractory fine aerosol particles were conducted using a High Resolution Time-Of-Flight Aerosol Mass Spectrometer (HR-ToF-AMS) and were used for a better estimation of the hygroscopic properties of particles organic fraction. The above results were also compared by the estimated hygroscopic parameters, when off-line chemical composition of particles having diameters smaller than 2.5 μm ($PM_{2.5}$) was used.

4.3 . A Cost-Effective Electrostatic Precipitator for Aerosol Nanoparticle Segregation

While in the two previous sections we provide measurements, mainly regarding atmospheric particles hygroscopic properties, in this section we introduce a simple and cost effective method for size segregating sub 100 nm aerosols. Measuring their size is important for assessing their environmental impacts (McMurry, 2000) and investigating their potential technological applications (Biskos *et al*., 2008). The most common and effective method in use, is the employment of DMAs, which have a high resolution, accuracy and repeatability, but come with the downside of high cost and bulky size, which limit their widespread application. On the other hand, Diffusion Batteries (DBs) can also be used as particle size classifiers (DeMarcus and Thomas, 1952), but a number

of technical limitations (cf. McMurry, 2000) has made them less favorable for particle size measurements compared to electrical mobility classifiers.

In this work we employed a tube composed by Electrostatic Dissipative Materials (EDMs), along which a potential difference was applied. The high surface resistivity (10^{12} Ω/sq) of the EDM tube allows the application of high voltages at its surface which result in an electrostatic field of varying strength which has a radial and an axial component. Charged particles, passing through the tube, are removed by electrostatic deposition caused by the radial field, while the axial field decelerates them, thus increasing their residence time and their chance for diffusional deposition. The result of these two processes resembles a combination of a DB and an electrostatic precipitator. The penetration efficiencies of charged monodisperse particles through the EDM tube were measured at different voltages, while numerical simulations of the flows and electric fields inside the tube were used for better understanding the processes of particle deposition. Most importantly, we provided a semi-empirical equation for predicting particle size, based in the measured particle relative penetration, flow rate and voltage.

REFERENCES

Alfarra, M.R., Coe, H., Allan, J.D., Bower, K.N., Boudries, H., Canagaratna, M.R., Jimenez, J.L., Jayne, J.T., Garforth, A., Li, S.-M., Worsnop, D.R.: Characterization of urban and rural organic particulate in the Lower Fraser Valley using two aerodyne aerosol mass spectrometers. *Atmos.Environ*. 38 (35), 5745–5758, 2004.

Biskos, G., Paulsen, D., Russell, L. M., Buseck, P. R., Martin, S. T.: Prompt deliquescence and efflorescence of aerosol nanoparticles. *Atmos.Chem. Phys*., 6, 4633-4642, doi:10.5194/acp-6-4633-2006, 2006a.

Clegg, S. L., Brimblecombe, P., Wexler, A. S.: Thermodynamic Model of the System H^+-NH_4^+ - SO_4^{2-} - NO_3^- - H_2O at TroposphericTemperatures. *J. Phys. Chem. A*, 102, 2137–2154, 1998.

DeMarcus, W. C. and Thomas, J. W.: Theory of a Diffusion Battery. *USAEC Report ORNL-1413*, Oak Ridge National Laboratory, Oak Ridge, TN, 1952.

Hallquist, M., Wenger, J. C., Baltensperger, U., Rudich, Y., Simpson, D., Claeys, M., Dommen, J., Donahue, N. M., George, C., Goldstein, A. H., Hamilton, J. F., Herrmann, H., Hoffmann, T., Iinuma, Y., Jang, M., Jenkin, M. E., Jimenez, J. L., Kiendler-Scharr, A., Maenhaut, W., McFiggans, G., Mentel, Th. F., Monod, A., Prévôt, A. S. H., Seinfeld, J. H., Surratt, J. D., Szmigielski, R., Wildt, J.: The formation, properties and impact of secondary organic aerosol: current and emerging issues, *Atmos. Chem. Phys*., 9, 5155–5236, doi:10.5194/acp-9-5155-2009, 2009.

Haywood, J. and Boucher, O.: Estimates of the direct and indirect radiative forcing due to tropospheric aerosols: a review, *Rev. Geophys*., 38, 513–543, 2000.

Heintzenberg J.: Fine particles in the global troposphere. A review , *Tellus, 41B*, 149-160, 1989.

Hinds, W. C.: Aerosol Technology: Properties, Behavior, and Measurement of Airborne Particles, 2nd Edition. *John Willey & Sons, Inc*., 1999.

IPCC, 2014: Climate Change 2014: Synthesis Report. Contribution of Working Groups I, II and III to the Fifth Assessment Report of the Intergovernmental Panel on Climate Change [Core Writing Team, R.K. Pachauri and L.A. Meyer (eds.)]. IPCC, Geneva, Switzerland, 151 pp.

Kalivitis, N., Birmili, W., Stock, M., Wehner, B., Massling, A., Wiedensohler, A., Gerasopoulos, E., and Mihalopoulos, N.: Particle size distributions in the Eastern Mediterranean troposphere, *Atmos. Chem. Phys*., 8, 6729–6738, doi:10.5194/acp-8-6729-2008, 2008.

Koulouri, E., Saarikoski, S., Theodosi, C., Markaki, Z., Gerasopoulos, E., Kouvarakis, G., Mäkelä, T., Hillamo, R., and Mihalopoulos, N.: Chemical composition and sources of fine and coarse aerosol particles in the eastern Mediterranean, *Atmos. Environ*., 42, 6542–6550, 2008.

Knutson, E.O., Whitby, K.T.: Aerosol classification by electric mobility: Apparatus, theory, and applications. *J. Aerosol Sci*., 6, 443-451, 1975.

Köhler, H.: The nucleus in and the growth of hygroscopic droplets, *Trans. Faraday Soc.*, 32, 1152-1161, (1936).

Lelieveld, J., Berresheim, H., Borrmann, S., Crutzen, P. J., Dentener, F. J., Fisher, H., Feichter, J., Flatau, P. J., Heland, J., Holzinger, R., Korrmann, R., Lawrence, M. G., Levin, Z., Markowitz, K. M., Mihalopoulos, N., Minikin, A., Ramanathan, V., de Reus, M., Roelofs, G. J., Scheeren, H. A., Sciare, J., Schlager, H., Schultz, M., Siegmund, P., Steil, B., Stephanou, E. G., Stier, P., Traub, M., Warneke, C., Williams, J., and Ziereis, H.: Global air pollution crossroads over the Mediterranean, *Science*, 298, 794–799, 2002.

Lohmann U., Ferrachat, S.: Impact of parametric uncertainties on the present-day climate and on the anthropogenic aerosol effect, *Atmos. Chem. Phys*., 10, 11373–11383, 2010

McInnes, L., Bergin, M., Ogren, J. and Schwartz, S.: Apportionment of light scattering and hygroscopic growth to aerosol composition, *Geophys. Res. Lett.*, 25, 513-516, 1998.

McMurry, P. H. (2000). A review of Atmospheric Aerosol Measurements. *Atmos. Environ.*, 34:1959-1999.

Mihalopoulos, N., Stephanou, E., Kanakidou, M., Pilitsidis, S.,Bousquet, P.: Tropospheric aerosol ionic compositionabove the Eastern Mediterranean Area, *Tellus B* 49B, 314–326, 1997.

Moore, Richard H., and Nenes, A.: Scanning flow CCN analysis - A method for fast measurements of CCN spectra. *Aerosol Sci. Tech*. 43.12, 1192-1207, 2009.

Moore, R.H., Cerully, K., Bahreini, R., Brock, C.A., Middelbrook, A.M., and Nenes, A.: Hygroscopicity and composition of California CCN during summer 2010, *J. Geophys. Res.*, 117, D00V12, doi:10.1029/2011JD017352, 2012a.

Moore, R.H., Raatikainen, T., Langridge, J.M., Bahreini, R., Brock, C.A., Holloway, J.S., Lack, D.A., Middlebrook, A.M., Perring, A.E., Schwarz, J.P., Spackman, J.R., and Nenes, A.: CCN spectra, hygroscopicity, and droplet activation kinetics of Secondary Organic Aerosol resulting from the 2010 Deepwater Horizon oil spill, Environ. *Sci. Technol.*, 46, 3093-3100, 2012b.

Ogren, J. and Charlson, J.: Implications for models and measurementsof chemical inhomogeneities among cloud droplets, *Tellus, 44B*, 489–504, 1992.

Peng C. and Chan, C. K.: The water cycles of water-soluble organic salts of atmospheric importance, *Atmos. Environ*. 35, 1183-1992, 2001.

Petäjä, T., Kerminen, V.-M., Dal Maso, M., Junninen, H., Koponen, I. K., Hussein, T., Aalto, P. P., Andronopoulos, S., Robin, D., Hämeri, K., Bartzis, J. G., Kulmala, M.: Sub-micron atmospheric aerosols in the surroundings of Marseille and Athens: physical characterization and new particle formation, *Atmos. Chem. Phys.*, 7, 2705–2720, 2007.

Petters, M. D. & Kreidenweis S. M.: A single parameter representation of hygroscopic growth and cloud condensation nucleus activity, *Atmos. Chem. Phys.*, 7, 1961–1971, doi:10.5194/acp-7-1961-2007, 2007.

Pikridas, M., Bougiatioti, A., Hildebrandt, L., Engelhart, G. J., Kostenidou, E., Mohr, C., Prévôt, A. S. H., Kouvarakis, G., Zarmpas, P., Burkhart, J. F., Lee, B.-H., Psichoudaki, M., Mihalopoulos, N., Pilinis, C., Stohl, A., Baltensperger, U., Kulmala, M., and Pandis, S. N.: The Finokalia Aerosol Measurement Experiment – 2008 (FAME-08): an overview, *Atmos. Chem. Phys.*, 10, 6793–6806, doi:10.5194/acp-10-6793-2010, 2010.

Rader, D.J., McMurry P.H.: Application of the tandem differential mobility analyzer to studies of droplet growth or evaporation, *J. Aerosol Sci*., 17, 771-787, 1986.

Raes, F., Van Dingenen, R., Vignati, E., Wilson, J., Putaud, J. P., Seinfeld, J H., Adams, P. (2000): Formation and cycling of aerosols in the global troposphere. *Atmos. Environ*., 34, 4214-4220.

Roberts, G. C., and Nenes, A.: A continuous-flow streamwise thermal-gradient CCN chamber for atmospheric measurements. *Aerosol Sci. Tech*. 39.3, 206-221, 2005.

Salisbury, G., Williams, J., Holzinger, R., Gros, V., Mihalopoulos, N., Vrekoussis, M., Sarda-Estéve, R., Berresheim, H., von Kuhlmann, R., Lawrence, M., and Lelieveld, J.: Ground-based PTR-MS measurements of reactive organic compounds during the MINOS campaign in Crete, July–August 2001, *Atmos. Chem. Phys.*, 3, 925–940, doi:10.5194/acp-3-925-2003, 2003.

Seinfeld, J. H. & Pandis, S.N., (2006): Atmospheric Chemistry And Physics. *John Wiley & Sons, inc.*

Stolzenburg, M.R. & McMurry, P.H.: An ultrafine aerosol Condensation Nucleus Counter, *Aerosol Sci. Technol*., 14, 48-65, 1991.

PART I: Physicochemical Properties of Atmospheric Aerosol Particles over Suburban and Remote Locations

2. Chemical Composition and Hygroscopic Properties of Aerosol Particles over the Aegean Sea

S. Bezantakos[1,2], K. Barmpounis[3], M. Giamarelou[1], E. Bossioli[4], M. Tombrou[4], N. Mihalopoulos[5], K. Eleftheriadis[2], J. Kalogiros[6], J. D. Allan[7], A. Bacak[7], C. J. Percival[7], H. Coe[7], and G. Biskos[1,3]

[1]*Department of Environment, University of the Aegean, Mytilene 81100, Greece*

[2]*ERL, Inst. of Nuclear Tech. & Rad. Protection, NCSR Demokritos, 15310 Ag. Paraskevi, Attiki, Greece*

[3]*Faculty of Applied Sciences, Delft University of Technology, Delft 2628-BL, The Netherlands*

[4]*Department of Physics, National and Kapodistrian University of Athens, Athens 15784, Greece*

[5]*Department of Chemistry, University of Crete, Heraklion 71003, Greece*

[6]*Institute of Environmental Research and Sustainable Development, National Observatory of Athens, Athens, Greece*

[7]*School of Earth, Atmospheric and Environmental Science, The University of Manchester, Manchester, United Kingdom*

Correspondence to: G. Biskos
(biskos@aegean.gr; g.biskos@tudelft.nl)
Published: 29 November 2013
Atmospheric Chemistry and Physics
(Atmos. Chem. Phys., 13, 11595–11608, 2013)

Abstract

The chemical composition and water uptake characteristics of sub-micrometre atmospheric particles over the region of the Aegean Sea were measured between 25 August and 11 September 2011 within the framework of the Aegean Game campaign. High temporal-resolution measurements of the chemical composition of the particles were conducted using an airborne compact time-of-flight aerosol mass spectrometer (cToF-AMS). These measurements were performed during two flights from the island of Crete to the island of Lemnos and back. A hygroscopic tandem differential mobility analyser (HTDMA) located on the island of Lemnos was used to measure the ability of the particles to take up water. The HTDMA measurements showed that the particles in the dominant mode were internally mixed, having hygroscopic growth factors that ranged from 1.00 to 1.59 when exposed to 85 % relative humidity. When the aircraft flew near the ground station on Lemnos, the cToF-AMS measurements showed that the organic volume fraction of the particles ranged from 43 to 56 %. These measurements corroborate the range of hygroscopic growth factors measured by the HTDMA during that time. Good closure between HTDMA and cToF-AMS measurements was achieved when assuming that the organic species were less hygroscopic and had an average density that corresponds to aged organic species. Using the results from the closure study, the cToF-AMS measurements were employed to determine vertical profiles of a representative aerosol hygroscopic parameter κ_{mix}. Calculated κmix values ranged from 0.19 to 0.84 during the first flight and from 0.22 to 0.80 during the second flight. Air masses of different origin as determined by back trajectory calculations can explain the spatial variation in chemical composition and κ_{mix} values of the particles observed in the region.

1. Introduction

Atmospheric aerosol particles affect the global radiative balance of the Earth by directly absorbing and scattering solar radiation (i.e., direct effect; Haywood and Boucher, 2000), and indirectly by acting as Cloud Condensation Nuclei (i.e., indirect effect; Ogren and Charlson, 1992). Scattering and absorption of aerosol particles strongly depends on their size and chemical composition, which are often characterised by high variability as a result of the large diversity of their sources and the different physicochemical processes they are involved in during their lifetime (Hallquist et al., 2009). The chemical composition of the particles also defines their hygroscopicity, i.e. their ability to take up water, which in turn can affect their interaction with incoming solar radiation. To predict the hygroscopic behaviour of pure or mixed inorganic particles one can use basic thermodynamic principles(e.g. Clegg et al., 1998). For particles that consist of organic species or mixtures of organic and inorganic compounds, however, existing knowledge does not allow accurate predictions of their hygroscopicity. This limited understanding is one of the greatest uncertainties in determining the role of atmospheric aerosols on climate.

To overcome the complexities involved in associating the chemical composition of atmospheric particles with their hygroscopic behaviour Petters and Kreidenweis(2007) proposed the use of a single hygroscopic parameter κ. The value of κ is 0 for completely insoluble but wettable particles whose water activity is not affected by water adsorbed on their surface. For typical atmospheric soluble-salt particles such as ammonium sulphate or sodium chloride the value of κ is 0.53 and 1.12, respectively, whereas for secondary organic aerosols (SOAs) it typically ranges between 0.0 and 0.2 (Petters and Kreidenweiss, 2007). Using the parameter κ, and information about the hygroscopic behaviour of the pure chemical species, one can make a good first approximation of the water uptake characteristics of internally mixed particles.

Particles observed in remote areas are typically suspended in the atmosphere long enough to reach an internally mixed state through coagulation and condensation of gaseous species (Heintzenberg 1989). This is typically the case for the wider area of Eastern Mediterranean, and particularly the region over the Aegean Sea, during July and August when the prevailing northern winds (i.e., the Etesians) carry polluted air masses

from central Europe, the Balkans (including Greece), and the Black Sea (Mihalopoulos et al., 1997; Lelieveld et al., 2002). The polluted air masses blend with natural primary and secondary particles, resulting in increased particle concentrations commonly observed in the region (Salisbury et al, 2003).

Although information about the size, the concentration, and the integrated chemical composition of particles found over the southern Aegean region has been extensively reported in the literature (Koulouri et al., 2008; Kalivitis et al., 2008), high temporal resolution measurements of their hygroscopicity and/or chemical composition has been rather scarce (Pikridas et al., 2010). To the best of our knowledge, only Stock et al. (2011) have carried out measurements using a hygroscopic tandem differential mobility analyser (HT-DMA) system at Finokalia on the island of Crete. During that study the observed hygroscopic growth factors of particles having dry mobility diameters of 50, 80 and 150 nm ranged from 1.12 to 1.59 when exposed at 90 % relative humidity.

In this work we report high temporal resolution chemical composition and hygroscopicity measurements of particles in the atmosphere over the Aegean Sea. Chemical composition measurements of non-refractory fine aerosol particles were conducted using an airborne compact time-of-flight aerosol mass spectrometer (cToF-AMS) onboard the UK BAe-146-301 Atmospheric Research Aircraft, which was operated through the Facility for Airborne Atmospheric Measurement (referred to as the FAAM BAe-146 aircraft from this point onwards). Particle hygroscopicity measurements were performed by an HTDMA system located in the northern region of the Aegean Sea. Good closure between cToF-AMS and HTDMA measurements (agreement within ±5% uncertainty) was achieved when the aircraft flew in the vicinity of the ground station. Using the parameterisation from the closure study, we employ the cToF-AMS measurements to determine vertical profiles of the hygroscopic parameter κ_{mix} of the particles in the region.

2. Methods

2.1 Instrumentation

2.1.1 Airborne measurements

The airborne measurements involved a total of three flights from Crete to Lemnos and back with the FAAM BAe146 aircraft (cf. Tombrou et al., 2012). The cToF-AMS was operational in only two of these flights; namely flights b637 and b641 performed on 1 and on 4 September, respectively. Detailed paths of these flights are shown in Fig. 1. In both cases the aircraft took off from Chania Airport, on Crete and headed east before turning north towards the island of Lemnos. The first flight took place from 09:00 to 13:45 UTC on 1 September. During that flight, the altitude of the aircraft was above 300 m on its way to Lemnos (eastern leg of the flight). To capture the vertical variation of the chemical composition of the particles along this path, the aircraft performed two missed approaches: one over the central Aegean Sea, and one over the island of Lemnos (Tombrou et al., 2012). The second flight took place from 11:13 to 15:38 UTC on 4 September. During that flight, the altitude of the aircraft along the leg from Crete to Lemnos (i.e. the part over the eastern Aegean Sea) was at lower altitude, almost constantly at 150 m above sea level (a.s.l.). The flight leg from Lemnos to Crete (i.e. the part over the western Aegean Sea) was in general at altitudes above 2.3 km during both flights, except for a small period during the second flight when the aircraft flew at 160 m a.s.l. on the southeast of Athens. Considering that the marine at mospheric boundary layer (MABL) was below 1 km, some parts of the flights were within and some above it.

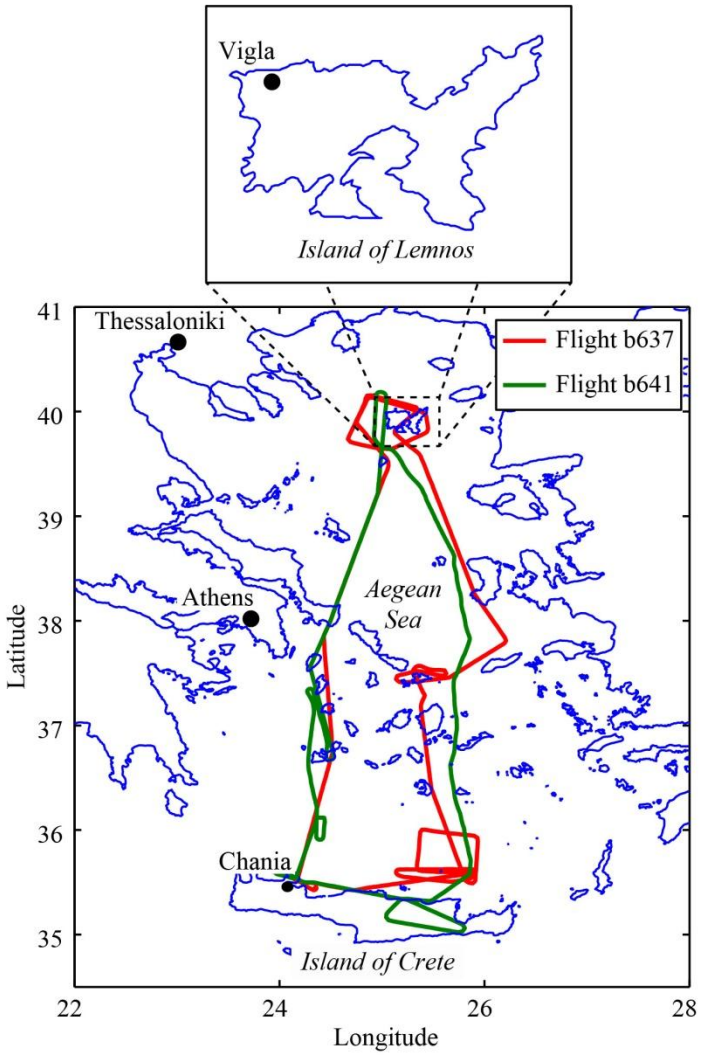

Fig. 1. Map of Greece showing the island of Lemnos and the location of the ground station at Vigla on the northwestern part of the island. The red and green lines show the paths followed by the FAAM BAe-146 aircraft on flights b637 and b641, performed on 1 and 4 September, respectively.

The non-refractory submicron chemical composition of the aerosol particles was determined by a cToF type (Canagaratna et al., 2007; Drewnick et al., 2005) AMS (Aerodyne Research Inc.) onboard the aircraft. Details of the airborne cToF-AMS instrument and the algorithm used for the analysis of the measurements are provided in Morgan et al. (2010). In brief, air was sampled through a Rosemount inlet (a forward facing, sub-isokinetic inlet with sampling efficiency close to unity for particles ≤600 nm; for more details cf. Foltescu et al., 1995), mounted on the aircraft fuselage. Inside the

AMS an aerodynamic lens (Wang et al., 2005) was used for focusing the sampled particles onto the heated surface, which was maintained at 600 ˚C. The vapours resulting from volatilising the particles on the heated surface were then ionised using electron impact at 70 eV, and the ion fragments were analysed by a quadruple mass spectrometer for specific ions, including NH_4^+, Cl^-, NO_3^-, SO_4^{2-} and organics. The cToF-AMS can measure particles having vacuum aerodynamic diameters (VADs) in the range from 50 to 700 nm (Liu et al., 2007), with a detection limit of ca. 50 ng m^{-3}.

The cToF-AMS was calibrated using monodisperse ammonium nitrate particles and the recorded measurements were analysed using the fragmentation table approach (Allan et al., 2003, 2004) with the modifications introduced by Aiken et al. (2008). Corrections for variations in the composition-dependent collection efficiency were applied according to the parameterisation introduced by Middlebrook et al. (2012).

2.1.2 Ground measurements

The ground-based hygroscopicity measurements were conducted at a station located 420 m a.s.l. in the area of Vigla, on the northwestern part of the island of Lemnos (39˚ 58' N, 25˚ 04' E; cf. Fig. 1). The area is far from any major city and from local anthropogenic sources. A custom-made HTDMA system (Rader and McMurry, 1986) and a commercially available scanning mobility particle sizer (SMPS, TSI Model 3034; Wang and Flagan, 1990) were used to measure the hygroscopic growth factor and the size distribution of the particles, respectively. For these measurements, ambient air was sampled through a 6-m long copper tube (ID = 26 mm) with a total flow rate of 30.0 lpm at atmospheric conditions. From this flow, 0.3 lpm were sampled by the HTDMA system and 1.0 lpm by the SMPS. A silica-gel diffusion drier was used upstream of the two systems in order to maintain the relative humidity (RH) of the sampled flow at 30±3 %. The SMPS system measured the particle size distribution from 10 to 487 nm, whereas the HTDMA measured the hygroscopicity of the particles having dry diameters from 50 to 170 nm.

The HTDMA system consisted of two differential mobility analysers (DMAs; Knutson and Whitby, 1975), and a condensation particle counter (CPC, TSI Model

3022A; Stolzenburg and McMurry, 1991). The first DMA (DMA-1, TSI 3080) included a ^{85}Kr aerosol neutraliser and a closed-loop system for recirculating the sheath flow. The second DMA (DMA-2) employed a custom-made system for the sheath flow recirculation with an RH controller (cf. Biskos et al., 2006a). For each measurement, the voltage on DMA-1 was adjusted to select dry aerosol particles having mobility diameters from 50 to 170 nm. The quasi-monodisperse particles downstream of DMA-1 were conditioned within a single Nafion-tube humidity exchanger (Perma Pure Model MD-110) to a constant RH of 85 %. The size distribution of the humidified particles was then measured by DMA-2 and the CPC. The aerosol and the sheath flows for both DMAs were 0.3 and 3.0 lpm, respectively.

The RH and temperature of the aerosol flow downstream the humidity exchanger and of the sheath flow in DMA-2 were measured by two humidity/temperature sensors (Rotronic Model SC-05). A proportional-integral-derivative (PID) controller was used to control the RH in both flows by adjusting the flow of a parallel stream of very high RH (ca. 100 %) on the outer annulus of each Nafion-tube humidity exchanger. The overall performance of the HTDMA was tested with ammonium sulfate and sodium chloride particles produced by atomisation. The uncertainty of the particle size measurements by the system was less than 1 % whereas RH variations were within less than 2 % of the set point.

2.2. Data Analysis

2.2.1. SMPS Measurements

The inversion of the SMPS measurements was performed using the Aerosol Instrument Manager software (AIM, TSI version 6.0), including correction for multiply charged particles. The inverted particle-number size distributions were then analyzed using a curve-fitting algorithm similar to that described in Hussein et al. (2005). This algorithm employed the least squares method to fit the sum of up to three lognormal distributions to the measurements. The first lognormal distribution corresponded to particles having a geometric mean mobility diameter from 10.0 to 25.0 nm (nucleation mode), the second from 25.1 to 90.0 nm (Aitken mode), and third from 90.1 to 500.0 nm

(accumulation mode). The geometric standard deviation of each lognormal distribution was allowed to vary between 1.2 and 2.1. The algorithm starts by fitting a tri-modal lognormal distribution to the measurements, and successively tests the possibility of reducing it to a bi- or to a uni-modal distribution based on the estimated number concentration of each mode, the geometric mean diameter, and the geometric standard deviation of the neighbouring modes.

2.2.2. HTDMA Measurements

The hygroscopic growth factor, g, determined by the HTDMA measurements is given by

$$g(\mathrm{RH})=\frac{d_m(\mathrm{RH})}{d_{m,dry}}, \quad (1)$$

where d_m(RH) and $d_{m,dry}$ are the geometric mean mobility diameters of the sampled particles at the hydrated state (i.e., RH = 85%) measured by DMA-2 and the CPC, and at the dry state, i.e., the mobility diameter selected by DMA-1, respectively. The RH at the inlet of DMA-1 varied between 27 and 33%, having an average value of 30% during the entire period of the measurements. As a result the measured growth factor can be more accurately expressed as

$$g(85\%|30\%)=\frac{d_m(85\%)}{d_m(30\%)}. \quad (2)$$

Here d_m(30%) is the nominal mobility diameter of the particles selected by DMA-1, and d_m(85%) is the mobility diameter measured by DMA-2 and the CPC of the HTDMA system.

Internally mixed monodisperse particles of uniform chemical composition will grow to the same size when subjected to identical RH conditions downstream of DMA-1. In this case, the size distribution of the humidified monodisperse particles can exhibit a single mode that is significantly broadened compared to that of the dry sample, or distinct monodisperse modes, depending on the hygroscopic variability of the particles.

To distinguish between modes that may correspond to different particle populations in a systematic way we employed the TDMAfit algorithm (Stolzenburg and McMurry, 1998) for inverting the HTDMA measurements. The algorithm uses the least

squares method to fit Gaussian-shaped transfer functions to the measured response of the system. To locate the peak positions and the associated concentrations that give the best fit, the algorithm employs a search routine that is based on a number of convergence criteria and constrains. When a chi-square function of the fit residual changes by less than 0.1% and each of the fitted parameters alters by less than 10% of its respective estimated uncertainty, the TDMAfit is considered to have converged to the best fit. Measurements inverted also by the TDMAinv algorithm developed by Gysel et al. (2009) gave hygroscopic growth factors that agreed within less than ±2.5 % with those calculated by TDMAfit.

For the analysis of the HTDMA measurements, we assumed that all the particles have a spherical shape when selected by DMA-1, and that particle shrinkage due to the presence of volatile species, (e.g. ammonium nitrate) was negligible. Under these assumptions, the measured hygroscopic growth factors less than 1.0, comprising ca. 3 % of all the measurements, were excluded.

2.2.3. Determining hygroscopic growth factors from the AMS measurements

The hygroscopic growth factor of internally mixed particles, g_{mix}, can be estimated using the AMS measurements as (Kreidenweis et al., 2008)

$$g_{mix}\,(\mathrm{RH}) = \left(1 + \kappa_{mix}\left(\frac{a_w}{1-a_w}\right)\right)^{1/3}, \qquad (3)$$

where a_{w} is the water activity of the solution droplet, which neglecting the Kelvin effect is equal to RH/100, and κ_{mix} is the hygroscopic parameter of the mixed particles given by

$$\kappa_{mix} = \sum_i \varepsilon_i \kappa_i. \qquad (4)$$

Here $\varepsilon_i = V_{si}/V_{\mathrm{s}}$ and κ_i are the volume fraction and the hygroscopic parameter of the *i*th chemical species of the particles, with V_{si} being the volume occupied by that species, and V_s the dry volume of the particle.

To estimate the volume fractions of each species of the particles from the cTOF-AMS measurements we first determined the molar fractions of the ions and the then those of the chemical compounds comprising the particles using the ion pairing algorithm proposed by Pilinis et al. (1987) and later simplified by Gysel et al. (2007). In this

simplified algorithm by setting the fraction of nitric acid to zero, the molar fraction of ammonium nitrate is equal to the molar fraction of nitrate ions. The rest of the ammonium ions are assigned to the sulfate ions, and depending on the ammonium to sulfate ratio, the molar fractions of sulfuric acid, ammonium bisulfate and ammonium sulfate are determined. To convert the mole fractions to volume fraction we used the bulk densities for every chemical species as summarized in Table 1 (Duplissy et al., 2011). The respective hygroscopic parameters are also shown in Table 1 (Petters and Kreidenweis, 2007). For the organic compounds commonly present in atmospheric particles, the density, ρ_{org}, and hygroscopic parameter, κ_{org}, can vary from 1200 to 1700 kg m^{-3} (Hallquist et al., 2009), and from 0.0 to 0.2 (Petters and Kreidenweis, 2007), respectively.

Table 1. *Hygroscopic parameters k* and densities used in the k-Köhler theory (Eq. 3).

Chemical species	κ	Density (kg m^{-3})
$(NH_4)_2SO_4$	0.53[a]	1769[b]
NH_4HSO_4	0.56[a]	1720[b]
NH_4NO_3	0.68[a]	1780[b]
H_2SO_4	0.97[d]	1830[b]
Organics	0.00-0.20[b]	1200-1700[c]

[a] Petters and Kreidenweis (2007);

[b]Duplissy et al. (2011);

[c]Hallquist et al. (2009);

[d]Biskos et al. (2009).

3. Results and Discussion

The prevailing synoptic conditions during the entire period of the measurements correspond mainly to north easterlies surface winds over the Aegean Sea, being

associated with a large-scale surface anticyclone. From 30 August to 3 September, however, the wind speeds were substantially lower with northwesterly directions. In particular, during the flight performed on 1 September (flight b637), a large-scale surface anticyclone prevailed over southeastern Europe, producing fair weather conditions and a moderate flow from the north-east sector over the Aegean Sea. During the flight performed on 4 September (flight b641), the low pressure pattern that prevailed over southeastern Europe, in combination with the anticyclone over Balkans, resulted in a strong channelled surface-wind flow over the Aegean Sea. Average wind speeds of up to 20 m s^{-1} were measured at altitudes 150 m a.s.l, but diminished above 4.5 km. When the aircraft flew in the vicinity of the station on Lemnos, the surface winds were from southwest direction and lower than 5 m s^{-1} during the first flight, and from northeast directions with speeds ranging from 9.5 to 13 m s^{-1} during the second flight. The surface temperature and RH at the ground station on Lemnos during the two missed approaches were 28 and 21˚C, and 45 and 75 %, respectively. For the entire period of the measurements, the surface temperature and the RH at the ground station ranged from 17.7 to 29.6 ˚C and from 16 to 87 %, respectively.

3.1. Measurements in the Atmosphere over the Ground Station

As described in Sect. 2.1, the size distributions and the hygroscopicities of the particles were continuously measured at the ground station during the entire period of the campaign. During each flight, the FAAM BAe146 aircraft flew in the vicinity of the ground station (i.e. ±300 m above or below the station and within a radius of 30 km) for approximately 10 to 15 min. The measurements performed by the airborne cToF-AMS during these two time windows were used to check the closure between hygroscopicity and chemical composition measurements. The following paragraphs provide an overview of the ground-based measurements and the closure study.

3.1.1. Particle Size Distributions

The evolution of the 1 h averaged particle size distributions measured by the SMPS, together with time series of the number concentration of particles having dry mobility diameter in the ranges of 50–80, 80–100 and 100–170 nm, for all the days of the

experiment are shown in Fig. 2. The total number concentration of the particles having diameters from 10 to 487 nm varied from ca. 4×10^2 to 1.0×10^4 particles cm^{-3} with median value of 1.9×10^3. Almost 72.1% of the samples exhibited bi-modal distributions, whereas 12.4% and 13.7% of them showed uni-modal and tri-modal distributions, respectively. The total particle number concentration in the nucleation mode varied from 1.7×10^2 to 3.2×10^3 particles cm^{-3}, with a median value of 7.7×10^2, in the Aitken mode 1.7×10^2 to 7.1×10^3 particles cm^{-3}, with a median value of 1.0×10^3, and in the accumulation mode from 1.8×10^2 to 3.4×10^3 particles cm^{-3}, with a median value of 9.9×10^2. Most often the particles were observed in the Aitken and the accumulation modes during the entire period of the measurements. Particle size distribution measurements over the region of the Aegean Sea are only available for the station of Finokalia on Crete (Pikridas et al., 2010). According to that study, the average total number concentration of particles having mobility diameters from 10 to 500 nm was ca. 2.7×10^3 particles cm^{-3}, which is very similar to the concentrations measured on Lemnos. From 30 August to 3 September, the majority of the particles resided in the accumulation and the Aitken modes. The rest of the period was characterised by wider size distributions with particles residing also in the nucleation mode (i.e. particles having diameter smaller than 25 nm). This pattern is well correlated with the variability in the origin of the air masses arriving at the station (cf. discussion in Sect. 3.2 and back-trajectory calculations shown in Fig. S1).

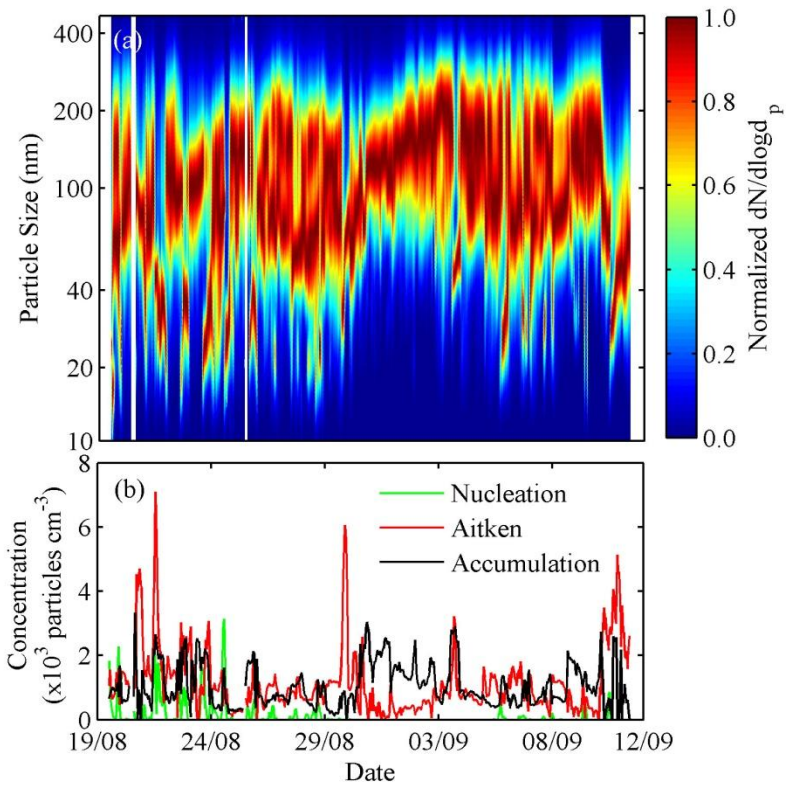

Fig. 2. Evolution of normalised, hourly averaged size distributions of particles having dry mobility diameters from 10 to 487 nm (**a**), and temporal variation of the respective number concentration of particles residing in the nucleation, Aitken and accumulation modes (**b**) throughout the whole period of the Aegean-Game field campaign.

3.1.2. Particle Hygroscopicity

Characteristic raw measurements by the ground-based HTDMA are shown in Fig. 3. The recorded size distributions correspond to particles having dry mobility diameters (i.e. diameters selected by DMA-1) of 70, 90, and 150 nm after being exposed to 85 % RH. The respective hygroscopic growth factors g(85%|30%) of those samples are 1.22, 1.22, and 1.21. In almost all the HTDMA measurements, the geometric standard deviation of the size distribution of the humidified particles was similar to that of the dry ones, indicating that the samples were internally mixed. This is expected in remote areas with no major local anthropogenic particle sources.

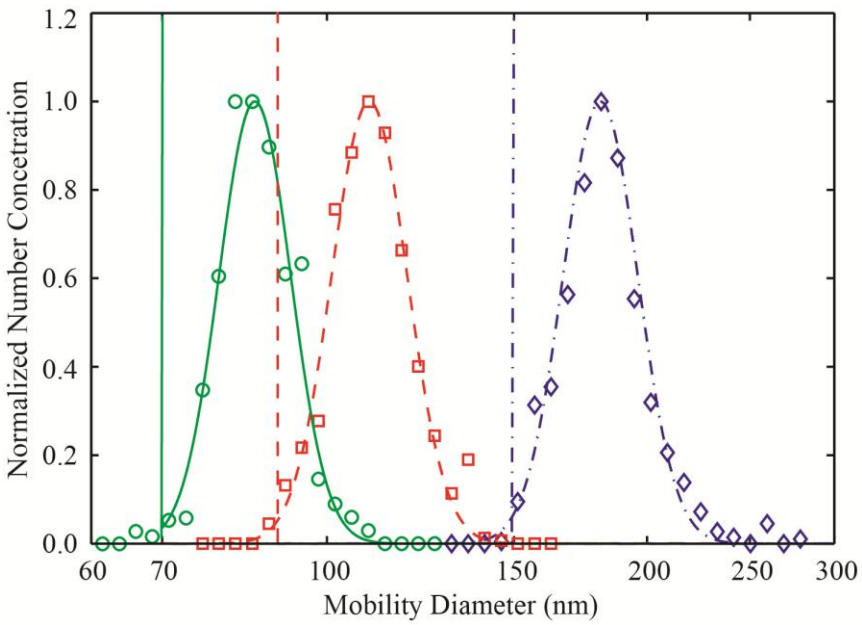

Fig. 3. Size distribution measurements of the humidified monodisperse particle samples recorded by the HTDMA system. Particles having dry mobility diameters of 70 (green), 90 (red), and 150 nm (blue) selected by DMA-1 at 30±3 % RH were exposed to 85 % RH and measured by DMA-2 and the CPC. Symbols represent the actual measurements and lines the fitted curves determined by the TDMAFIT algorithm. One hygroscopic mode is observed in all the measurements, corresponding to growth factors of 1.22, 1.22 and 1.21, for the 70-, 90- and 150-nm dry particles, respectively.

Figure 4 shows the hygroscopic growth factors $g(85\%|30\%)$ measured by the HTDMA (Fig. 4a) together with the measured (SMPS data) number concentrations of the particles having dry diameters in the ranges selected by DMA-1 (Fig. 4b) during the entire period of the campaign. The measurements are grouped in three different classes depending on the dry mobility diameters selected by DMA-1: green circles and curve correspond to measurements of particles having dry mobility diameter from 50 to 80 nm, red squares and curve from 80 to 100 nm, and blue diamonds and curve from 100 to 170 nm. Note that although the dry diameter was selected to be close to the peak of the most dominant mode of the particle size distribution as measured by the SMPS, measurements of dry particles in other modes were randomly sampled to investigate potential differences in their hygroscopicity. For the Aitken (19 % of the samples) and accumulation (81 % of the samples) mode particles, the average growth factors were 1.18 (ranging from 1.00 to 1.56) and 1.21 (ranging from 1.00 to 1.59), respectively. The

average growth factor for all particle sizes was 1.20, having a minimum value of 1.00 and a maximum of 1.59. Periods with particles of high (from 25 to 30 August), low (from 30 August to 2 September) and moderate (from 2 to 9 September) variation in the growth factor can be identified in the HTDMA measurements. This difference is well correlated with the variability in the origin of the air masses arriving at the station. During the days with the low variation in particle hygroscopicity, the air masses reaching the station had almost the same origin (i.e. the Black Sea), as indicated in Fig. S1 in the Supplement.

Although the selected dry diameters correspond to different periods during the campaign, they exhibit very similar growth factors when comparing nearby measurements. Considering also that the variability and the average growth factors corresponding to particles having different dry diameters are also very similar, in most of the cases, suggests that there is no noticeable variation of chemical composition as a function of particles size. It should also be pointed out that the selected dry particles had diameters in the range from 50 to 170 nm, within which the contribution of the Kelvin effect to the hygroscopic growth of the particles is negligible (Biskos et al., 2006b; Park et al., 2009).

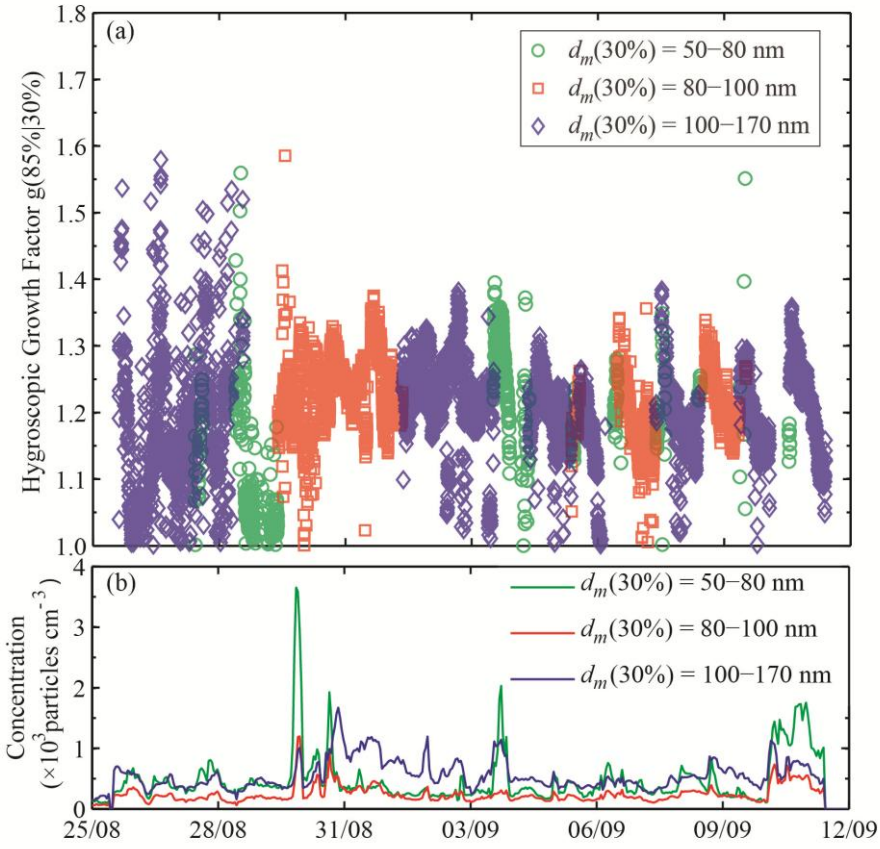

Fig. 4. Time series of the hygroscopic growth factors of atmospheric aerosol particles measured with the HTDMA (**a**) and number concentrations of the particles having dry mobility diameters in the ranges sampled by the HTDMA (**b**) at the ground station on Lemnos Island. Aerosol particles are grouped in three different regions based on their dry mobility diameters: from 50 to 80 nm (green circles and curve), from 80 to 100 nm (red squares and curve), and from 100 to 170 nm (blue diamonds and curve).

The average hygroscopic growth factor measured in our work is ca. 12 % lower compared to those reported by Stock et al. (2011), who also employed an HTDMA system at Finokalia, on the island of Crete, from 12 August to 20 October 2005. The hygroscopic growth factors of particles having dry diameters 50, 80, and 150 nm observed during that study ranged from 1.12 (nearly hydrophobic particles) to 1.59 (more hygroscopic particles). Considering that those HTDMA measurements were conducted at 90 % RH using the κ-Köhler theory (i.e. Eqs. 3 and 4), we calculate the corresponding growth factors at 85 % RH to be in the range from 1.08 to 1.43. Although this range is

similar to that observed in our study, the occurrence frequency of the more hygroscopic particles reported by Stock et al. (2011) was significantly higher (of the order of 84 to 90 %) compared to that in our study (i.e. ca. 35 %).

3.1.3. Particle Chemical Composition and Hygroscopicity

Figure 5 shows the chemical composition of the atmospheric particles when the aircraft was flying within a 30 km radius from the ground station and between 100 and 700 m altitude (i.e., ca. ± 300 m from the altitude of the ground station). The reported volume fractions are estimated by applying the ion pairing algorithm (cf. sect. 2.2.3) to the cTOF-AMS measurements. The organic species comprised almost 50% of the total particle dry volume, whereas ammonium sulfate and ammonium bisulfate accounted for the rest. Although the volume fraction of the organic species was similar during both days, the inorganic fraction of the particles was more acidic during the flight on 1 September (Fig. 5a). Considering that during both flights the chemical composition of the particles did not show high variability with size (data not shown), the cToF-AMS measurements can be considered as representative for the entire particle size range and therefore can be used to predict the hygroscopic growth of the particles using the κ-Köhler theory.

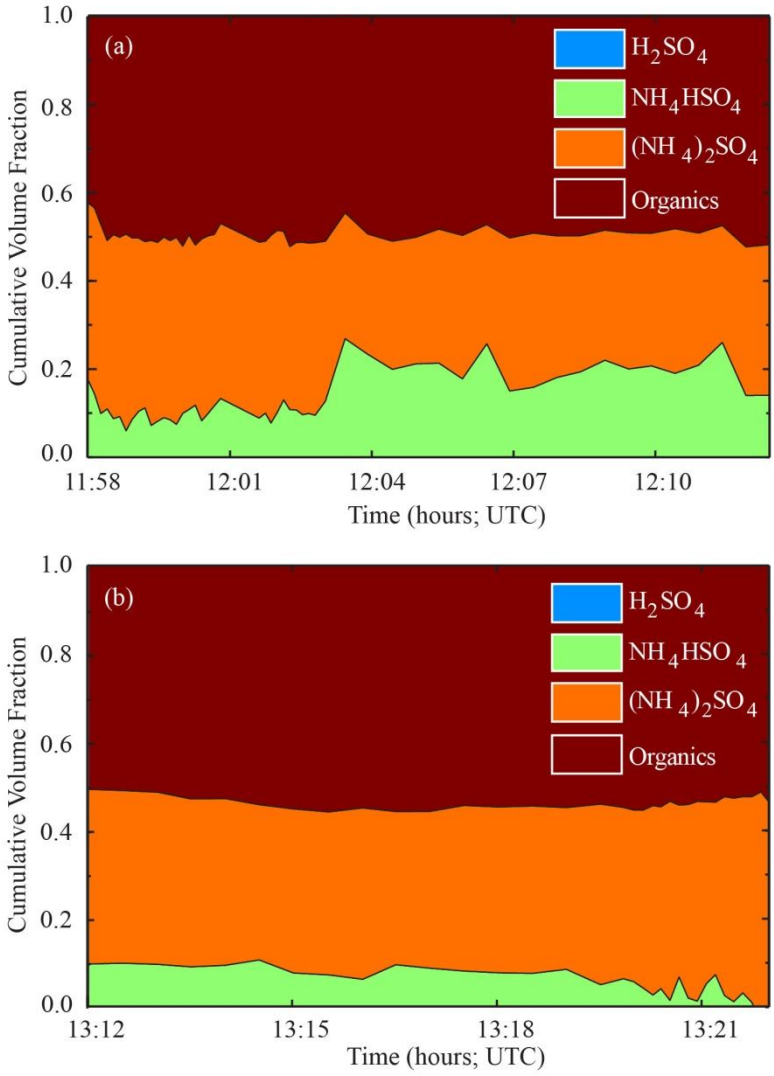

Fig. 5. Cumulative volume fractions of the chemical species comprising the particles in the atmosphere over the ground station on Lemnos Island during the flights performed on 1 September (flight b637) (**a**) and on 4 September (flight b641) (**b**). The volume fractions are estimated by the ion pairing algorithm and the chemical composition measurements from the airborne cToF-AMS.

The comparison between predicted (i.e. using Eqs. (3) and (4) and the cToF-AMS measurements) and measured (i.e. using Eq. (2) and the HTDMA measurements) hygroscopic growth factors is shown in Fig. 6. The particles measured by the HTDMA had dry mobility diameters of 100 nm. To account for the fact that the relative humidity of the dry sample was 30 %, and therefore the particles entering the HTDMA may have

already had some water due to their acidity (cf. Biskos et al. 2009; Engelhaart et al. 2011), and/or their organic content (c.f. Marcolli et al., 2004), we calculate the absolute growth factor at 85% RH as

$$g(85\%)=\frac{d_m(85\%)}{d_{m,dry}}=\frac{d_m(30\%)}{d_{m,dry}}\times\frac{d_m(85\%)}{d_m(30\%)}=g(30\%)\times g(85\%|30\%). \quad (5)$$

Here $g(85\%|30\%)$ is the measured growth factor (cf. Eq. 2), and $g(30\%)$ is the growth factor of the particles entering the HTDMA at 30% RH. The latter is estimated using the κ-Köhler theory and the composition measurements provided by the cTOF-AMS. The estimated $g(30\%)$ values varied from 1.03 to 1.06 during the specific measurements.

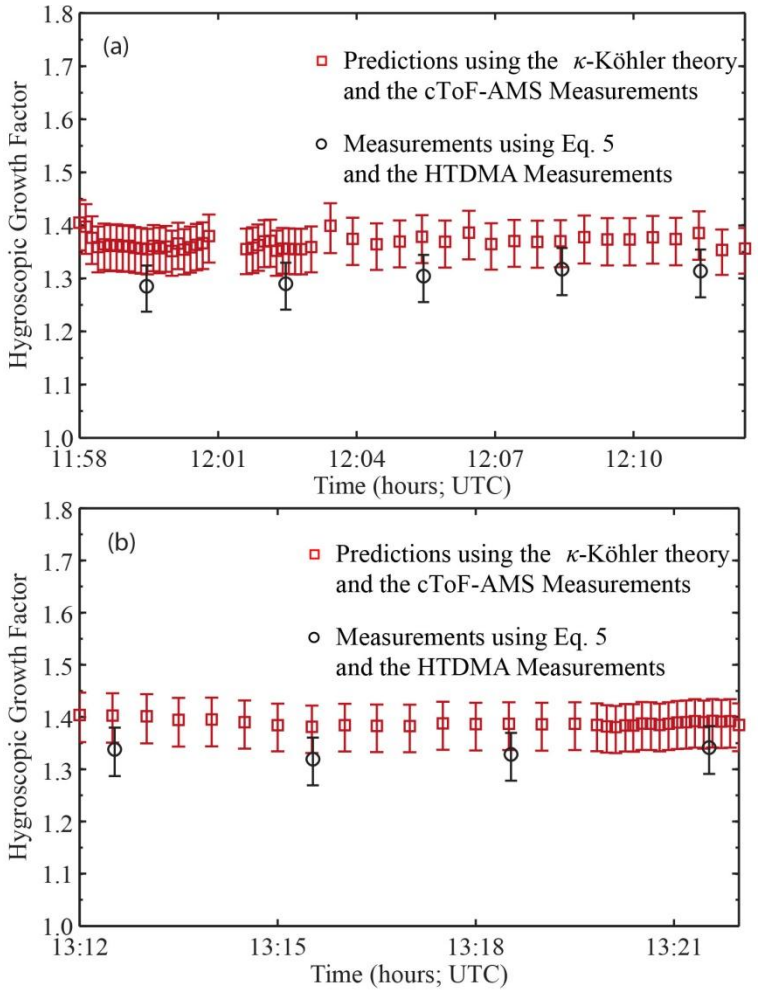

Fig. 6. Hygroscopic growth factors measured by the HTDMA (black dots) and predicted by κ-Köhler

theory using the chemical composition measurements from the airborne cToF-AMS (red squares) when the aircraft was flying close to Vigla station on 1 (flight b637) September 2011 (**a**) and on 4 (flight b641) (**b**) September 2011. The HTDMA growth factors correspond to particles having dry mobility diameter of 100 nm, whereas the chemical composition corresponds to particles having Vacuum Aerodynamic Diameters (VADs) in the range 50–700 nm. Error bars represent the 2 % uncertainty in the RH measurements.

For the predicted growth factors shown in Fig. 6, we used the fixed κ and ρ values for the inorganic species shown in Table 1. The values of κ_{org} and ρ_{org} were determined as follows. By keeping κ_{org} = 1200 kg m^{-3} (i.e. the lowest density of organic species as indicated from the literature; cf. Hallquist et al., 2009), we increased κ_{org} from 0 up to the value that the predicted hygroscopic growth factors agreed with the measured ones within 5 %. In a similar manner, we increased ρ_{org} from 1200 kg m^{-3} by keeping κ_{org} = 0. From the resulting ranges of κ_{org} and ρ_{org}, we used the mean values as the most representative for each day. Following this procedure we estimated κ_{org} = 0.03 and ρ_{org} = 1300 kg m^{-3} during the flight on 1 September, and κ_{org} = 0.1 and ρ_{org} = 1400 kg m^{-3} during the flight on 4 September. Evidently, the organic fraction of the particles observed during the closure on 4 September was more hygroscopic and slightly more dense compared to that on 1 September. In either case, the organic fraction of the particles was far less hygroscopic than the inorganic fraction, resulting in a reduction of the amount of water they could uptake as compared to their pure inorganic counterparts.

3.2. Measurements in the Atmosphere over the Aegean Sea

In the paragraphs that follow we provide an overview of the cToF-AMS chemical composition measurements conducted over the Aegean Sea during the two flights of the campaign, and employ them to predict the representative hygroscopic parameter of the particles using the κ-Köhler theory.

3.2.1. Particle Chemical Composition

The volume fractions of the compounds comprising the particles observed during the entire flights on 1 and 4 September are shown in Figs. 7 and 8, respectively. During

the flight on 1 September (data shown in Fig. 7) the volume fraction of sulfuric acid, ammonium bisulfate, and ammonium sulfate ranged from zero to 0.86 with a median value of zero; from zero to 0.66 with a median value of 0.22, and from zero to 1.00 with a median value of 0.31; respectively. In two of the four vertical paths of the flight (i.e. above the central Aegean Sea and above the island of Lemnos), the acidity of the particles appeared to increase with increasing height, indicating that the concentration of ammonia was very low at high altitudes, as had been observed in other regions (e.g. Spengler et al., 1990). The volume fraction of ammonium sulfate was almost zero at lower altitudes, rising to 0.5 at 2.5 km a.s.l. This pattern was inverted in the two vertical paths above Crete. The volume fractions of ammonium bisulfate in this case were high at lower altitudes (<700 m a.s.l.) and, with the exception of a couple of points (one around 2.0 and one 3.7 km a.s.l.), decreased with increasing height. In all cases, the concentration of H_2SO_4 was almost zero for the entire flight, with the exception of a few measurements higher than 4.0 km a.s.l. over Crete.

As shown by back trajectory calculations (cf. Fig. S2), low-altitude air masses arriving over the north or central Aegean Sea originated from eastern Europe and the wider Black Sea region. These air masses appeared to carry particles of very low acidity, as shown in Fig. 7. The low-altitude air masses arriving over Crete, on the other hand, originated either from the marine environment or from the mainland, but in both cases they passed over the wider Athens region. This can explain the high acidity of the particles observed at lower altitudes in that area. Acidic particles formed or directly emitted from anthropogenic activities in the region of Athens travelled over the central Aegean Sea towards Crete. The acidity of these particles did not change significantly during advection as a result of the low concentrations of ammonia over the marine environment (Clarisse et al., 2009). Acidic particles coming from eastern Europe (i.e. those arriving over the north Aegean Sea) have a greater chance of being neutralised due to the higher concentration of ammonia over the mainland.

The organic volume fraction of the particles observed during the flight conducted on 1 September ranged from zero to 0.74, with a median value of 0.46. Their vertical variability during all four vertical parts of the flight was similar, starting with low values at the lower altitudes, increasing at intermediated heights and decreasing again at even

higher levels. The height of the layers with particles of high organic fractions differed from place to place, with the highest layer observed over the central Aegean Sea. Considering that the air masses arriving over Lemnos and the central Aegean Sea during the respective missed approaches have passed over urban, rural and marine environments, and that their origin was similar (i.e. from eastern Europe), the organic fraction of the particles could be either biogenic or anthropogenic.

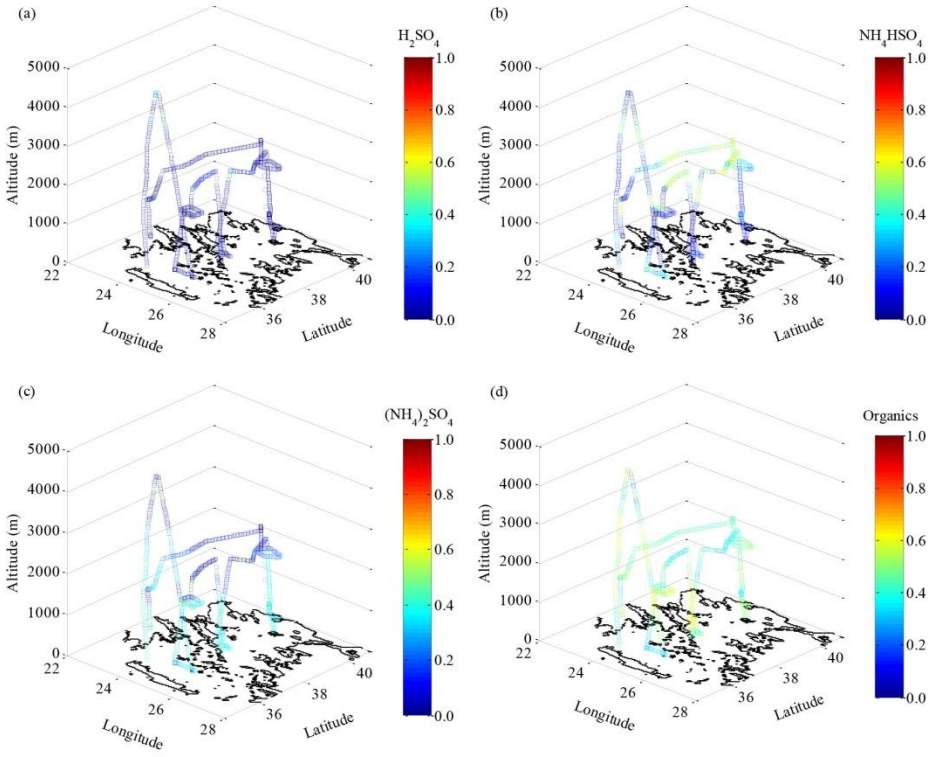

Fig. 7. Composition of the non-refractory compounds measured by the cToF-AMS during the flight performed on 1 September 2011 (flight b637) over the Aegean Sea. The reported volume fractions for H_2SO_4 (**a**), NH_4HSO_4 (**b**), $(NH_4)_2SO_4$ (**c**) and organic matter (**d**) are estimated using the mole fractions determined by the cToF-AMS measurements and the simplified ion pairing algorithm proposed by Gysel et al. (2007).

The chemical composition of the particles observed during the flight on 4 September is shown in Fig. 8. During that flight the aircraft flew at lower altitudes from Crete to Lemnos (eastern leg of the flight) and at higher altitudes from Lemnos to Crete

(western leg of the flight). Three of the four vertical parts of the flight in this case ended at substantially higher altitudes (ca. 4.0 km a.s.l.) compared to those of the first one. The vertical part of the flight over the central Aegean Sea was limited to ca. 1.0 km. The volume fraction of sulfuric acid, ammonium bisulfate, and ammonium sulfate ranged from zero to 0.79, with a median value of zero; from zero to 0.69, with a median value of 0.10; and from zero to 0.97, with a median value of 0.35; respectively. Similarly to the measurements recorded during the flight on 1 September, particle acidity increased with increasing altitude. In this case, however, the particles observed at ca. 2.5 km a.s.l. (i.e. similar to the altitude of the eastern leg of the first flight) were even more acidic, having a H_2SO_4 volume fraction that reached values as high as ca. 0.4. High volume fractions of NH_4HSO_4 were observed at a layer between 1.0 and 2.0 km a.s.l. over the west/northwest of Crete.

The respective fractions for the organic compounds of the particles during the flight conducted on 4 September ranged from 0.03 to 0.84, with a median value of 0.48. An increasing particle organic content is observed with increasing altitude, having median volume fractions of 0.44 and 0.54 for altitudes below and above 2.0 km, respectively. Compared to the flight on 1 September, the vertical distributions of the second flight (i.e. 4 September) exhibited a higher uniformity. This can be explained by the fact that the air masses arriving in many regions over the study area all originated from central/western Europe and followed similar paths (cf. Fig. S3 in the Supplement).

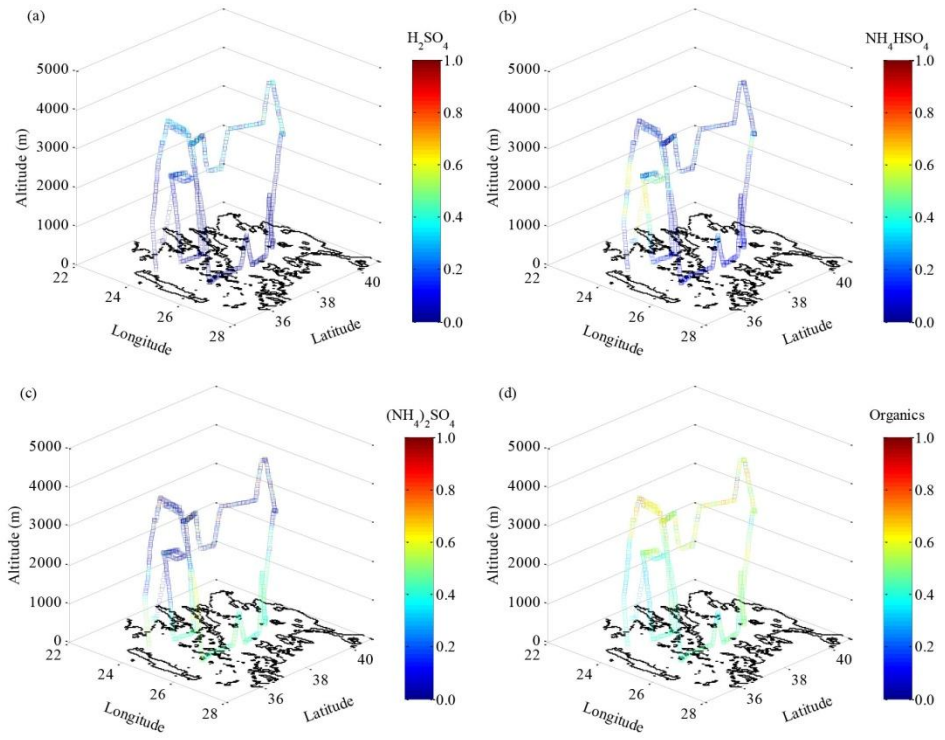

Fig. 8. Composition of the non-refractory compounds measured by the cToF-AMS during the flight performed on 4 September 2011 (flight b641) over the Aegean Sea. The reported volume fractions for H_2SO_4 (**a**), NH_4HSO_4 (**b**), $(NH_4)_2SO_4$ (**c**) and organic matter (**d**) are estimated using the mole fractions determined by the cToF-AMS measurements and the simplified ion pairing algorithm proposed by Gysel et al. (2007).

3.2.2. Particle Hygroscopicity

Using the bulk chemical composition measurements discussed above, we calculated vertical profiles of the aerosol hygroscopic parameter κ_{mix} (Eq. 4) during the two flights (cf. Figs. 9 and 10). For these calculations we used the hygroscopic parameters and the densities of the organic fraction of the particles derived from the closure study (i.e. $\kappa_{org} = 0.03$, $\rho_{org} = 1300$ kg m^{-3} and $\kappa_{org} = 0.1$, $\rho_{org} = 1400$ kg m^{-3} for the flights conducted on 1 and 4 September, respectively; cf. Sect. 3.1.3 and Fig. 6), and assumed that all the samples were internally mixed. During the flight on 1 September (Fig. 9), the hygroscopic parameter ranged from 0.19 to 0.84, with a median value of 0.31. The hygroscopic parameter κ_{mix} within the MABL (i.e. up to 1 km a.s.l.) exhibited a decreasing trend with increasing altitude over the southern and central Aegean Sea (Fig. 9a–c). At higher altitudes κ_{mix} showed a noticeably higher variability, with values ranging

from 0.21 at lower altitudes to 0.84 at altitudes above 4 km where the particles were highly acidic. The vertical variability of κ_{mix} over the northern Aegean Sea was significantly lower, having values that ranged from 0.19 to 0.38. Overall, the hygroscopic parameter κ_{mix} below the MABL was higher over the southern Aegean sea due to the influence of air masses arriving from the wider Athens region, as described in Sect. 3.2.1.

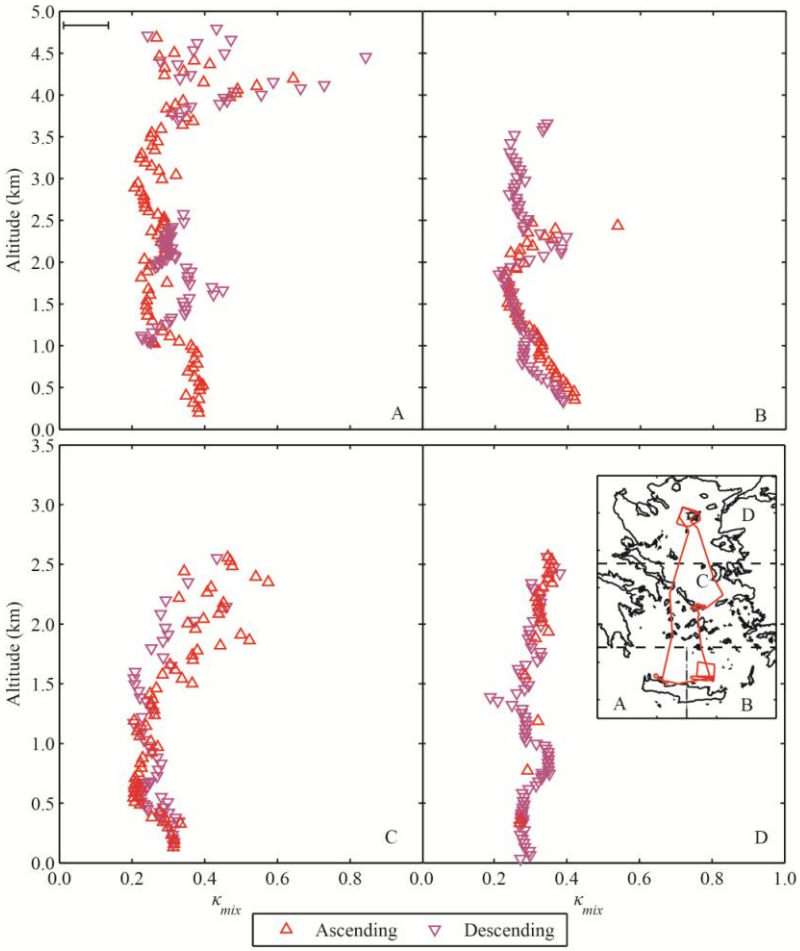

Fig. 9. Vertical profiles of the estimated hygroscopic parameters κ_{mix} of aerosol particles observed over southwestern (**a**) southeastern (**b**), central (**c**) and northern (**d**) Aegean Sea, during ascends (up triangles) and descends (down triangles) performed on the flight of 1 September 2011 (flight b637). The inset shows the locations corresponding to the vertical profiles of κ_{mix} shown in the different subplots. The hygroscopic parameters are calculated using the κ-Köhler theory (Eq. 3) and the bulk chemical composition measurements from the airborne cToF-AMS. For the calculations we assumed that the particles were internally mixed, and that all the organic species had κ_{org} = 0.03 and ρ_{org} = 1300 kg m^{-3}. The error bar represents the spread of the estimated κmix values when adopting the level of uncertainty used in our closure study.

The vertical profiles of the hygroscopic parameters predicted for the flight on 4 September are shown in Fig. 10. In this case, the calculated κ_{mix} values ranged from 0.22 to 0.80, with a median value of 0.36, which is comparable to that calculated for the first flight. However, the vertical variability of κ_{mix} for altitudes even up to 2–3 km was significantly lower compared to that observed during the first flight. The median value of κ_{mix} was of the order of 0.3 for the whole region as a result of the low acidity (i.e. the inorganic fraction of the particles was mostly ammonium sulfate) and relatively low organic volume fractions of the particles. The variability of κ_{mix} was higher at higher altitudes, with values reaching up to 0.80. This increase is explained by the increasing acidity of the particles, i.e. their higher volume fraction of sulfuric acid with increasing altitude, as shown in Fig. 8a.

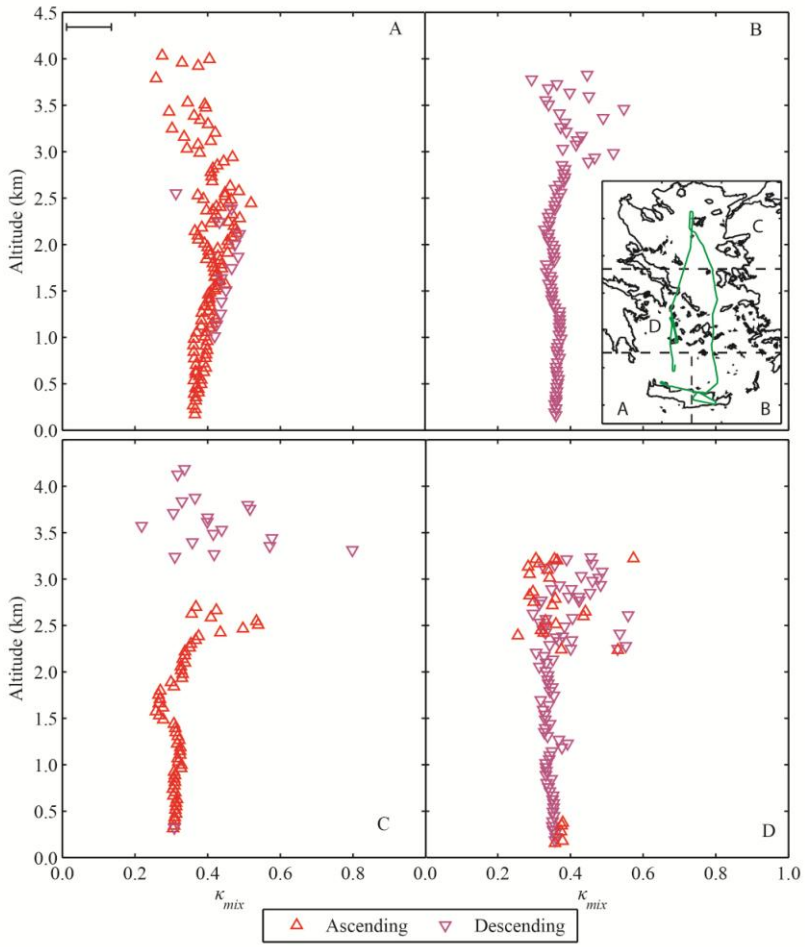

Fig. 10. Vertical profiles of the estimated hygroscopic parameters κ_{mix} of aerosol particles observed over southwestern (**a**) southeastern (**b**), central (**c**) and northern (**d**) Aegean Sea, during ascends (up triangles) and descends (down triangles) performed on the flight of 4 September 2011 (flight b641). The inset shows the locations corresponding to the vertical profiles of κ_{mix}, shown in the different subplots. The hygroscopic parameters are calculated using the κ-Köhler theory (Eq. 3) and the bulk chemical composition measurements from the airborne cToF-AMS. For the calculations we assumed that the particles were internally mixed, and that all the organic species had κ_{org} = 0.1 and ρ_{org} = 1400 kg m^{-3}. The error bar represents the spread of the estimated κ_{mix} values when adopting the level of uncertainty used in our closure study.

Despite the part that the measurements are performed in a marine environment of the Aegean Sea, the estimated median κ_{mix} values, during both flights, reside well within the range measured in urban and rural regions (Wex et al., 2010) and modelled for continental Europe (Pringle et al., 2010).

4. Conclusions

Measurements of the chemical composition and hygroscopicity of atmospheric particles were conducted over the region of the Aegean Sea using a cToF-AMS onboard the FAAM BAe-146 aircraft, and a ground-based HTDMA system located on a remote station on the island of Lemnos. The HTDMA measurements showed that the mean hygroscopic growth factor of particles having dry diameters from 50 to 170 nm was ca. 1.2, and that the aerosol samples were internally mixed during the entire period of the campaign. Good closure between cToF-AMS and HTDMA measurements was achieved when the aircraft flew in the vicinity of the ground station. For these cases, the most representative values of κ_{org} and ρ_{org} were respectively 0.03 and 1300 kg m^{-3} for the flight on 1 September (b637), and 0.10 and 1400 kg m^{-3} for the flight on 4 September (b641).

The particles observed over the wider region of the Aegean Sea during the two flights exhibited high variability in their acidity and organic volume fraction, which can be attributed to differences in the origin of the air masses arriving in the region. During the flight conducted on 1 September, the air masses arriving over the northern and central Aegean Sea had origins ranging from eastern Europe, the Black Sea, and the Balkans, while those arriving over Crete had passed near the city of Athens, transferring anthropogenic emissions. During the flight conducted on 4 September, air masses

originated mainly from western and central Europe and the wind patterns were more uniform and representative of the summer period in the region. For both flights we observed that the organic species accounted for almost 50 % of the volume of the particles, and that their acidity increased with increasing altitude. Higher spatial uniformity of the chemical composition of the particles was observed during the second flight as a result of the low variability in the origin and the paths of the air masses arriving in the region. The acidity of the particles observed during that flight was significantly high at high altitudes, exhibiting H_2SO_4 volume fractions of up to 0.4.

Using the particle parameters κ_{org} and ρ_{org} obtained from the closure study when the aircraft flew in the vicinity of the ground station, the cToF-AMS chemical composition measurements were used to estimate vertical profiles of the aerosol single hygroscopic parameter κ_{mix}. Although the median hygroscopic parameter was not significantly different for both flights (i.e. 0.31 and 0.36 during the flights on 1 and 4 September, respectively), its vertical variability was higher during the first flight. This can be explained by the high diversity in the origin of the air masses arriving in the study region, and the contribution of polluted air from the wider Athens area over the southern Aegean Sea during that flight. Despite that the measurements were performed in the marine environment of the Aegean Sea, the estimated median hygroscopic parameters were more representative of continental aerosol particles.

Acknowledgements

The airborne measurements reported in this work have been supported by the EUFAR (227159) EC grant agreement under the Aegean-Game-2 project. Airborne data were obtained using the BAe-146-301 Atmospheric Research Aircraft (ARA) flown by Directflight Ltd and managed by the Facility for Airborne Atmospheric Measurements (FAAM), which is a joint entity of the Natural Environment Research Council (NERC) and the Met Office. The ground measurements have been co-financed by the European Union (European Social Fund – ESF) and Greek national funds through the operational program "Education and Lifelong Learning" of the National Strategic Reference Framework (NSRF) – research funding program: Heracleitus II, Investing in knowledge society through the European Social Fund.

Literature Cited

Aiken, A. C., Decarlo, P. F., Kroll, J. H., Worsnop, D. R., Huffman, J. A., Docherty, K. S., Ulbrich, I. M., Mohr, C., Kimmel, J. R., Sueper, D., Sun, Y., Zhang, Q., Trimborn, A., Northway, M., Ziemann, P. J., Canagaratna, M. R., Onasch, T. B., Alfarra, M. R., Prévôt, A. S. H., Dommen, J., Duplissy, J., Metzger, A., Baltensperger, U., and Jimenez, J. L.: O/C and OM/OC ratios of primary, secondary, and ambient organic aerosols with high-resolution time-of-flight aerosol mass spectrometry, Environ. Sci. Technol., 42, 4478-4485, 2008.

Allan, J. D., Jimenez, J. L., Williams, P. I., Alfarra, M. R., Bower, K. N., Jayne, J. T., Coe, H., and Worsnop, D. R.: Quantitative sampling using an aerodyne aerosol mass spectrometer - 1. Techniques of data interpretation and error analysis", J. Geophys. Res. Atmos., 108, 4090, doi:10.1029/2002JD002358, 2003.

Allan, J. D., Coe, H., Bower, K. N., Alfarra, M. R., Delia, A. E., Jimenez, J. L., Middlebrook, A. M., Drewnick, F., Onasch, T. B., Canagaratna, M. R., Jayne, J. T., and Worsnop, D. R.: A generalised method for the extraction of chemically resolved mass spectra from aerodyne aerosol mass spectrometer data, J. Aerosol Sci., 35, 909-922, 2004.

Biskos, G., Paulsen, D., Russell, L. M., Buseck, P. R., Martin, S. T.: Prompt deliquescence and efflorescence of aerosol nanoparticles. Atmos.Chem. Phys., 6, 4633-4642, doi:10.5194/acp-6-4633-2006, 2006a.

Biskos, G., Russel, L. M., Buseck, P. R., Martin, S. T.: Nanosize effect on the hygroscopic growth factor of aerosol particles, Geoph.Res. Lett., 33, L07801 doi:10.1029/2005GL025199, 2006b.

Biskos, G., Buseck, P. R., Martin, S. T.: Hygroscopic Growth of Nucleation-mode Acidic Sulfate Particles, J. Aerosol Sci., 40, 338-347, 2009.

Canagaratna, M. R., Jayne, J. T., Jimenez, J. L., Allan, J. D., Alfarra, M. R., Zhang, Q., Onasch, T. B., Drewnick, F., Coe, H., Middlebrook, A., Delia, A., Williams, L. R., Trimborn, A. M., Northway, M. J., DeCarlo, P. F., Kolb, C. E., Davidovits, P., and Worsnop, D. R.: Chemical and microphysical characterization of ambient aerosols with the aerodyne aerosol mass spectrometer, Mass Spectrom. Rev., 26, 185–222, 2007.

Clarisse, L., Clerbaux, C., Dentener, F., Hurtmans, D., and Coheur, P.-F.: Global ammonia distribution derived from infrared satellite observations, Nature Geosci., 2, 479–483, 2009.

Clegg, S. L., Brimblecombe, P., Wexler, A. S.: Thermodynamic Model of the System H^+-NH_4^+ - SO_4^{2-} - NO_3^- - H_2O at TroposphericTemperatures. J. Phys. Chem. A, 102, 2137–2154, 1998.

Drewnick, F., Hings, S. S., DeCarlo, P., Jayne, J. T., Gonin, M., Fuhrer, K., Weimer, S., Jimenez, J. L., Demerjian, K. L., Borrmann, S., and Worsnop, D. R.: A new time-of-flight aerosol mass spectrometer (TOF-AMS)-instrument description and first field deployment, Aerosol Sci. Tech., 39, 637-658, 2005.

Duplissy, J., DeCarlo, P. F., Dommen, J., Alfarra, M. R.: Relating hygroscopicity and composition of organic aerosol particulate matter. Atmos. Chem. Phys., 11, 1155–1165, doi:10.5194/acp-11-1155-2011, 2011.

Engelhart, G. J., Hildebrandt, L., Kostenidou, E., Mihalopoulos, N., Donahue, N. M., and Pandis, S. N.: Water Content of aged aerosol, Atmos. Chem. Phys., 11, 911–920, doi:10.5194/acp-11-911-2011, 2011.

Foltescu, V. L., Selin, E., and Below, M.: Corrections for particle losses and sizing errors during aircraft aerosol sampling using a rosemount inlet and the pms las-x, Atmos. Environ., 29, 449–453, 1995.

Gysel, M., Crosier, J., Topping, D. O., Whitehead J. D.: Closure study between chemical composition and hygroscopic growth of aerosol particles during TORCH2, Atmos. Chem. Phys., 7, 6131–6144, doi:10.5194/acp-7-6131-2007, 2007.

Gysel, M. McFiggans, G.B. Coe, H.: Inversion of tandem differential mobility analyser (TDMA) measurements, J. Aerosol Sci., 40, 134-151, 2009.

Hallquist, M., Wenger, J. C., Baltensperger, U., Rudich, Y., Simpson, D., Claeys, M., Dommen, J., Donahue, N. M., George, C., Goldstein, A. H., Hamilton, J. F., Herrmann, H., Hoffmann, T., Iinuma, Y., Jang, M., Jenkin, M. E., Jimenez, J. L., Kiendler-Scharr, A., Maenhaut, W., McFiggans, G., Mentel, Th. F., Monod, A., Prévôt, A. S. H., Seinfeld, J. H., Surratt, J. D., Szmigielski, R., Wildt, J.: The formation, properties and impact of secondary organic aerosol: current and

emerging issues, Atmos. Chem. Phys., 9, 5155–5236, doi:10.5194/acp-9-5155-2009, 2009.

Haywood, J. and Boucher, O.: Estimates of the direct and indirect radiative forcing due to tropospheric aerosols: a review, Rev. Geophys., 38, 513–543, 2000.

Heintzenberg J.: Fine particles in the global troposphere. A review , Tellus, 41B, 149-160, 1989.

Hussein, T., Maso, M. D., Petäjä, T., Koponen I. S., Paatero, P.: Evaluation of an automatic algorithm for fitting the particle number size distributions, Boreal Environ. Res., 10, 337–355, 2005.

Kalivitis, N., Birmili, W., Stock, M., Wehner, B., Massling, A., Wiedensohler, A., Gerasopoulos, E., and Mihalopoulos, N.: Particle size distributions in the Eastern Mediterranean troposphere, Atmos. Chem. Phys., 8, 6729–6738, doi:10.5194/acp-8-6729-2008, 2008.

Koulouri, E., Saarikoski, S., Theodosi, C., Markaki, Z., Gerasopoulos, E., Kouvarakis, G., Mäkelä, T., Hillamo, R., and Mihalopoulos, N.: Chemical composition and sources of fine and coarse aerosol particles in the eastern Mediterranean, Atmos. Environ., 42, 6542–6550, 2008.

Knutson, E. O. and Whitby, K. T.: Aerosol classification by electric mobility: apparatus, theory, and applications, J. Aerosol Sci., 6, 443–451, 1975.

Kreidenweis, S. M., Petters, M. D., and DeMott, P. J.: Single parameter estimates of aerosol water content, Environ. Res. Lett., 3, 035002, doi:10.1088/1748-9326/3/3/035002, 2008.

Lelieveld, J., Berresheim, H., Borrmann, S., Crutzen, P. J., Dentener, F. J., Fisher, H., Feichter, J., Flatau, P. J., Heland, J., Holzinger, R., Korrmann, R., Lawrence, M. G., Levin, Z., Markowitz, K. M., Mihalopoulos, N., Minikin, A., Ramanathan, V., de Reus, M., Roelofs, G. J., Scheeren, H. A., Sciare, J., Schlager, H., Schultz, M., Siegmund, P., Steil, B., Stephanou, E. G., Stier, P., Traub, M., Warneke, C., Williams, J., and Ziereis, H.: Global air pollution crossroads over the Mediterranean, Science, 298, 794–799, 2002.

Liu, P. S. K., Deng, R., Smith, K. A., Williams, L. R., Jayne, J. T., Canagaratna, M. R., Moore, K., Onasch, T. B., Worsnop, D. R., and Deshler, T.: Transmission

efficiency of an aerodynamic focusing lens system: comparison of model calculations and laboratory measurements for the aerodyne aerosol mass spectrometer, Aerosol Sci. Tech., 41, 721–733, 2007.

Marcolli, C., Luo, B. P. and Peter, T.: Mixing of the organic aerosol fractions: liquids as the thermodynamically stable phases, J. Phys. Chem. A, 108, 2216–2224, 2004.

Middlebrook, A. M., Bahreini, R., Jimenez, J. L., and Canagaratna, M. R.: Evaluation of composition-dependent collection efficiencies for the aerodyne aerosol mass spectrometer using field data, Aerosol Sci. Tech., 46, 258–271, 2012.

Mihalopoulos, N., Stephanou, E., Kanakidou, M., Pilitsidis, S.,Bousquet, P.: Tropospheric aerosol ionic compositionabove the Eastern Mediterranean Area, Tellus B 49B, 314–326, 1997.

Morgan, W. T., Allan, J. D., Bower, K. N., Highwood, E. J., Liu, D., McMeeking, G. R., Northway, M. J., Williams, P. I., Krejci, R., and Coe, H.: Airborne measurements of the spatial distribution of aerosol chemical composition across Europe and evolution of the organic fraction, Atmos. Chem. Phys., 10, 4065–4083, doi:10.5194/acp-10-4065-2010, 2010.

Ogren, J. and Charlson, J.: Implications for models and measurementsof chemical inhomogeneities among cloud droplets, Tellus, 44B, 489–504, 1992.

Park, K., Kim, J. S., Miller, A. L.: A study on effects of size and structure on hygroscopicity of nanoparticles using a tandem differential mobility analyzer and TEM, J. Nanopart. Res., 11,175–183, 2009.

Petters, M. D. & Kreidenweis S. M.: A single parameter representation of hygroscopic growth and cloud condensation nucleus activity, Atmos. Chem. Phys., 7, 1961–1971, doi:10.5194/acp-7-1961-2007, 2007.

Pikridas, M., Bougiatioti, A., Hildebrandt, L., Engelhart, G. J., Kostenidou, E., Mohr, C., Prévôt, A. S. H., Kouvarakis, G., Zarmpas, P., Burkhart, J. F., Lee, B.-H., Psichoudaki, M., Mihalopoulos, N., Pilinis, C., Stohl, A., Baltensperger, U., Kulmala, M., and Pandis, S. N.: The Finokalia Aerosol Measurement Experiment – 2008 (FAME-08): an overview, Atmos. Chem. Phys., 10, 6793–6806, doi:10.5194/acp-10-6793-2010, 2010.

Pilinis, C. and Seinfeld, J. H.: Continued development of a general equilibrium model for inorganic multicomponent atmospheric aerosols, Atmos. Environ., 21, 2453–2466, 1987.

Pringle, K. J., Tost, H., Pozzer, A., Pöschl, U., and Lelieveld, J.: Global distribution of the effective aerosol hygroscopicity parameter for CCN activation, Atmos. Chem. Phys., 10, 5241–5255, doi:10.5194/acp-10-5241-2010, 2010.

Rader, D. J. and McMurry, P. H.: Application of the tandem differential mobility analyzer to studies of droplet growth or evaporation, J. Aerosol Sci., 17, 771–787, 1986.

Salisbury, G., Williams, J., Holzinger, R., Gros, V., Mihalopoulos, N., Vrekoussis, M., Sarda-Estéve, R., Berresheim, H., von Kuhlmann, R., Lawrence, M., and Lelieveld, J.: Ground-based PTR-MS measurements of reactive organic compounds during the MINOS campaign in Crete, July–August 2001, Atmos. Chem. Phys., 3, 925–940, doi:10.5194/acp-3-925-2003, 2003.

Spengler, J. D., Brauer, M., and Koutrakis, P.: Acid air and health, Environ. Sci. Technol., 24, 946–955, 1990.

Stock, M., Cheng, Y. F., Birmili, W., Massling, A., Wehner, B., Müller, T., Leinert, S., Kalivitis, N., Mihalopoulos, N., and Wiedensohler, A.: Hygroscopic properties of atmospheric aerosol particles over the Eastern Mediterranean: implications for regional direct radiative forcing under clean and polluted conditions, Atmos. Chem. Phys., 11, 4251–4271, doi:10.5194/acp-11-4251-2011, 2011.

Stolzenburg, M. R. and McMurry, P. H.: TDMAFIT user's manual, Particle Technology Laboratory, Department of Mechanical Engineering, Univercity of Minnesota, Minneapolis, 1–61, 1988.

Stolzenburg, M. R. and McMurry, P. H.: An ultrafine aerosol condensation nucleus counter, Aerosol Sci. Technol., 14, 48–65,1991.

Tombrou, M., Bossioli, E., Kalogiros, J., Allan, J., Bacak, A., Biskos, G., Coe, H.,Dandou, A., Kouvarakis, G., Mihalopoulos, N., Protonotariou, A. P., Szabó-Takács, B., and Triantafillou, E.: Physical and chemical processes of polluted air masses during etesians: Aegean-Game airborne campaign – an out-line, in

advances in meteorology, climatology and atmospheric physics, Springer Atmospheric Sciences, 1239–1244, Springer Verlag Berlin Heidelberg, 2012.

Wang, C. S. and Flagan C. R.: Scanning electrical mobility spectrometer, Aerosol Sci. Technol., 13, 230–240, 1990.

Wang, X., Kruis, F. E., and McMurry, P. H.: Aerodynamic focusing of nanoparticles: I. Guidelines for designing aerodynamic lenses for nanoparticles, Aerosol Sci. Tech., 39, 611–623, 2005.

Wex, H., McFiggans, G., Henning, S., and Stratmann, F.: Influence of the external mixing state of atmospheric aerosol on derived CCN number concentrations, Geophys. Res. Lett., 37, L10805, doi:10.1029/2010GL043337, 2010.

Supplement

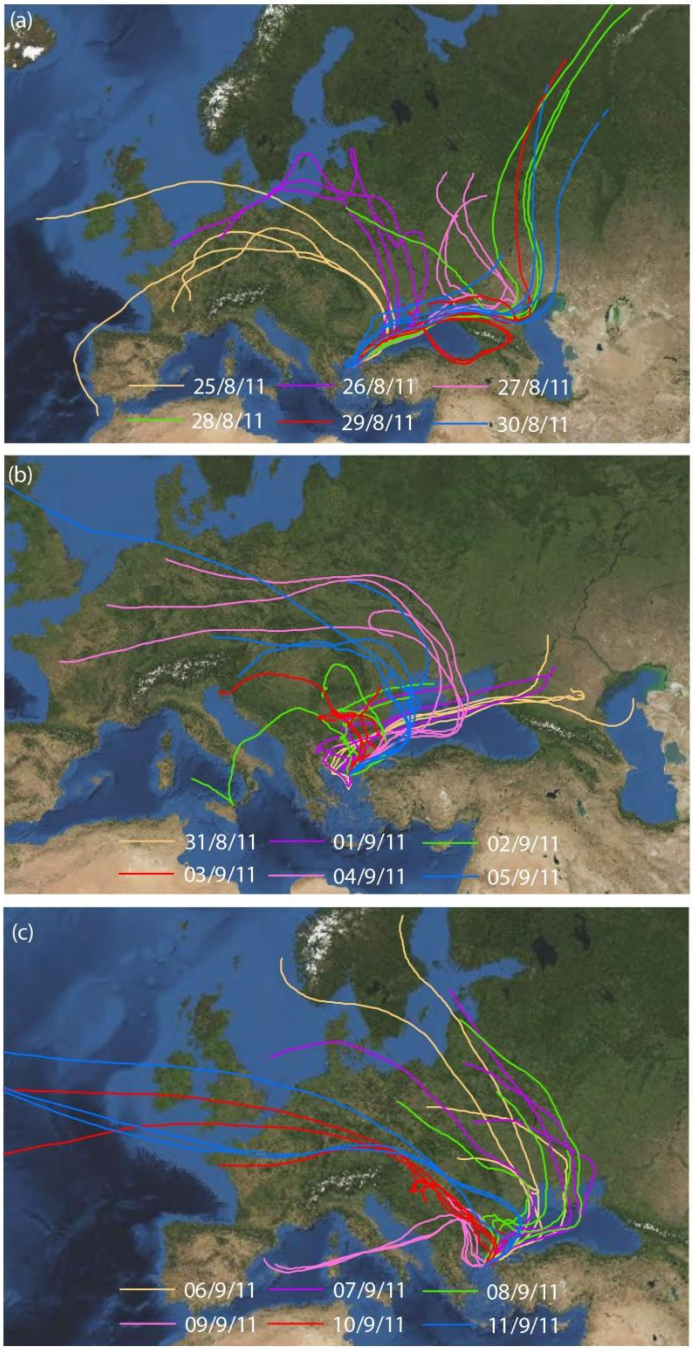

Figure S1. Wind back trajectories (120-hours long) caclulated by NOAA's HYSPLIT model for the ground station station located at Vigla on the island of Lemnos at an altitude of 420 m asl. Different colors corespond to back trajec tories arriving at the station on different dates during the field campaign.

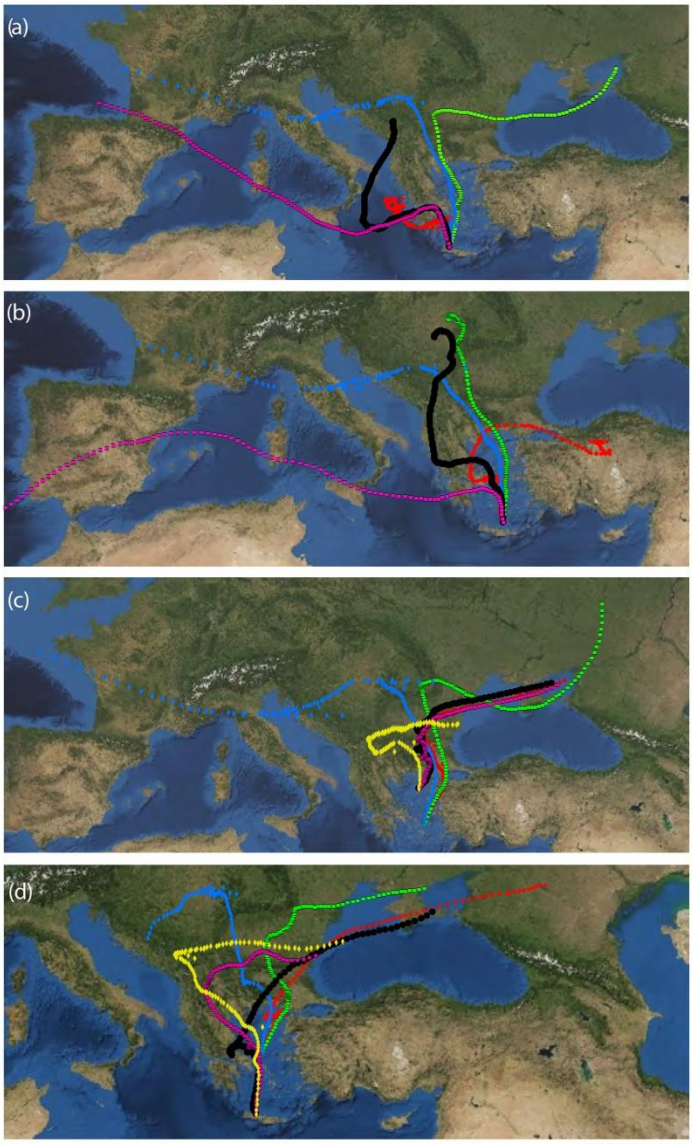

Figure S2. Wind back trajectories (120-hours long) caclulated by NOAA's HYSPLIT model for the different positions of the aircraft during the flight on the 1st of September 2011. The calculations have been performed when the aircraft was over Chania at 09:00 UTC (a), over north of Crete at 10:00 UTC (b), over the central Aegean Sea and Lemnos at 11:00 and 12:00 UTC, respectively (c), and over the central Aegean Sea and Chania on the way back at 13:00 and 14:00 UTC, respectively (d). Different colors of the trajectories correspond to different flight altitudes: 500 m (red), 1500 m (green), 2500 m (blue), 3500 m (black), and 4500 m (magenta).

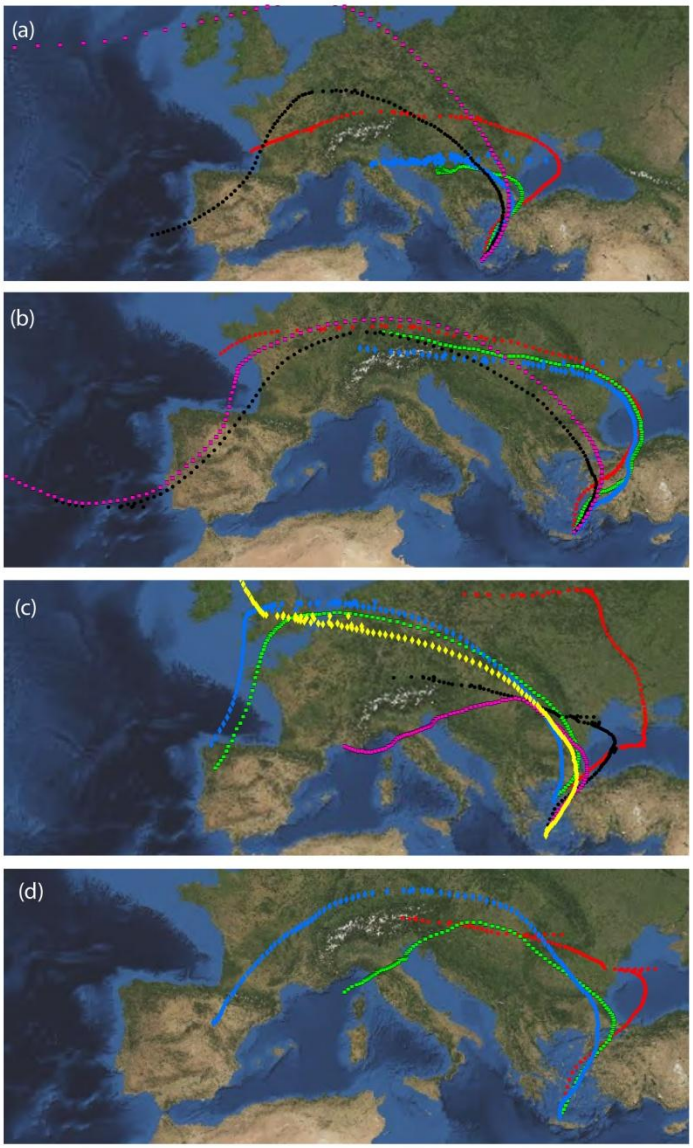

Figure S3. Wind back trajectories (120-hours long) caclulated by NOAA's HYSPLIT model for the different positions of the aircraft during the flight on the 4th of September 2011. The calculations have been performed when the aircraft was over Chania at 11:00 UTC (a), over eastern Crete at 12:00 UTC (b), over the Lemnos and northwestern of Crete at 13:00 and 14:00 UTC, respectively (c), and over Chania on the way back at 15:00 UTC, respectively (d). Different colors of the trajectories correspond to different flight altitudes: 500 m (red), 1500 m (green), 2500 m (blue), 3500 m (black), and 4500 m (magenta).

C. Hygroscopic Properties and Mixing State of Ultrafine Aerosol Particles in Urban Background Sites

Abstract

The hygroscopicity and mixing state of atmospheric ultrafine particles over suburban areas of two large cities in Greece, namely Athens and Patras, were measured using a combination of a Hygroscopic Tandem Differential Mobility Analyzer (HTDMA) and a continuous-flow streamwise-thermal-gradient Cloud Condensation Nuclei Counter (CCNC). The chemical composition of the particles was also measured using a High-Resolution Time-of-Flight Aerosol Mass Spectrometer (HR-ToF-AMS) and filter samples. Although both sites are affected by local and long range transported emissions, the measurements showed that the observed particles were more hygroscopic, more CCN active and more often externally mixed in Athens than in Patras. The frequency of externally mixed samples in both cases, was higher when long-range transported air masses passed above the city centers as indicated by wind back-trajectory calculations. Closure between HR-ToF-AMS and HTDMA/CCNC using the κ-Köhler theory indicated that the hygroscopicity of the organic fraction of the particles κ_{org} observed in Athens is higher compared to that observed in Patras and other studies conducted in eastern Mediterranean region. This can be explained by either the presence of highly hygroscopic refractory matter or of a more hygroscopic organic fraction than the one assumed in most field measurements. In both cases, however, the values obtained at sub- and super-saturation conditions exhibited systematic differences of up to 80%.

1. Introduction

Atmospheric particles scatter and absorb the incoming solar radiation, thereby affecting the radiative balance of the Earth in a direct way (Haywood and Boucher, 2000). In addition, by acting as cloud condensation nuclei (CCN) they can affect the energy balance of the planet in an indirect way (Ogren and Charlson, 1992). Both the direct and indirect effect of atmospheric particles on climate depends strongly on their size and chemical composition, as well as on the amount of water they hold at different atmospheric conditions. The later is determined by the hygroscopicity of the particles, i.e. their ability to take up water from the vapour phase when exposed to different relative humidity (RH) conditions.

Basic thermodynamic models (e.g., Clegg et al., 1998) have been developed for predicting the hygroscopic behaviour of pure or mixed inorganic particles. However, existing knowledge provides inaccurate predictions on the hygroscopicity of particles that consist of organic species or mixtures of organic and inorganic compounds. To simplify the association of particle chemical composition with hygroscopicity, Peters and Kreidenweiss (2007) proposed the use of a single hygroscopic parameter κ. Typical atmospheric soluble-salt particles such as ammonium sulphate or sodium chloride have κ values of 0.53 and 1.12, respectively, whereas those of organic compounds lie in the range between zero and 0.3 (Petters and Kreidenweiss, 2007). For completely insoluble but wettable particles, whose water activity is not affected by water adsorbed on their surface, the κ value is zero. Using the parameter κ, and information about the hygroscopic behaviour of the pure chemical species, one can make a good approximation of the water uptake characteristics of mixed atmospheric particles.

The use of a single hygroscopic parameter κ proposed by Petters and Kreidenweis has been one way for describing the hygroscopic behaviour of atmospheric aerosols in atmospheric-climate models (e.g. Liu and Wang, 2010). For the accurate consideration of aerosol microphysics processes required to improve the predictability in these models, however, observations of aerosol hygroscopicity and mixing state are needed for different regions (Pringle et al., 2010). Such measurements are available for remote environments in the region of the Aegean Sea and Eastern Mediterranean (Stock et al., 2011; Bougiatioti et al., 2009 and 2011; Bezantakos et al., 2013). However, to the best of our knowledge, the only data available for suburban environments in the broader region of Southeastern Europe and especially for the mainland of Greece are those reported by

Petäjä et al. (2007), which measured the hygroscopic growth factor of sub 50 nm particles in a suburban site close to Athens.

In this work we report measurements of the CCN activity, hygroscopicity, and mixing state of particles observed in the atmosphere over suburban areas in Patras and Athens. The measurements were conducted using a combination of one Hygroscopic Tandem Differential Mobility Analyzer (HTDMA; Rader and McMurry, 1986) and a continuous flow streamwise thermal gradient Cloud Condensation Nuclei Counter (CCNC; Roberts and Nenes, 2005). Particle chemical composition measurements were also conducted using a High-Resolution Time-Of-Flight Aerosol Mass Spectrometer (HR-ToF-AMS; DeCarlo et al., 2006) and filter samplers used to collect particles having diameters smaller than 2.5 μm ($PM_{2.5}$). The HTDMA and CCNC were coupled so that the hygroscopic behavior of dry monodisperse particles was measured simultaneously at sub- and super-saturated conditions. The mixing state of the particles was also derived by the HTDMA measurements. Closure between the HTDMA/CCNC and chemical composition measurements was used to estimate the hygroscopicity of the organic fraction of the particles.

2. Experimental

Hygroscopicity measurements at sub- and super-saturated conditions were performed from 8 to 26 June 2012 in Patras and from 4 to 26 July 2012 in Athens. Particles chemical composition was measured during the total sampling period in Patras and from 12 to 26 July 2012 in Athens. The measuring site at Patras was located at FORTH/ICE-HT (38.297º N, 21.809º E), at a height of 85 m and ca. 10 km far from the center of the city. The measuring site in Athens was located in Demokritos GAW station (37.995º N, 23.816º E), at 250 m height, having a distance of ca. 8 km from the city center. The sampling locations were influenced by particles emitted from the cities when the wind had western and south- to northwestern direction in case of Patras and Athens, respectively (cf. Fig. 1). Five-day wind back-trajectories, which were calculated on a 6-h basis using NOAA's HYSPLIT model, were employed to distinguish sub-periods during which air masses of different origin arrived at the two stations.

Fig 1. Map of Greece showing the locations of the ground stations in Patras and Athens.

2.1 Instrumentation

An HTDMA and a CCNC were used to measure the hygroscopic properties of particles in sub- and super-saturated conditions, respectively (cf. Fig. S1 in the supplement for the details). The whole system sampled air with a total flow rate of 1.8 lpm. Dried particles were selected by the first Differential Mobility Analyzer (DMA-1; TSI Model 3080; Knutsen and Whitby 1975) of the HTDMA. The closed-loop sheath flow and the monodisperse aerosol outlet flow of DMA-1 were 10.8 and 1.8 lpm, while the voltage on the central rod was changed every 6 minutes in order to select particles having mobility diameters of 60, 80, 100 and 120 nm. The aerosol flow upstream DMA-1 was dried to below 35% using a silica gel diffusion drier in Patras site, and below 15% using a dried air system and a nafion exchange membrane in Athens. A fraction (0.3 lpm) of the quasi-monodisperse flow downstream DMA-1 was passed through a nafion-tube humidity exchanger where its RH was increased to 87%, before the size distribution of the particles was measured with a second DMA (DMA-2; custom-made DMA using a closed-loop sheath flow with RH control; cf. Biskos et al., 2006a) and the Condensation Particle Counter (CPC, TSI Model 3772; Stolzenburg and McMurry, 1991). The RH in both the aerosol and the sheath flow in DMA-2 was controlled by PID controllers within a ±2% accuracy. Both DMAs in the HTDMA system were calibrated with Polystyrene Latex (PSL) spheres, while the overall performance of the HTDMA was investigated with

ammonium sulfate particles. The rest (1.5 lpm) of the quasi-monodisperse flow downstream DMA-1 was sampled by the CCNC, which was operated in a scanning flow mode (Moore and Nenes, 2009). In this mode particles were exposed to super-saturation conditions that progressively varied from 0.1 to 1.0%, allowing the rapid and continuous measurement of super-saturation spectra with high temporal resolution. A more detailed description of the specific CCNC can be found in Bougiatioti et al. (2009).

An HR-ToF-AMS and filter samplers under an impactor with cutoff diameter of 2.5 μm were used to determine the chemical composition of the particles. Details of the HR-ToF-AMS can be found in DeCarlo et al. (2006). In brief, particles are focused by an aerodynamic lens onto a heated surface, where the non refractory compounds are flash vaporized at 600^{o}C. The resulted vapours are then ionized using electron impact at 70 eV and analyzed using mass spectrometry. Particles Vacuum Aerodynamic Diameters (VADs) are determined by measuring their time of flight (ToF) between a chopper and the vaporizer surface. The AMS was deployed alternatively between V and W mode measuring 3 min in each mode. In this work the V mode data are used. The collection efficiency (CE) was calculated using the algorithm of Kostenidou et al. (2007).

The filter samples were collected daily on quartz pre-treated filters and were analyzed using ion chromatography for inorganic species of atmospheric relevance.

2.2. Data Analysis

2.2.1. HTDMA Measurements

The hygroscopic growth factor, *g*, determined by the HTDMA measurements is given by:

$$g(\mathrm{RH}) = \frac{d_m(\mathrm{RH})}{d_{\mathrm{dry}}}, \quad (1)$$

where d_m(RH) and d_{dry} are respectively the geometric mean mobility diameters of the sampled particles at the hydrated state (i.e., at RH = 87%) as measured by DMA-2 and the CPC, and at the dry state as dictated by the settings (i.e., flow rates and voltage) used in DMA-1.

Internally mixed monodisperse dry particles exposed to elevated RH conditions within the HTDMA system will grow by the same amount due to water uptake. As a result they will exhibit a unimodal size distribution when measured by DMA-2 and the CPC of the HTDMA. Externally mixed dry monodisperse particles, on the other hand,

may grow to different sizes exhibiting either a wider unimodal or a bimodal size distribution when measured by the HTDMA. The TDMAfit algorithm (Stolzenburg and McMurry, 1988) was employed for inverting the HTDMA measurements and distinguishing between internally and externally mixed aerosols (cf. Bezantakos et al., 2013). Characteristic HTDMA measurements of internally and externally mixed particles after data inversion are provided in the supplement (Fig. S2).

2.2.2. CCNC Measurements

The super-saturated conditions within the CCNC were calibrated in terms of the temperature difference between the inlet and the outlet (ΔT = 5 °C), the instantaneous flow rate and the overall flow rate range. The relationship between super-saturation and instantaneous flow rate was determined by the procedure described by Moore and Nenes (2009). According to that, size-classified ammonium sulfate particles from DMA-1 were introduced into the CCNC whose flow, the range of super-saturated conditions, was scanned. For each particle size, the critical super-saturation value $S_{c,}$ above which particles act as CCN was obtained from Köhler theory (Moore et al., 2012a). The process was repeated with five different particles sizes. The calibration measurements were fitted with sigmoidal curves where the inflection point, corresponding to the S_c of the selected ammonium sulfate particles, was used to determine the critical activation flow rate Q_{50}. The absolute uncertainty of the calibrated CCNC super-saturation is estimated to be ±0.04% (Moore et al., 2012a; 2012b).

The CCN activity of the particles is characterized by the activation ratio given by:

$$R_a \equiv \frac{CCN}{CN} = a_0 + \frac{a_1 - a_0}{1 + (Q/Q_{50})^{-a_2}}, \quad (2)$$

where CCN and CN are the activated and total particle concentrations, while a_0, a_1, a_2 and Q_{50} are constants that describe the minimum, maximum, slope and inflection point of the sigmoidal, respectively, while Q is the instantaneous volumetric flow rate. Ideally, a_0 is zero and a_1 is expected to be unity; however, values for a_1 varied throughout the measurement period depending on the selected aerosol particle size and the mixing state. The inflection point (i.e. Q_{50} or "critical flow rate"), corresponds to the instantaneous flow rate, that produces a level of super-saturation within the CCNC, required to activate the measured monodisperse aerosol. Characteristic sigmoid activation curve of particles

having dry mobility diameter of 120 nm at super-saturated conditions ranging from 0.1 to 1.0% is shown in Fig. S3.

2.2.3. AMS Measurements

The standard HR-AMS data analysis software SQUIRREL v1.51C and PIKA v1.10C (Sueper, 2011) with Igor Pro 6.22A (Wavemetrics) was used for the AMS data analysis. For the organic mass spectra we applied the fragmentation table of Aiken et al. (2008) modifying the *m/z* ratio 18 and 28 (Kostenidou et, in preparation). Positive Matrix Factorization, PMF, (Paatero and Tapper, 1994; Lanz et al., 2007) was applied to the high-resolution organic mass spectra using the *m/z* ratios 12-200 according to the approach of Ulbrich et al. (2009). PMF, which is a bilinear unmixing model, reproduces the measurements as a linear combination of factors to indentify the different organic aerosol sources.

2.3. Estimation of the hygroscopic parameter κ

2.3.1. Determining the hygroscopic parameter κ from HTDMA measurements

The hygroscopic parameter κ can be determined by the hygroscopic growth factor measured by HTDMA as follows (Kreidenweis et al., 2008):

$$\kappa_{\mathrm{HTDMA}} = \frac{\left(g(\mathrm{RH})^3\text{-}1\right)}{a_{\mathrm{w}}/(1\text{-}a_{\mathrm{w}})} \ , \qquad (3)$$

where g(RH) is the measured hygroscopic growth factor (i.e., at 87% RH in our measurements) and a_{w} is the water activity of the solution droplet, which can be calculated by:

$$a_{\mathrm{w}} \approx \frac{\mathrm{RH}}{100} \left(exp\left(\frac{4\sigma_{s/\alpha} \ M_w}{RT\rho_w d_m(RH)} \right) \right)^{-1} . \qquad (4)$$

Here $\sigma_{s/a}$ and M_w are the surface tension and molecular weight of pure water (0.072 J m^{-2} and 18^{-3} kg/mol, respectively), R is the universal gas constant, T is the absolute temperature, ρ_{w} is the density of water and d_m is the diameter of the particles at elevated RH. Note that the exponential term, i.e., the Kelvin term, provides only a small correction for particles larger than 60 nm.

For externally mixed particles κ_{HTDMA} corresponding to each mode can be obtained. An average value of the hygroscopic parameter, which is representative of the hygroscopic properties of the entire particle population, can be also obtained as follows:

$$\bar{\kappa}_{\mathrm{HTDMA}} = \frac{\left(g_{\mathrm{avg}}(\mathrm{RH})^3 - 1\right)}{a_{\mathrm{w}}/(1-a_{\mathrm{w}})}. \quad (5)$$

Here g_{avg}(RH) is the average hygroscopic growth factor of the entire monodisperse particle population.

2.3.2. Determining the hygroscopic parameter κ from CCNC measurements

The hygroscopic parameter of the particles can also be obtained using the CCNC measurements (i.e., critical super-saturation) as follows:

$$\kappa_{\mathrm{CCN}} = \frac{4A^3}{d_{\mathrm{dry}}^3 S_c^2} \quad (6)$$

where S_c is the critical super-saturation at which half of the monodisperse particles activate (cf. sect. 2.2.2), d_{dry} is the dry mobility diameter selected by DMA-1, and

$$A = \frac{4M_{\mathrm{w}}\sigma_{\mathrm{w}}}{RT\rho_{\mathrm{w}}} \quad (7)$$

Here M_{w}, σ_{w} and ρ_{w} are the molecular weight, the surface tension and the density of water, while R and T are the universal gas constant and temperature of the system, respectively.

2.3.3. Estimating the hygroscopic parameter κ from particle chemical composition measurements

The hygroscopic parameter of the particles can be estimated using measurements of their chemical composition as follows:

$$\kappa_{\mathrm{CHEM}} = \sum_{\mathrm{i}} \varepsilon_{\mathrm{i}}\, \kappa_{\mathrm{i}}\,. \quad (8)$$

Here $\varepsilon_i = V_{\mathrm{si}}/V_{\mathrm{s}}$ and κ_{i} are the volume fraction and the hygroscopic parameter of the ith chemical species comprising the particles, with V_{si} being the volume occupied by that species and V_{s} the volume of the dry particle. The volume fractions of each species were estimated using fixed densities for the inorganic compounds (cf. Bezantakos et al., 2013 and Table 1 therein). To determine the organic volume fraction of the particles the corresponding density of the organics ρ_{org} was derived by combining the HR-ToF-AMS and the SMPS measurements (cf. DeCarlo et al., 2004). The hygroscopic parameters of

the inorganic species were taken by Petters and Kreidenweis (2007; cf. Table 1 therein). For the organic fraction, κ_{org} was estimated by fitting the predicted hygroscopic parameters κ_{CHEM} to that determined by the HTDMA and the CCNC (i.e., $\bar{\kappa}_{HTDMA}$ and κ_{CCN}, respectively), for the 120-nm particles. The hygroscopic parameter κ_{CHEM} was estimated using 2-h averaged size resolved HR-ToF-AMS measurements corresponding to particles with vacuum aerodynamic diameters (VADs) from ca. 165 to 209 nm. The reason for using such a wide range of particle sizes was to improve the signal to noise ratio in the measurements. The fitted hygroscopic parameter of the organic fraction (i.e. κ_{org}) was allowed to vary from 0.0 to 0.3 (Kreidenweis et al., 2007).

Values of κ_{org} were also estimated on a 24-hour basis, were also estimated by fitting κ_{CHEM} obtained by the off-line chemical composition measurements with the corresponding 24-h averaged $\bar{\kappa}_{HTDMA}$and κ_{CCN} values. In this case, the mass of the inorganic fraction of the particles was obtained from the filter samples, while the mass and density of the organic fraction was obtained by the HR-ToF-AMS. A similar procedure, as described above was followed to estimate the aerosol hygroscopic parameter. The simplified ion-pairing scheme described by Gysel et al., (2007), was used for the measurements conducted in Patras. For the measurements in Athens, due to the presence of Na^+, Cl^-, Ca^{2+}, K^+ in the filter samples we used ISORROPIA II (Fountoukis and Nenes, 2007) for the ion-pairing of the inorganic fraction.

3. Results and Discussion

3.1. Measurements in the atmosphere over the suburban site of Patras

The measuring period in Patras was divided into three distinct sub-periods based on the origin of the air masses arriving at the monitoring station as determined by 5-day wind back-trajectories using the NOAA HYSPLIT model. During the first and the third sub-period (i.e., 8-17 and 24-27 June, respectively) the air masses had western and north western origin while during the second (18-23 June), their origin was north-eastern. Discussion of the measurements in the sections that follows is based on the wind patterns observed in each sub-period.

3.1.1. Particle Hygroscopicity at sub-saturated conditions (HTDMA measurements)

Figure 2 shows the calculated 5-day wind back-trajectories for characteristic days corresponding to each sub-period, together with the measured growth factor distributions for 60- and 120-nm particles exposed to 87% RH. On 11 and 26 June (i.e., representative

days of the first and the third period) the air masses were passing over the city of Patras (Fig. 2a and c) carrying local-emitted and long-range transported particles. The observed aerosols during these days were both internally and externally mixed depending on the time, with the fraction of the latter being higher for the smaller dry mobility diameters (i.e., $d_{m,dry}$ = 60 nm) as shown in Fig. 2d, e and h, i. On 20 June (i.e., characteristic day of the second period) the air masses were not influenced by emissions from the city of Patras (Fig. 2b). For the entire day both the 60- and 120-nm particles were internally mixed, as indicated by the sharper measured growth factor distributions (Figs. 2f and g).

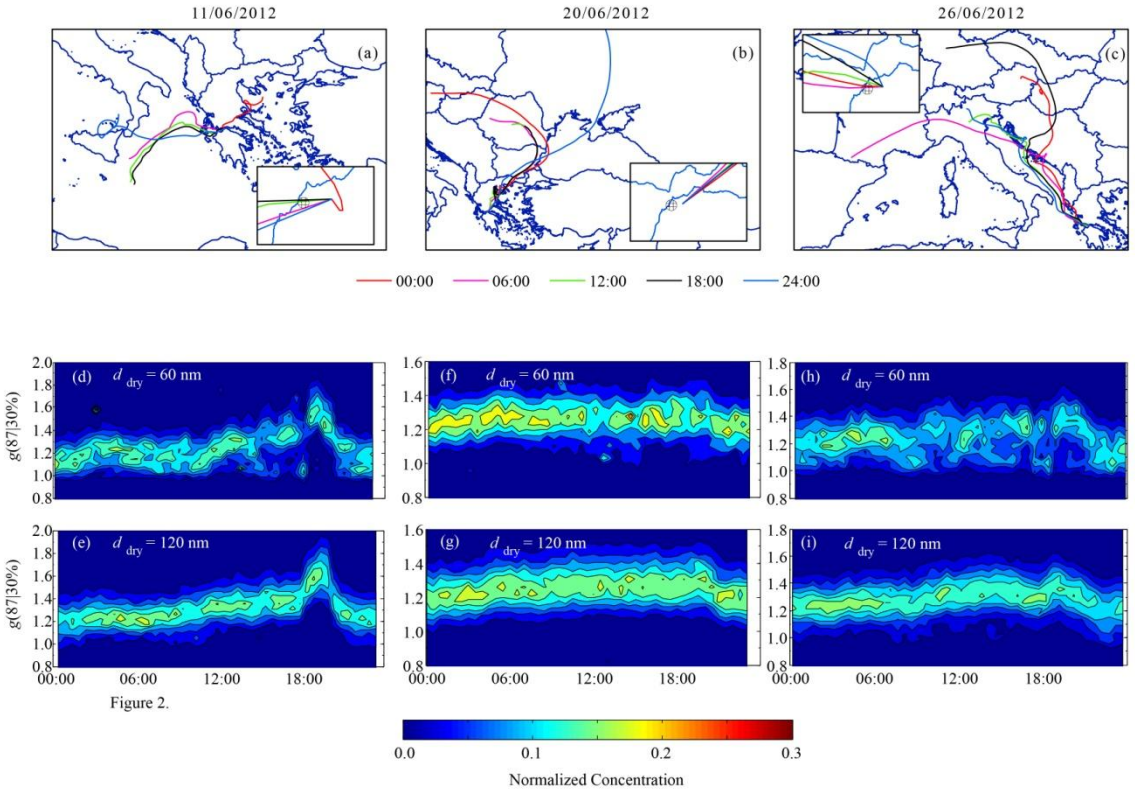

Figure 2.

Fig 2. Calculated 5-day wind back-trajectories and the growth factor distributions of 60- and 120-nm particles, when exposed to 87±2% RH, on 11 (**a, d, e**), 20 (**b, f, g**) and 26 (**c, h, i**) June. Three characteristic days that represent three distinct sub-periods during the measurements in Patras.

Figure 3 shows 6-h averaged hygroscopic growth factors of particles having dry mobility diameters of 60, 80, 100 and 120 nm after being exposed at 87% RH, for the entire period of the measurements in Patras. The particles can be divided in more and less hygroscopic fractions, depending on whether they exhibit g(87|30%) values above or below 1.15, as indicated by solid red or open blue circles, respectively. The size of the

circles in Fig. 3 indicates the relative population of the more or less hygroscopic fraction, while Table 1 summarizes the median values and the range of the more hygroscopic relative population in each sub-period.

Table 1. Median values and range (in brackets) of the number fractions of particles residing in the more hygroscopic mode (i.e., $g(87\%|30\%) > 1.15$) during the three different sub-periods (P1 8-17 June; P2 18-23 June; P3: 24-27 June) of the measurements in Patras.

d_{dry} (nm)	P1	P2	P3
60	0.90 (0.34-1.00)	0.99 (0.75-1.00)	0.88 (0.47-1.00)
80	0.97 (0.60-1.00)	0.98 (0.89-1.00)	0.92 (0.73-1.00)
100	0.97 (0.86-1.00)	1.00 (0.92-1.00)	0.97 (0.86-1.00)
120	0.97 (0.89-1.00)	1.00 (0.93-1.00)	0.96 (0.89-1.00)

Overall, the majority of the particle population resided in the more hygroscopic mode. Compared to the larger dry particles investigated in this work, particles having dry mobility diameters of 60 nm exhibited the highest fraction of less hygroscopic particles. The variability of the number concentration fraction of the more hygroscopic mode was decreasing with increasing dry mobility diameter. Higher fractions of particles residing in the less hygroscopic mode were observed during the first and the third sub-period (i.e., 8-17 and 24-27 June, respectively) when more than 10% of the aerosol samples were externally mixed. During these two periods the concentration of the less oxygenated Hydrocarbon and Cooking-like Organic Aerosol (HOA and COA, respectively) determined by the HR-ToF-AMS (cf.: section 2.2.3) were increased (cf. Fig. S4) indicating the presence of anthropogenic particles.

The median values and ranges of the hygroscopic growth factors of particles residing in either the less or the more hygroscopic mode during each sub-period of the measurements in Patras are summarized in Table 2. The observed particles exhibited hygroscopic growth factors similar to the ones observed in North Aegean Sea (c.f. Bezantakos et al., 2013) and 10% lower than the ones observed in South Aegean (c.f. Stock et al., 2011).

Table 2. Median values and range (in brackets) of externally mixed particles classified as less hygroscopic (lh; $g \leq 1.15$) and as more hygroscopic (mh; $g > 1.15$) when exposed to 87% RH, during each sub-period in Patras.

d_{dry} (nm)	P1		P2		P3	
	lh	mh	lh	mh	lh	mh
60	1.10 (1.00-1.15)	1.23 (1.15-1.59)	1.13 (1.03-1.15)	1.24 (1.15-1.38)	1.08 (1.02-1.15)	1.26 (1.15-1.69)
80	1.05 (1.00-1.15)	1.24 (1.15-1.59)	1.06 (1.03-1.15)	1.24 (1.15-1.44)	1.05 (1.01-1.15)	1.27 (1.15-1.44)
100	1.05 (1.00-1.15)	1.25 (1.16-1.60)	1.06 (1.03-1.15)	1.24 (1.15-1.62)	1.03 (1.00-1.14)	1.27 (1.15-1.44)
120	1.04 (1.00-1.15)	1.25 (1.15-1.63)	1.13 (1.11-1.14)	1.24 (1.16-1.43)	1.03 (1.00-1.12)	1.27 (1.15-1.45)

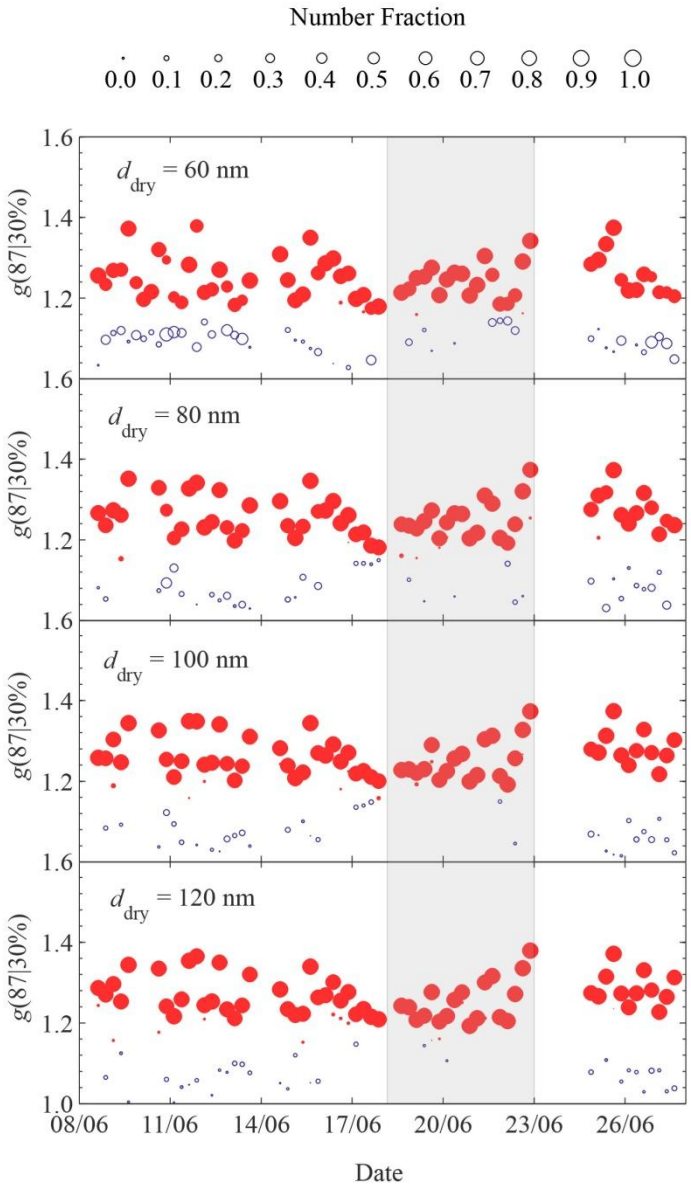

Fig 3: HTDMA measurements of 60-, 80-, 100-, 120-nm particles for the entire period of the measurements in Patras. The size of the symbols (i.e., the size of the circles) is proportional to the number fraction of each mode. Particles which exhibited hygroscopic growth factor below 1.15 (less hygroscopic) are denoted with different symbols (i.e. open blue circles). The grayed area marks the second sub-period.

3.1.2. Particle hygroscopicity at supersaturated conditions (CCNC measurements)

The hygroscopic parameters κ and activation fractions of the monodisperse particles determined by the CCNC measurements (i.e., when the particles were exposed to super-saturated conditions) averaged over 6 h are shown in Figure 4 and summarized in Table 3. The lowest activation fractions but with the highest variability were observed for

60-nm particles in all three sub-periods. The larger particle exhibited similar activation fractions with values almost unity during most of the first sub-period. During the second and the third sub-period, however, the larger particles exhibited somewhat lower activation fractions with values as low as 70%. Overall, the activation fraction decreased with increasing dry mobility diameter from 80 nm. A significant deviation from these trends were observed on 17 June, where the activation fraction of all the particles was lower than 50%, possible due to transport of aerosols from wildfires in Balkans from low altitude winds (cf. Fig. S8).

The variability of κ_{CCN} increased with increasing particle size but overall exhibited moderate values that are indicative of mixed particles composed of inorganic and organic species. Only the largest sampled particles (i.e., those having dry diameters of 100 and 120 nm) exhibited hygroscopic properties representative of pure inorganic particles during a short period around 22 June. The observed κ_{CCN} values were not significantly different than the ones reported by Bougiatioti et al. (2009) for the South Aegean region.

Table 3. Median values together with the range (in brackets) of hygroscopicity parameters κ and activation fractions R_a of particles having dry mobility diameters of 60, 80, 100 and 120 nm at various super-saturation conditions, rating from 0.1 to 1.0, in Patras suburban sampling site.

d_{dry} (nm)	P1		P2		P3	
	κ_{CCN}	Ra	κ_{CCN}	Ra	κ_{CCN}	Ra
60	0.12 (0.06-0.23)	0.82 (0.21-1.00)	0.10 (0.06-0.24)	0.77 (0.26-1.00)	0.13 (0.06-0.19)	0.83 (0.33-1.00)
80	0.18 (0.07-0.39)	1.00 (0.46-1.00)	0.20 (0.07-0.36)	0.91 (0.53-1.00)	0.23 (0.12-0.32)	0.88 (0.64-1.00)
100	0.23 (0.10-0.51)	1.00 (0.42-1.00)	0.27 (0.12-0.60)	0.83 (0.55-1.00)	0.24 (0.15-0.40)	0.87 (0.65-1.00)
120	0.23 (0.09-0.66)	1.00 (0.43-1.00)	0.26 (0.10-0.71)	0.79 (0.56-1.00)	0.23 (0.13-0.44)	0.84 (0.64-1.00)

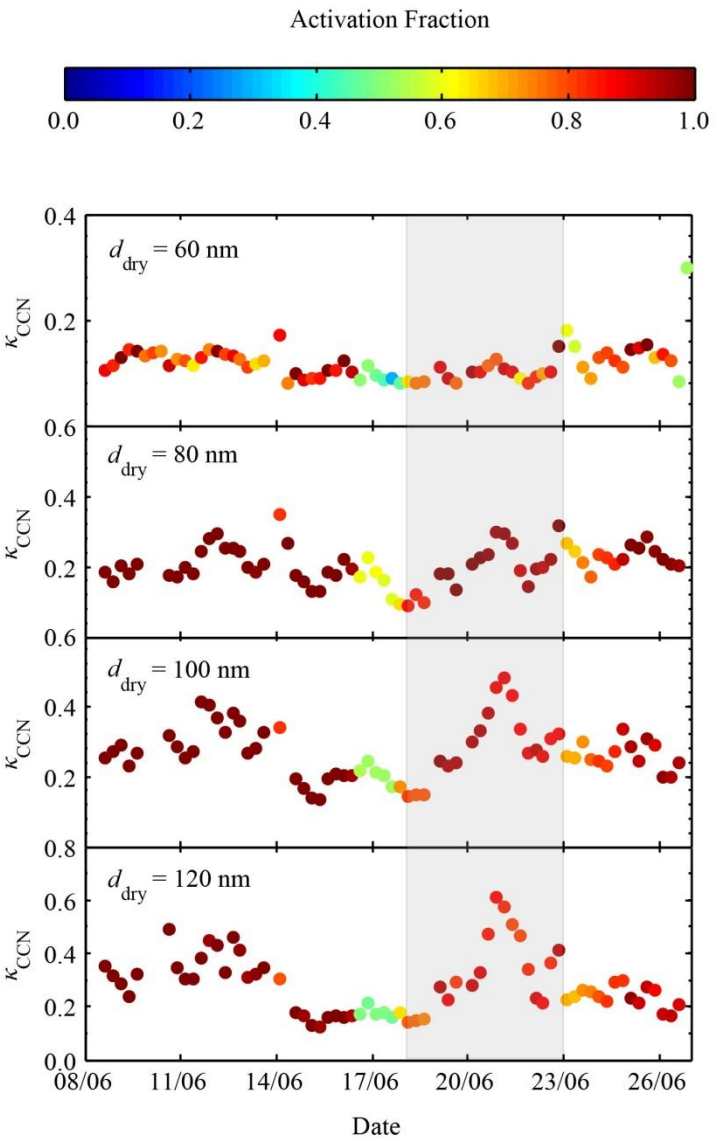

Fig 4. Hygroscopic parameters κ_{CCN} and their activation fractions (Color bar) of 60-, 80-, 100-, 120-nm particles, measured by the CCNC in Patras. The grayed area marks the second sub-period.

3.1.3. Predicted hygroscopic parameter κ from particles chemical composition

Figure 5 shows 2-h averaged hygroscopic parameters derived from the HTDMA and CCNC measurements together with predictions using the size resolved particle chemical composition from the HR-ToF-AMS and the κ-Köhler theory as described in sect. 2.3.3. The hygroscopic parameter of the organic fraction κ_{org} shown in Fig. 5b and 5d, which was allowed to vary between zero and 0.3, was estimated by matching κ_{CHEM} with $\bar{\kappa}_{HTDMA}$ and κ_{CCN}, respectively. The median values and the range of the estimated κ_{CHEM} and κ_{org} parameters at both sub- and super-saturation conditions for the three sub-periods are shown in Table 4.

Table 4. Median values and range (in brackets) of the estimated aerosol and organic fraction's, hygroscopic parameters (κ_{CHEM} and κ_{org}) at different saturation (S) conditions in Patras. For the estimation κ_{CHEM} was fitted to the measured hygroscopic parameters of particles having dry mobility diameter of 120 nm by varying κ_{org}.

S	Variable	P1	P2	P3
Sub	κ_{CHEM}	0.2 (0.12-0.31)	0.17 (0.11-0.33)	0.21 (0.12-0.32)
	κ_{org}	0.00 (0.00-0.18)	0.00 (0.00-0.19)	0.00 (0.00-0.13)
Super	κ_{CHEM}	0.29 (0.16-0.49)	0.27 (0.13-0.47)	0.27 (0.21-0.35)
	κ_{org}	0.10 (0.00-0.30) (0.00-0.30)	0.13 (0.00-0.30) (0.00-0.30)	0.00 (0.00-0.18) (0.00-0.11)

The median value of the hygroscopic parameter of the organic fraction κ_{org} throughout the entire period of the measurements was zero when estimated at sub-saturated conditions (i.e., by fitting κ_{CHEM} to $\bar{\kappa}_{HTDMA}$) in all three sub-periods. Values of κ_{org} higher than 0.1 were used only in 15% of the cases during the first and the second sub-period and only in 4% during the third. The corresponding median value of κ_{org} estimated at super-saturated conditions (i.e., by fitting κ_{CHEM} to κ_{CCNC}) was 0.10 and 0.13 during the first and the second sub-period, respectively and zero during the third. During the first and the second sub-period κ_{org} values of zero were used in 37 and 12%, respectively. During the third sub-period values of κ_{org} higher than 0.1 accounted for 18% of the cases.

Differences in estimated κ_{org} values under different saturation conditions indicate that the atmospheric organic species exhibit different hygroscopic behavior in sub- and

super-saturated conditions. Such differences have been observed in other field campaigns (e.g., Irwin et al., 2010, Wu et al., 2013) providing speculations that they can be attributed to limitations of the κ-Köhler model and surface tension reductions, non ideality effects in the solution droplet, co-condensation of semi-volatile species and limited solubility of the organic species. Similar differences in the sub- and super-saturation hygroscopic properties were observed in laboratory studies conducted with SOAs (Wex et. al., 2009) and soot particles coated by organic acids (Henning et al., 2012).

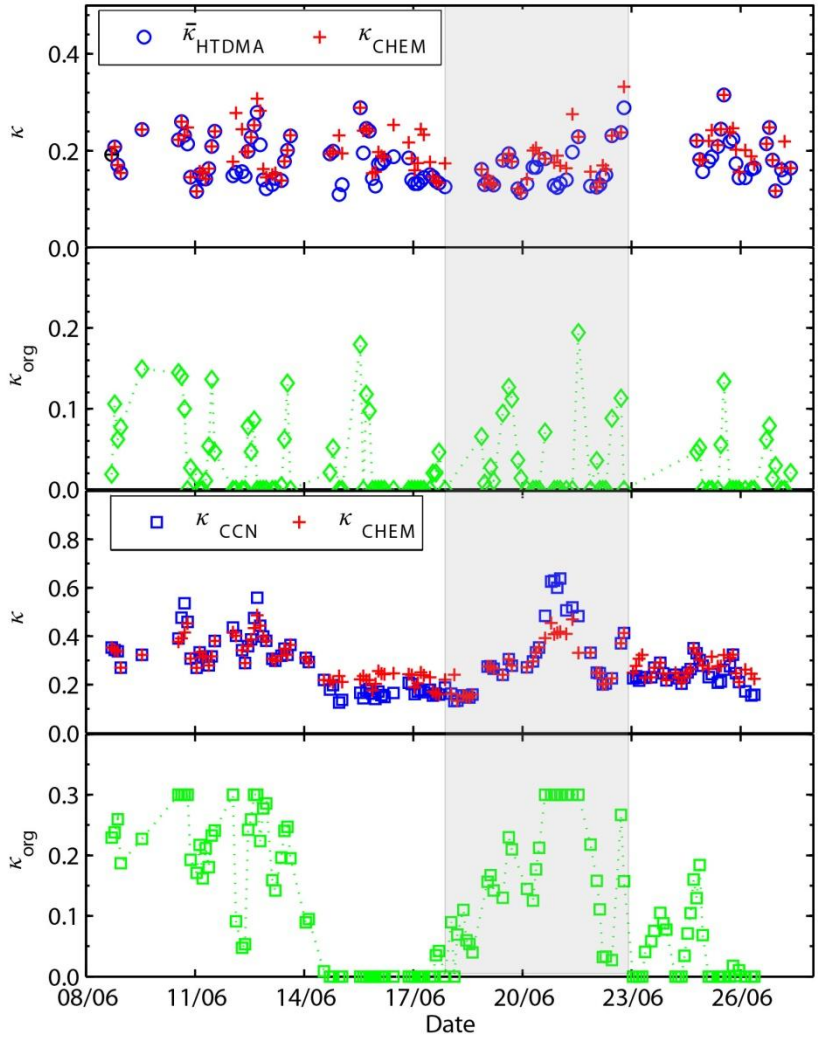

Fig 5. Comparison of predicted κ_{CHEM} from the AMS measurements with κ derived from HTDMA ($\bar{\kappa}_{HTDMA}$) and CCNC measurements (κ_{CCN}) in Patras. κ_{CHEM} was predicted by applying the κ-Köhler theory on the size resolved chemical composition of the particles. The hygroscopic parameter of the organic fraction (κ_{org}) was estimated by fitting the predicted κ_{CHEM} values to the measurements by varying κ_{org} from 0.0 to 0.3.

A possible correlation between hygroscopicity of the organic fraction (i.e. κ_{org}) and the degree of its oxygenation or O:C ratio, had been proposed in other field and laboratory studies, like Chang et al., (2010) and Kuwata et al., (2013). In our case, however, no correlation was observed between O:C and estimated κ_{org} values. Despite that the organic fraction of the particles was dominated by Secondary Oxygenated Organics as indicated by the HR-ToF-AMS measurements (cf. Fig. S4), in many cases we had to use a κ_{org} value of zero to obtain the best fit between the estimated κ_{CHEM} and the measured $\bar{\kappa}_{HTDMA}$ or $\kappa_{CCN.}$

To investigate the consistency of our analysis, estimates of κ_{org} were also made using the chemical composition of $PM_{2.5}$ filter samples collected over 24-h and the procedure described above. In this case κ_{CHEM} predictions were fitted to 24-h averaged hygroscopic parameters derived from HTDMA and the CCNC measurements (cf. Fig. S5 and Table S1). The estimated κ_{org} at sub-saturated conditions (i.e., by fitting κ_{CHEM} derived from the filter samples to κ_{HTDMA}) indicated that the organic fraction of the sampled particles was hydrophobic on 42% of the cases during the first sub-period and larger than 66% during the third and the second. At super-saturated conditions the estimated κ_{org} corresponded to slightly and mildly hygroscopic organic species. The estimated κ_{org} values obtained from filter samples indicated that the organic fraction exhibited higher water affinity when exposed to super-saturated conditions, which is similar to the observation made when κ_{org} values were estimated from HR-ToF-AMS measurements.

3.2. Measurements in the atmosphere over the suburban site of Athens

Five sub-periods could be distinguished on the basis of the 5-day wind back-trajectories calculated by the NOAA HYSPLIT model. During the first sub-period (4 to 8 July) the air masses had northwestern to northeastern origin. The second and the fourth sub-periods (9 to 10, and from 14 to 23 July, respectively) were characterized of winds with northeastern direction, while the winds during the third and the fifth period (11 to 14 and 24 to 26 July, respectively) had directions that ranged from northeast to west. It should be noted that winds carrying air masses coming over the Aegean Sea (i.e. winds with northeast direction), are less affected by land emissions. The following sections provide a discussion of the measurements conducted by taking into account the different wind patterns of each sub-period.

3.2.1. Particle Hygroscopicity at sub-saturated conditions (HTDMA measurements)

Figure 6 shows the calculated 5-day wind back-trajectories together with the measured growth factor distributions for 60- and 120-nm particles when exposed to 87% RH, for three characteristic days. On 4 July (i.e., representative day of the first sub-period) the air masses reached the sampling site from the northwest or from the north until ca. 12:00, passing above residential areas, while their direction changed to northeastern encountering less populated areas in the afternoon (Fig. 6a). The growth factor distributions measured on 4 July (Figs. 6d and e) indicate the particles were mainly externally mixed particles with an increased fraction at lower dry mobility diameters (i.e., d_m = 60 nm) until noon, but switched to mostly internally mixed, coinciding with the change in wind direction.

On 13 July (i.e., representative day of sub-periods 3 and 5) the air masses had variable directions and were passing above densely populated city areas before reaching the sampling site (Fig. 6b). Particles were mostly externally mixed until the early evening hours (i.e., around 18:00) and internally mixed afterwards, as indicated by the growth factor distributions (Fig. 6f and g). The fraction of the externally mixed samples was higher for the smaller dry particles as indicated by the broader growth factor distributions. On 22 July, which is a representative day of sub-periods 2 and 4, the calculated wind back-trajectories indicated that the air masses had the same paths passing over the Aegean Sea throughout the entire day (Fig. 6c). Particles observed on 22 July were in most of the cases internally mixed, exhibiting a decreasing fraction of internally mixtures with decreasing dry mobility diameters (Fig. 6h and i). Despite the different wind origins, particles appear to be externally mixed in the early morning hours (from ca. 6:00 to 10:00) in all three characteristic days, probably because of the morning traffic.

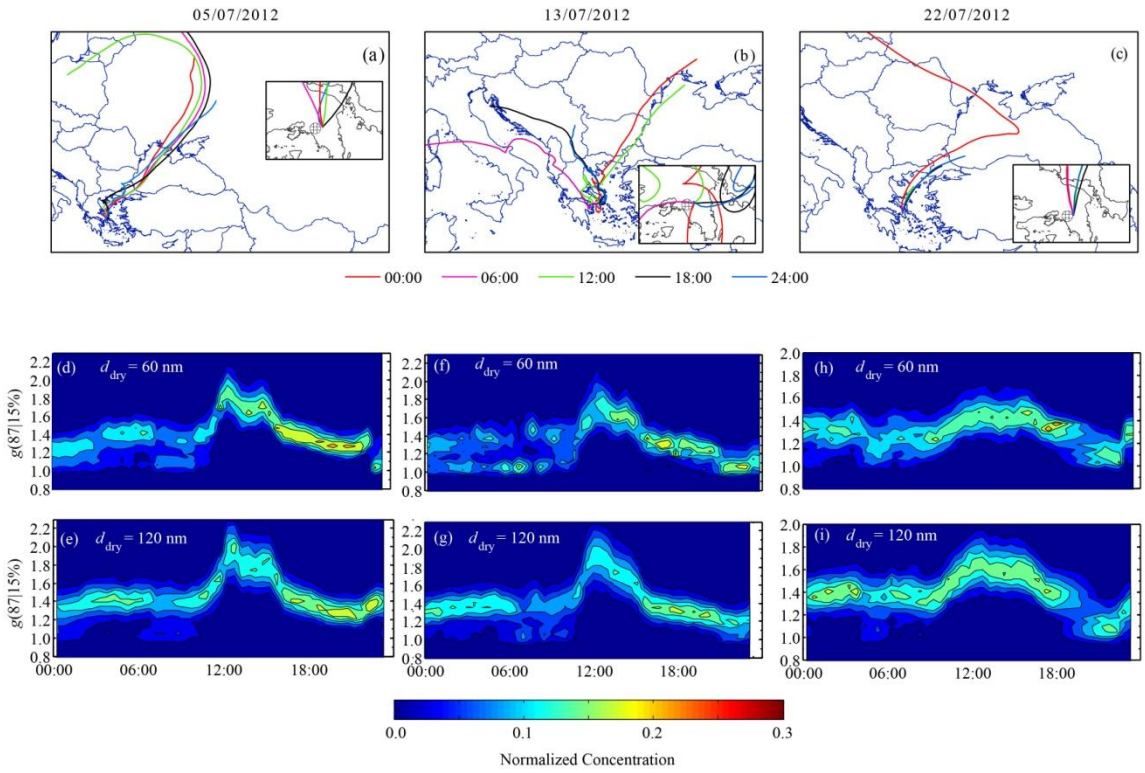

Fig 6. Calculated 5-day wind back-trajectories and growth factor distributions of 60- and 120-nm particles, when exposed to 87±2% RH on 5 (**a, d, e**), 13 (**b, f, g**) and 22 (**c, h, i**) July. These days are characteristic and represent five distinct sub-periods during the measurements in Athens. Sub-period one is represented by 5 July, sub-periods 3 and 5 by 13 July and sub-periods 2 and 4 by 22 July.

The 6-hour averaged *g*(87|15%) hygroscopic growth factors together with the relative population (i.e. size of circles) of more or less hygroscopic particles during the entire period of the measurements in Athens are shown in Fig. 7. The median values and range of the relative populations of the more hygroscopic fraction for each sub-period is summarized in Table 5. Compared to the measurements conducted in Patras, externally mixed particles were observed more often. Overall, the majority of the particles resided in the more hygroscopic mode. Higher fractions of the more hygroscopic group were observed during the second and the fourth sub-periods, when the particles were mostly internally mixed. An extended period of internally mixed aerosol during the fourth sub-period can be explained by a reduction of anthropogenic emitted particles, since from 14 July a number of inhabitants left the city for their summer vacations.

Table 5. Median values and range (in brackets) of the number fractions of particles residing in the more hygroscopic mode (i.e., $g(87|15\%) > 1.15$) during the five different sub-periods (P1 4-8 July; P2 9-10 July; P3 11-14 July; P4 14-23 July; P5 24-26 July) of the measurements in Athens.

d_{dry} (nm)	P1	P2	P3	P4	P5
60	0.81 (0.17-1.00)	1.00 (0.40-1.00)	0.66 (0.14-0.97)	0.98 (0.27-1.00)	0.89 (0.59-1.00)
80	0.88 (0.26-1.00)	0.99 (0.70-1.00)	0.85 (0.45-1.00)	1.00 (0.47-1.00)	0.89 (0.65-1.00)
100	0.88 (0.48-1.00)	1.00 (0.74-1.00)	0.83 (0.52-1.00)	1.00 (0.66-1.00)	0.91 (0.78-1.00)
120	0.90 (0.51-1.00)	0.97 (0.76-1.00)	0.85 (0.55-1.00)	1.00 (0.63-1.00)	0.89 (0.78-1.00)

Interestingly, even during the other sub-periods the fraction of the internally mixed and hygroscopic particles was higher from ca. 12:00 to 16:00, corroborated by the decrease of the less oxygenated HOA, COA fractions (i.e. by applying PMF over the HR-AMS measurements; cf. sect. 2.2.3), during these hours (cf. Fig. S6). The observations above suggest that the aerosol mixing state could not be attributed to the wind direction alone but to a combination of the later with other factors like the variation of particles produced from local and distant sources.

Overall, the hygroscopicity of the sampled particles was higher in Athens than in Patras. Particles indicated the highest hygroscopic behavior during the second sub-period, while during the other sub-periods their hygroscopicity was similar. Particles having dry mobility diameters of 60 nm and that were classified as less hygroscopic, exhibited higher hygroscopic growth factors compared to the larger particles of the same group, during sub-periods with higher anthropogenic influence (i.e. during first, third and fifth sub-periods. The median values and ranges of the hygroscopic growth factors exhibited by

either less or more hygroscopic particles during each sub-period are summarized in Table 6. The hygroscopic growth factors of the observed 60 nm particles were on average similar to ones reported by Petäjä et al. (2007), however their variability and maximum values were higher.

Table 6. Median values and range (in brackets) of externally mixed particles classified as less hygroscopic (lh; $g \leq 1.15$) and as more hygroscopic (mh; $g > 1.15$) when exposed to 87% RH, during each sub-period in Athens.

d_{dry} (nm)	P1		P2		P3		P4		P5	
	lh	mh	lh	mh	lh	mh	lh	mh	lh	mh
60	1.08	1.37	1.05	1.44	1.07	1.36	1.07	1.36	1.07	1.38
	(1.04-1.13)	(1.17-1.76)	(1.03-1.08)	(1.22-1.87)	(1.04-1.12)	(1.20-1.67)	(1.02-1.15)	(1.18-1.77)	(1.04-1.14)	(1.26-1.92)
80	1.06	1.38	1.06	1.45	1.06	1.36	1.05	1.36	1.06	1.4
	(1.04-1.11)	(1.19-1.82)	(1.02-1.13)	(1.23-1.92)	(1.03-1.15)	(1.20-1.75)	(1.01-1.13)	(1.20-1.81)	(1.05-1.14)	(1.27-1.87)
100	1.05	1.37	1.09	1.44	1.05	1.37	1.07	1.38	1.05	1.38
	(1.02-1.14)	(1.22-1.84)	(1.04-1.11)	(1.23-1.87)	(1.03-1.13)	(1.21-1.80)	(1.03-1.15)	(1.22-1.90)	(1.04-1.14)	(1.28-1.86)
120	1.06	1.39	1.12	1.45	1.05	1.38	1.08	1.39	1.05	1.39
	(1.03-1.15)	(1.23-1.85)	(1.04-1.15)	(1.25-1.87)	(1.02-1.12)	(1.20-1.87)	(1.05-1.14)	(1.22-1.91)	(1.05-1.11)	(1.28-1.89)

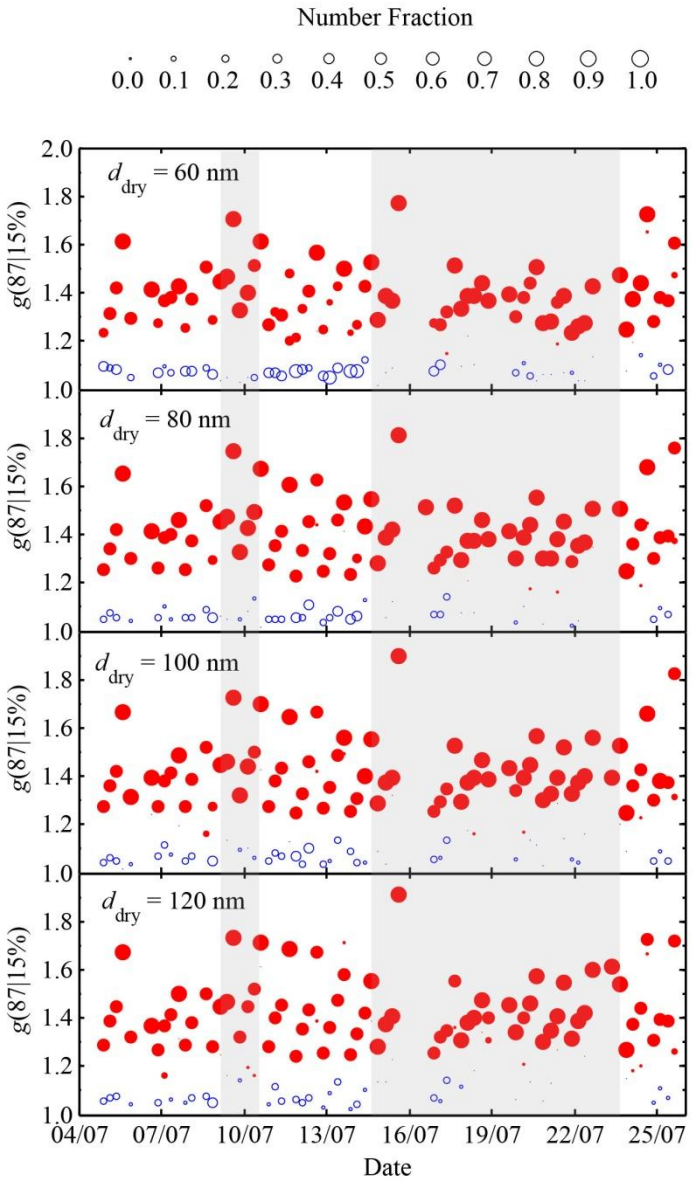

Fig 7: HTDMA measurements of 60-, 80-, 100-, 120-nm particles for the entire period of the measurements in Athens. The size of the symbols (i.e., the size of the circles) is proportional to the number fraction of each mode. Particles which exhibited hygroscopic growth factor below 1.15 (less hygroscopic) are denoted with different symbols (i.e. open blue circles). The grayed areas mark the second and fourth sub-periods.

In contrast to the observations in Patras, the hygroscopic growth factors of all samples observed in Athens exhibited a strong diurnal variation throughout the entire measuring period. As shown in Fig. 8, the hygroscopic growth factors for the 60- and 120-nm exhibited a peak from ca. 12:00 to 16:00 local time. During the same time the particles exhibit highest hygroscopic growths with g(87%|15%) reaching up to ca. 2. Such high values have been either associated with sea-salt particles or organic salts, like

sodium formate or sodium acetate (Peng and Chan, 2001; Wu et al., 2011). Sodium organic salts have been found to be present in marine environments and are products of sub-micron sea salt particles reacting with organic acids (Kerminen et al., 1998). The corroborating wind directions were northeastern in most cases, during those hours, thus possible carrying particles of marine origin.

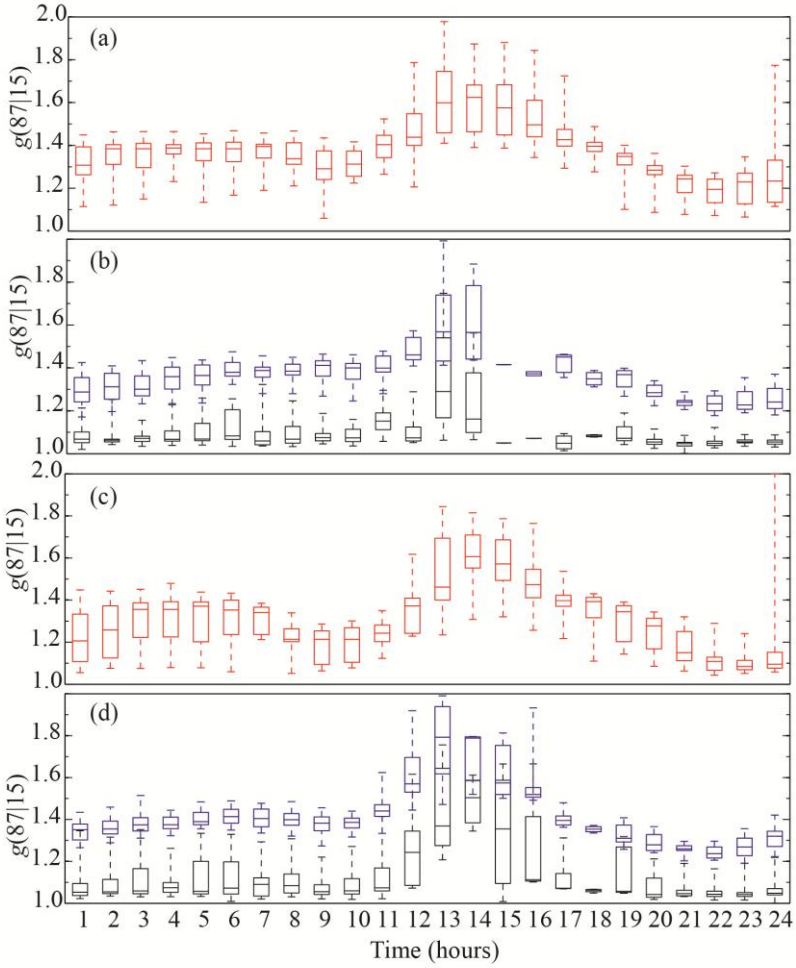

Fig 8. Diurnal variation of the hygroscopic growth factors of internally (**a, c**) and externally (**b, d**) mixed, which had dry mobility diameters of 60- (**a, b**) and 120- nm (**c, d**), in Athens.

3.2.2. Particle hygroscopicity at super-saturated conditions (CCNC measurements)

The 6-hour averaged activation fractions and hygroscopic parameters of the monodisperse particles determined by the CCNC are shown in Fig. 9 and summarized in Table 7. Compared to the κ_{CCN} values reported from the measurements in Patras, the hygroscopicity of the particles in Athens was higher. The lowest activation fractions were observed for 60-, while the highest for 120-nm particles in all sub-periods. Although highly hygroscopic particles were observed occasionally during the entire period of the

measurements, the highest κ_{CCN} values were systematically observed during the second sub-period. Particles having dry mobility diameters of 60 nm were the less hygroscopic while those having 100- and 120- nm were the most hygroscopic in all sub-periods.

Table 7. Median values together with the range (in brackets) of hygroscopicity parameters κ and activation fractions R_a of particles having dry mobility diameters of 60, 80, 100 and 120 nm at various super-saturation conditions, rating from 0.1 to 1.0, in Athens suburban sampling site.

d_{dry} (nm)	P1		P2		P3		P4		P5	
	κ_{CCN}	*R*a	κ_{CCN}	*R*a	κ_{CCN}	*R*a	κ_{CCN}	*R*a	κ_{CCN}	*R*a
60	0.28	0.72	0.33	0.76	0.29	0.49	0.28	0.64	0.35	0.66
	(0.15-0.45)	(0.26-0.94)	(0.21-0.52)	(0.23-0.96)	(0.14-0.50)	(0.22-0.93)	(0.16-0.49)	(0.13-1.00)	(0.21-0.49)	(0.22-0.95)
80	0.44	0.84	0.59	0.94	0.37	0.77	0.42	0.91	0.44	0.93
	(0.20-0.67)	(0.59-1.00)	(0.30-0.74)	(0.77-1.00)	(0.17-0.61)	(0.46-1.00)	(0.14-0.70)	(0.61-1.00)	(0.27-0.57)	(0.68-1.00)
100	0.54	0.87	0.67	0.97	0.47	0.9	0.5	0.99	0.53	1
	(0.15-0.84)	(0.65-1.00)	(0.37-0.83)	(0.81-1.00)	(0.22-0.69)	(0.67-1.00)	(0.24-0.76)	(0.41-1.00)	(0.37-0.68)	(0.62-1.00)
120	0.53	0.88	0.54	0.99	0.5	0.99	0.45	1	0.45	1
	(0.17-0.81)	(0.71-1.00)	(0.32-0.86)	(0.81-1.00)	(0.17-0.83)	(0.83-1.00)	(0.20-0.80)	(0.80-1.00)	(0.30-0.61)	(0.89-1.00)

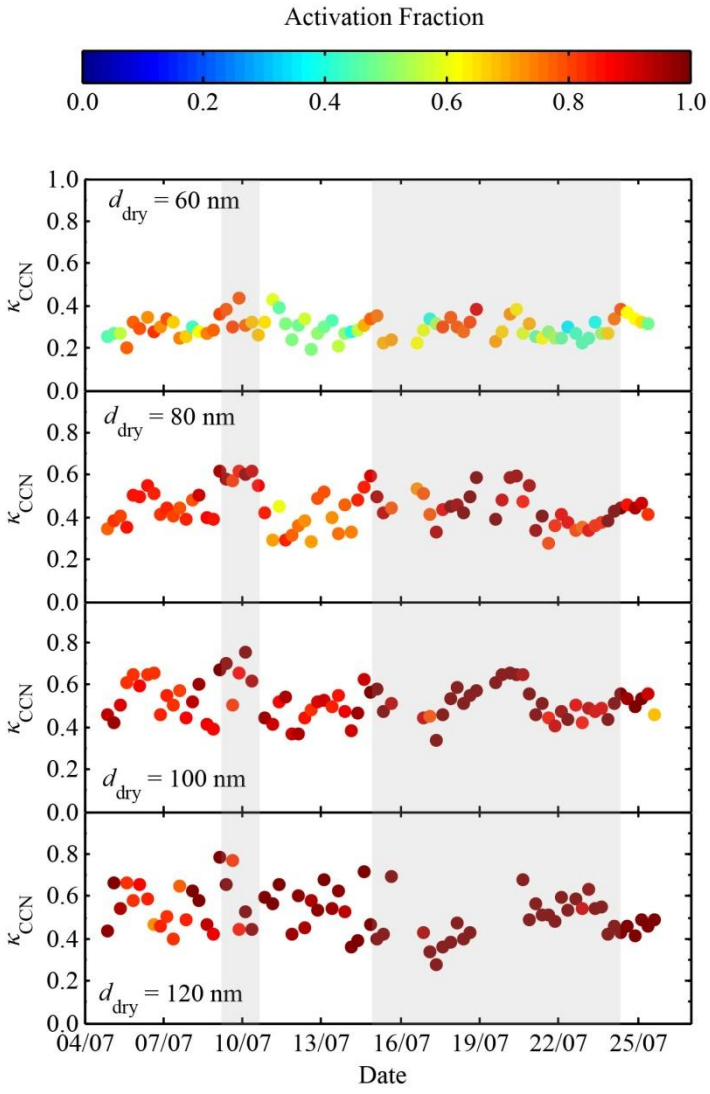

Fig 9. Hygroscopic parameters κ_{CCN} and their activation fractions (Color bar) of 60-, 80-, 100-, 120-nm particles, measured by the CCNC in Athens. The grayed areas mark the second and fourth sub-periods.

3.2.3. Predicted hygroscopic parameter κ from particles chemical composition

Estimations of the hygroscopic parameter of the organic fraction κ_{org} of the 120-nm particles when they were exposed to sub- and super-saturated conditions are shown in Fig. 10. The median values and the range of the estimated κ_{CHEM} and κ_{org} parameters at both sub- and super-saturation conditions are shown in Table 8.

Table 8. Median values and range (in brackets) of the estimated aerosol and organic fraction's, hygroscopic parameters (κ_{CHEM} and κ_{org}) at different saturation (S) conditions in Athens. For the

estimation, κ_{CHEM} was fitted to the measured hygroscopic parameters of particles having dry mobility diameter of 120 nm by varying κ_{org}.

S	Variable	P3	P4	P5
Sub	κ_{CHEM}	0.24 (0.12-0.39)	0.29 (0.14-0.46)	0.28 (0.20-0.42)
	κ_{org}	0.09 (0.00-0.30)	0.17 (0.00-0.30)	0.15 (0.00-0.30)
Super	κ_{CHEM}	0.38 (0.32-0.44)	0.39 (0.29-0.56)	0.41 (0.35-0.46)
	κ_{org}	0.3 (0.2-0.30)	0.3 (0.05-0.30)	0.3 (0.12-0.30)

In order to obtain the best fit between the estimated κ_{CHEM} and the measured $\bar{\kappa}_{HTDMA}$ or κ_{CCN} we had to use in many cases a κ_{org} value of 0.3. Higher κ_{org} values would result in a better fitting, but to the best of our knowledge this is the highest value for organic species used in studies of atmospheric relevance. The high hygroscopicity observed with the HTDMA and the CCN can therefore be attributed to highly hygroscopic refractory compounds which cannot be detected by the HR-ToF-AMS.

Compared to the κ_{org} values estimated for the measurements conducted in Patras the estimated κ_{org} values in Athens were higher. The corresponding median value of κ_{org} when estimated at sub-saturated conditions was 0.09, 0.17 and 0.15 during the third, fourth and fifth sub-periods, respectively. During the third sub-period κ_{org} values above 0.1 accounted for almost 39%, while during the fourth and the fifth sub-periods κ_{org} values less than 0.1 accounted for 28 and 25%, respectively. The corresponding median value of κ_{org} when estimated at super-saturated conditions was 0.30 in all three sub-periods, while values of κ_{org} smaller than 0.3 accounted for 25% of the measurements during the fourth and 12% during the third and fifth sub-period.

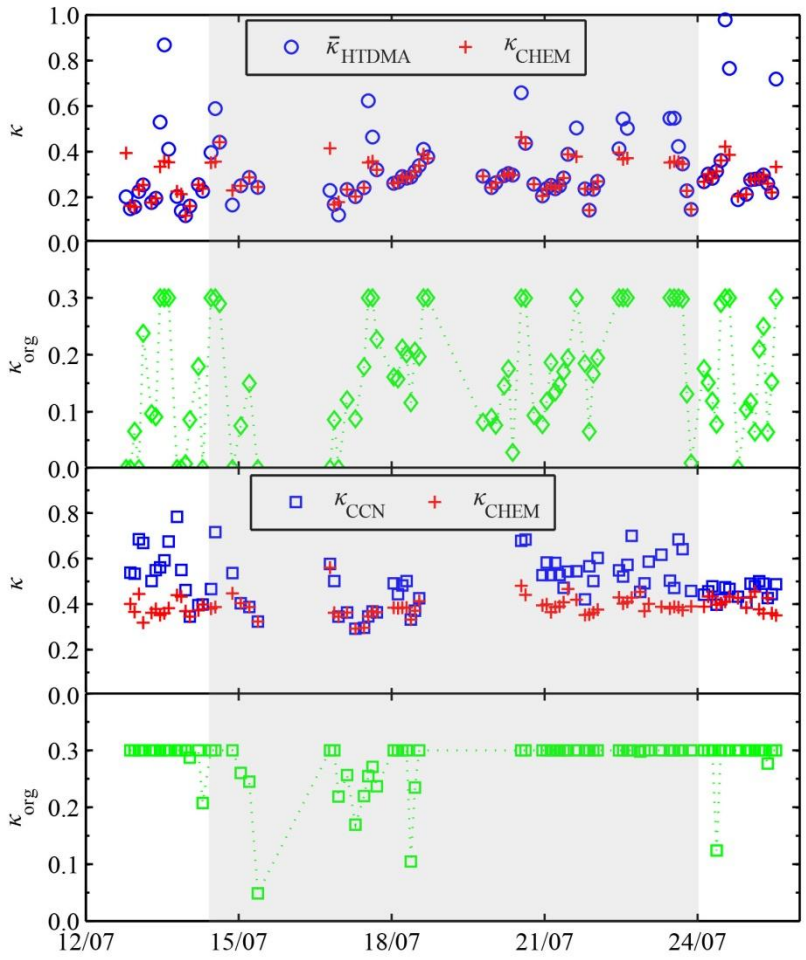

Fig 10. Comparison of predicted κ_{CHEM} from the AMS measurements with κ derived from HTDMA ($\bar{\kappa}_{HTDMA}$) and CCNC measurements (κ_{CCN}) in Athens. κ_{CHEM} was predicted by applying the κ-Köhler theory on the size resolved chemical composition of the particles. The hygroscopic parameter of the organic fraction (κ_{org}) was estimated by fitting the predicted κ_{CHEM} values to the measurements by varying κ_{org} from 0.0 to 0.3. The grayed area marks the fourth sub-period.

The estimated κ_{org} values obtained from the off-line chemical composition measurements (cf. Fig. S7 and table S2) indicated no significant differences with those obtained from the HR-ToF-AMS, except for the fourth and the fifth sub-period at sub- and super-saturated conditions, respectively. Since the 24-h average hygroscopicity of the organic fraction is not radically affected by either using the filter samples or the HR-ToF-AMS there is the possibility either the mass concentration of refractory matter to be limited and concentrated on specific hours or the organic components to be more hygroscopic than the value of 0.30 we assumed.

4. Conclusions

In this work we report the mixing state and the hygroscopicity of aerosol particles observed at two suburban sites in the cities of Patras and Athens. The measurements were performed with dried size-selected particles having diameters from 60 to 120 nm that were exposed to sub- and super-saturation conditions using a combination of an HTDMA and a CCNC. Five-day wind back-trajectories were used to distinguish the measurements in sub-periods depending on whether the air masses arriving at the stations passed over the cities or not. Chemical composition measurements by an HR-ToF-AMS and $PM_{2.5}$ filter samples were used to estimate the hygroscopic parameter of the organic fraction κ_{org}.

Observing the behavior of the particles when exposed to sub-saturated conditions indicated that the aerosols over Athens were more often externally mixed and significantly more hygroscopic than those in Patras. For both stations the majority of the particles resided in the more hygroscopic mode (i.e., g(87%) > 1.15), while the population of the less hygroscopic mode (i.e. g(87%) <1.15) was increased during sub-periods with city influences. A strong diurnal variation in the particles hygroscopic growth factors was only observable in Athens exhibiting a peak during the early afternoon.

At super-saturated conditions the sampled particles were more CCN active and more hygroscopic in Athens. In both sampling sites the lowest κ_{CCN} values and activation fractions were observed for 60 nm particles while the highest for larger particles (i.e. particles having dry mobility diameters of 100 and 120 nm.

The estimated hygroscopic parameters of the organic fraction (κ_{org}) using the HR-ToF-AMS measurements indicated that the organic fraction was more hygroscopic in Athens than in Patras, and in both cases when the particles were exposed to super-saturated conditions. In Patras the organic fraction was in many cases hydrophobic when exposed to sub-saturated conditions and despite the slightly higher median κ_{org} values which were obtained using the chemical composition provided by filter samples never exceeded 0.2. However, employing the HR-ToF-AMS measurements to estimate κ_{org} in Athens resulted in many cases of poor fitting even when we used the maximum κ_{org} value of 0.3, especially for super-saturated conditions. Combining this result with the observation of highly hygroscopic particles we suspected the presence of refractory and highly hygroscopic matter. However, the use of the chemical composition provided by

filter samples did not radically altered the resulted κ_{org} values leading to the possibility of either limited mass concentration of refractory matter, which was present only for short periods during the day or of organic components which are more hygroscopic than we assumed.

Acknowledgements

This research has been co-financed by the European Union (European Social Fund – ESF) and Greek national funds through the Operational Program "Education and Lifelong Learning" of the National Strategic Reference Framework (NSRF) - Research Funding Program: THALES. Investing in knowledge society through the European Social Fund.

Literature Cited

Aiken, A.C., Decarlo, P.F., Kroll, J.H., Worsnop, D.R., Huffman, J.A., Docherty, K.S., Ulbrich, I.M., Mohr, C., Kimmel, J.R., Sueper, D., Sun, Y., Zhang, Q., Trimborn, A., Northway, M., Ziemann, P.J., Canagaratna, M.R., Onasch, T.B., Alfarra, M. R., Prévôt, A.S.H., Dommen, J., Duplissy, J., Metzger, A., Baltensperger, U., and Jimenez, J.L.: O/C and OM/OC ratios of primary, secondary, and ambient organic aerosols with high-resolution time-of-flight aerosol mass spectrometry, Environ. Sci. Technol., 42, 4478–4485, 2008.

Bezantakos, S., Barmpounis, K., Giamarelou, M., Bossioli, E., Tombrou, M., Mihalopoulos, N., Eleftheriadis, K., Kalogiros, J., Allan, J. D., Bacak, A., Percival, C. J., Coe, H. and Biskos, G.: Chemical composition and hygroscopic properties of aerosol particles over the Aegean Sea, Atmos. Chem. Phys., 13, 11595–11608, 2013, doi:10.5194/acp-13-11595-2013.

Biskos, G., Paulsen, D., Russell, L.M., Buseck, P.R., Martin, S.T.: Prompt deliquescence and efflorescence of aerosol nanoparticles. Atmos. Chem. Phys. 6, 4633-4642, 2006a.

Bougiatioti, A., Fountoukis, C., Kalivitis, N., Pandis, S. N., Nenes, A. and Mihalopoulos N.: Cloud condensation nuclei measurements in the marine boundary layer of the eastern Mediterranean: CCN closure and droplet growth kinetics, Atmos. Chem. Phys., 9, 7053–7066, 2009.

Bougiatioti, A., Nenes, A., Fountoukis, C., Kalivitis, N., Pandis, S. N. and Mihalopoulos N.: Size-resolved CCN distributions and activation kinetics of aged continental and marine aerosol, Atmos. Chem. Phys., 11, 8791–8808, 2011, doi:10.5194/acp-11-8791-2011.

Chang, R. Y.-W., Slowik, J. G., Shantz, N. C., Vlasenko, A., Liggio, J., Sjostedt, S. J., Leaitch, W. R. and Abbatt, J. P. D.: The hygroscopicity parameter (κ) of ambient organic aerosol at a field site subject to biogenic and anthropogenic influences: relationship to degree of aerosol oxidation, Atmos. Chem. Phys., 10, 5047–5064, 2010, doi:10.5194/acp-10-5047-2010.

Clegg, S.L., Brimblecombe, P., Wexler, A.S.: Thermodynamic model of the system H^+-NH_4^+ - SO_4^{2-} - NO_3^- - H_2O at tropospheric temperatures. J. Phys. Chem. A, 102, 2137-2154, 1998b.

DeCarlo, P., Worsnop, D. R., Slowik, J. G., Davidovits, P., and Jimenez, J. L.: Characterizing Particle Morphology and Density Effects by Combining Mobility

and Aerodynamic Diameter Measurements. Aerosol Sci. Technol., 38, 1206–1222, 2004.

DeCarlo, P.F., Kimmel, J. R., Trimborn, A., Northway, M. J., Jayne, J. T., Aiken, A. C., M. Gonin, Fuhrer, K., Horvath, T., Docherty, K., Worsnop, D. R., and Jimenez, J. L.: Field-deployable, high-resolution, time-of-flight aerosol mass spectrometer. Analytical Chemistry, 78: 8281-8289, 2006.

Fountoukis, C. and Nenes, A.: ISORROPIA II: a computationaly efficient thermodynamic equilibrium model for K^+-Ca^{2+}-Mg^{2+}- NH_4^+-SO_4^{2-}-NO_3^--Cl^--H_2O aerosols. Atmos. Chem. Phys., 7, 4639-4659, 2007.

Gysel, M., Crosier, J., Topping, D.O., Whitehead J.D.: Closure study between chemical composition and hygroscopic growth of aerosol particles during TORCH2. Atmos. Chem.and Phys., 7, 6131-6144, 2007.

Haywood, J. and Boucher, O.: Estimates of the direct and indirect radiative forcing due to tropospheric aerosols: a review. Rev. Geophys., 38, 513–543, 2000.

Henning, S., Ziese, M., Kiselev, A., Saathoff, H., Möhler, O., Mentel, T. F., Buchholz, A., Spindler, C., Michaud, V., Monier, M., Sellegri, K. and Stratmann, F.: Hygroscopic growth and droplet activation of soot particles: uncoated, succinic or sulfuric acid coated, Atmos. Chem. Phys., 12, 4525–4537, 2012, doi:10.5194/acp-12-4525-2012

Irwin, M., Good, N., Crosier, J., Choularton, T. W. and McFiggans, G.: Reconciliation of measurements of hygroscopic growth and critical supersaturation of aerosol particles in central Germany, Atmos. Chem. Phys., 10, 11737–11752, 2010, doi:10.5194/acp-10-11737-2010.

Kerminen, V. M., Teinila, K., Hillamo, R., and Pakkanen, T.: Substitution of chloride in sea-salt particles by inorganic and organic anions, J. Aerosol Sci., 29, 929–942, 1998.

Knutson, E.O., Whitby, K.T.: Aerosol classification by electric mobility: Apparatus, theory, and applications. J. Aerosol Sci., 6, 443-451, 1975.

Kreidenweis, S.M., Petters, M.D., DeMott, P.J.: Single parameter estimates of aerosol water content, Environ. Res. Lett., 3, 035002, 2008.

Kostenidou, E., Pathak, R. K., and Pandis, S. N.: An algorithm for the calculation of secondary organic aerosol density combining AMS and SMPS data, Aerosol Sci. Technol., 41, 1002–1010, 2007.

Kostenidou, E., Florou, K., Kaltsonoudis, C., Tsiflikiotou, M., and Pandis, S. N., Sources and Chemical Processing of Organic Aerosol during the Summer in the Eastern Mediterranean (in preparation).

Kuwata, M., Shao, W., Lebouteiller, R. and Martin, S. T.: Classifying organic materials by oxygen-to-carbon elemental ratio to predict the activation regime of Cloud Condensation Nuclei (CCN), Atmos. Chem. Phys., 13, 5309–5324, 2013

Lanz, V. A., Alfarra, M. R., Baltensperger, U., Buchmann, B., Hueglin, C., and Prevot, A. S. H.: Source apportionment of submicron organic aerosols at an urban site by factor analytical modeling of aerosol mass spectra, Atmos. Chem. Phys., 7, 1503–1522, 2007.

Liu, X and Wang, j.: How important is organic aerosol hygroscopicity to aerosol indirect forcing?, Environ. Res. Lett., 5, 044010 (10pp), 2010, doi:10.1088/1748-9326/5/4/044010

Moore, Richard H., and Nenes, A.: Scanning flow CCN analysis - A method for fast measurements of CCN spectra. Aerosol Sci. Tech. 43.12, 1192-1207, 2009.

Moore, R.H., Cerully, K., Bahreini, R., Brock, C.A., Middelbrook, A.M., and Nenes, A.: Hygroscopicity and composition of California CCN during summer 2010, J. Geophys. Res., 117, D00V12, doi:10.1029/2011JD017352, 2012a.

Moore, R.H., Raatikainen, T., Langridge, J.M., Bahreini, R., Brock, C.A., Holloway, J.S., Lack, D.A., Middlebrook, A.M., Perring, A.E., Schwarz, J.P., Spackman, J.R., and Nenes, A.: CCN spectra, hygroscopicity, and droplet activation kinetics of Secondary Organic Aerosol resulting from the 2010 Deepwater Horizon oil spill, Environ. Sci. Technol., 46, 3093-3100, 2012b.

Ogren, J., Charlson, J.: Implications for models and measurementsof chemical inhomogeneities among cloud droplets, Tellus B, 44, 489–504, 1992.

Paatero, P. and Tapper, U.: Positive matrix factorization – a nonnegative factor model with optimal utilization of error-estimates of data values, Environmetrics, 5, 111–126, 1994.

Peng C. and Chan, C. K.: The water cycles of water-soluble organic salts of atmospheric importance, Atmos. Environ. 35, 1183-1992, 2001.

Petäjä, T., Kerminen, V.-M., Dal Maso, M., Junninen, H., Koponen, I. K., Hussein, T., Aalto, P. P., Andronopoulos, S., Robin, D., Hämeri, K., Bartzis, J. G., Kulmala, M.: Sub-micron atmospheric aerosols in the surroundings of Marseille and Athens:

physical characterization and new particle formation, Atmos. Chem. Phys., 7, 2705–2720, 2007.

Petters, M.D. & Kreidenweis S.M.: A single parameter representation of hygroscopic growth and cloud condensation nucleus activity, Atmos. Chem. Phys., 7, 1961-1971, 2007.

Pringle K. J., Tost, H., Pozzer, A., Pöschl, U. and Lelieveld, J.: Global distribution of the effective aerosol hygroscopicity parameter for CCN activation, Atmos. Chem. Phys., 10, 5241-5255, 2010.

Rader, D.J., McMurry P.H.: Application of the tandem differential mobility analyzer to studies of droplet growth or evaporation, J. Aerosol Sci., 17, 771-787, 1986.

Roberts, G. C., and Nenes, A.: A continuous-flow streamwise thermal-gradient CCN chamber for atmospheric measurements. Aerosol Sci. Tech. 39.3, 206-221, 2005.

Stock, M., Cheng, Y.F., Birmili, W., Massling, A., Wehner, B., Müller, T., Leinert, S., Kalivitis, N., Mihalopoulos, N. and Wiedensohler, A.: Hygroscopic properties of atmospheric aerosol particles over the Eastern Mediterranean: implications for regional direct radiative forcing under clean and polluted conditions, Atmos. Chem. Phys., 11, 4251-4271, 2011.

Stolzenburg, M. R. and McMurry, P.H.: TDMAFIT User's Manual, Particle Technology Laboratory, Department of Mechanical Engineering, Univercity of Minnesota, Minneapolis, 1-61, 1988.

Stolzenburg, M.R. & McMurry, P.H.: An ultrafine aerosol Condensation Nucleus Counter, Aerosol Sci. Technol., 14, 48-65, 1991.

Sueper, D.: ToF-AMS high resolution analysis software – Pika, online available at: http://cires.colorado.edu/jimenez-group/ ToFAMSResources/ToFSoftware, 2011.

Ulbrich, I. M., Canagaratna, M. R., Zhang, Q., Worsnop, D. R., and Jimenez, J. L.: Interpretation of organic components from positive matrix factorization of aerosol mass spectrometric data, Atmos. Chem. Phys., 9, 2891–2918, 2009.

Wex, H., Petters, M. D., Carrico, C. M., Hallbauer, E., Massling, A., McMeeking, G. R., Poulain, L., Wu, Z., Kreidenweis, S. M. and Stratmann, F.: Towards closing the gap between hygroscopic growth and activation for secondary organic aerosol: Part 1 – Evidence from measurements, Atmos. Chem. Phys., 9, 3987–3997, 2009.

Wu, Z. J., Nowak, A., Poulain, L., Herrmann, H., Wiedensohler, A.: Hygroscopic behavior of atmospherically relevant water-soluble carboxylic salts and their

influence on the water uptake of ammonium sulfate, Atmos. Chem. Phys., 11, 12617–12626, 2011, doi:10.5194/acp-11-12617-2011.

Wu, Z. J., Poulain, L., Henning, S., Dieckmann, K., Birmili, W., Merkel, M., van Pinxteren, D., Spindler, G., Müller, K., Stratmann, F. Herrmann, H. and Wiedensohler A.: Relating particle hygroscopicity and CCN activity to chemical composition during the HCCT-2010 field campaign, Atmos. Chem. Phys., 13, 7983–7996, 2013, doi:10.5194/acp-13-7983-2013.

Supplement

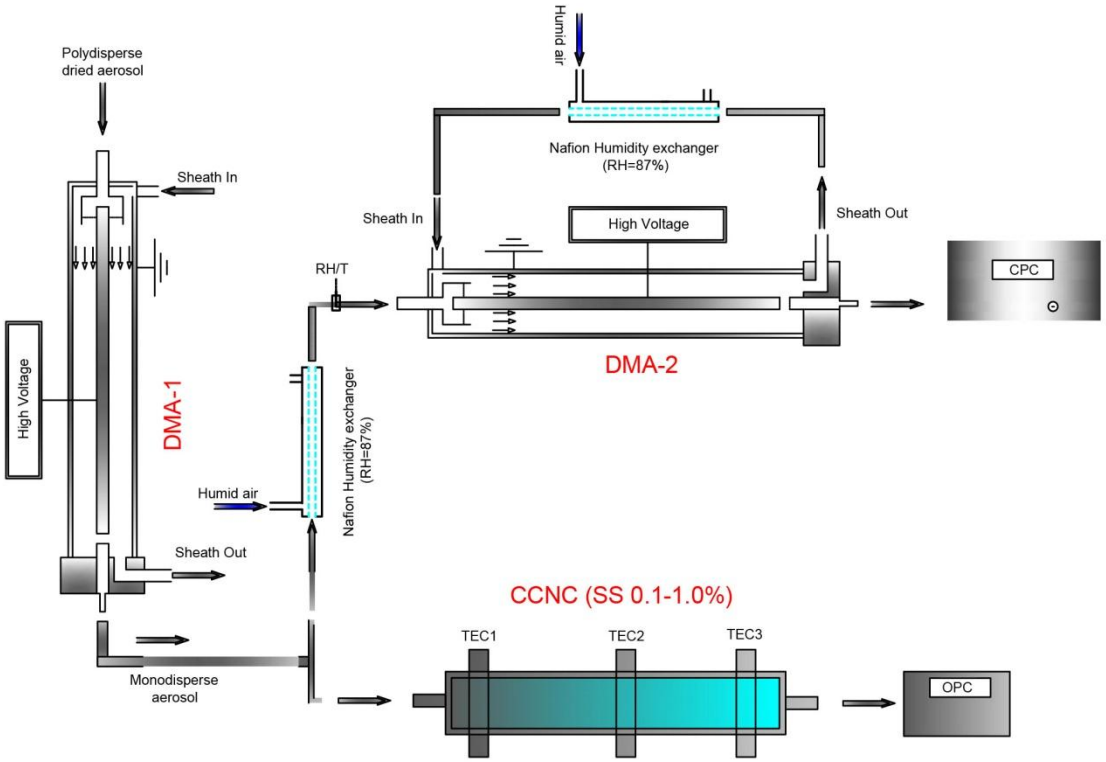

Fig S1. Experimental setup of HTDMA-CCNC combo. In brief, ambient air was sampled at a rate of 1.8 lpm. Particles passed through a drier, a ^{85}Kr neutralizer and DMA-1, where particles of 40, 60, 80, 100 and 120 nm were selected. 0.3 lpm of the monodisperse flow downstream DMA-1 was passed through a nafion humidifier, where its RH was increased to 87 ±2%, before measured by DMA-2 and the CPC. The rest of the monodisperse flow (1.5 lpm) was directed through the CCNC, where it was super-saturated from 0.1 to 1.0% with water vapors. Particles that activated as Cloud Condensation Nuclei were detected downstream by an Optical Particle Counter.

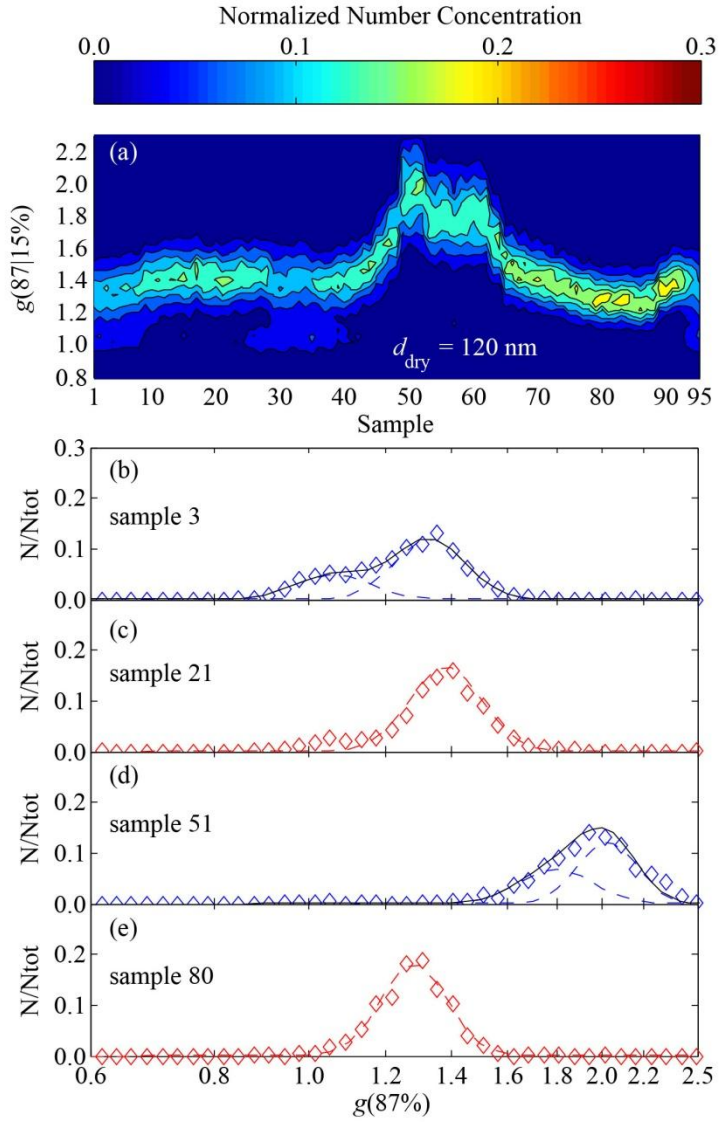

Fig S2. Examples of growth factor distributions of sampled particles having 120 nm dry mobility diameters, when exposed at 87±2% RH inside the HTDMA (**a**) and results of the inversion algorithm for selected samples (**b-e**).

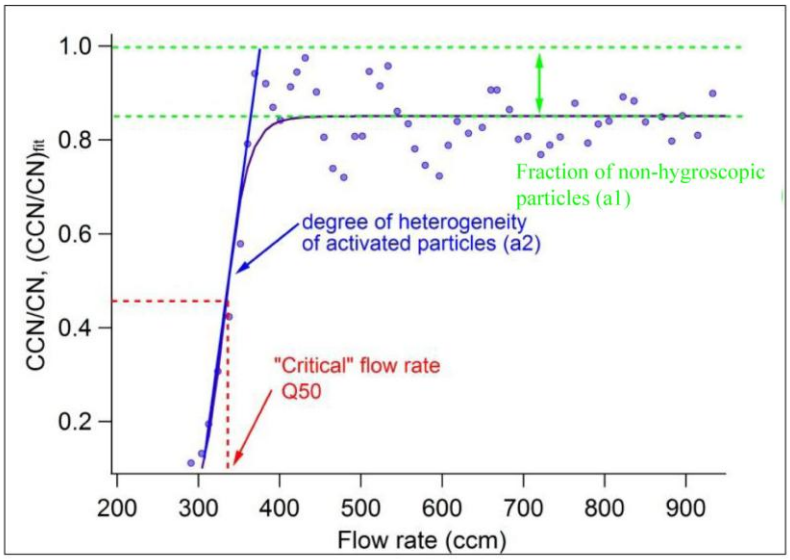

Fig S3. Example of CCN activation ratio for monodisperse particles of 120 nm dry mobility diameters, when exposed at super-saturated conditions ranging from 0.1 to 1.0 inside the CCN.

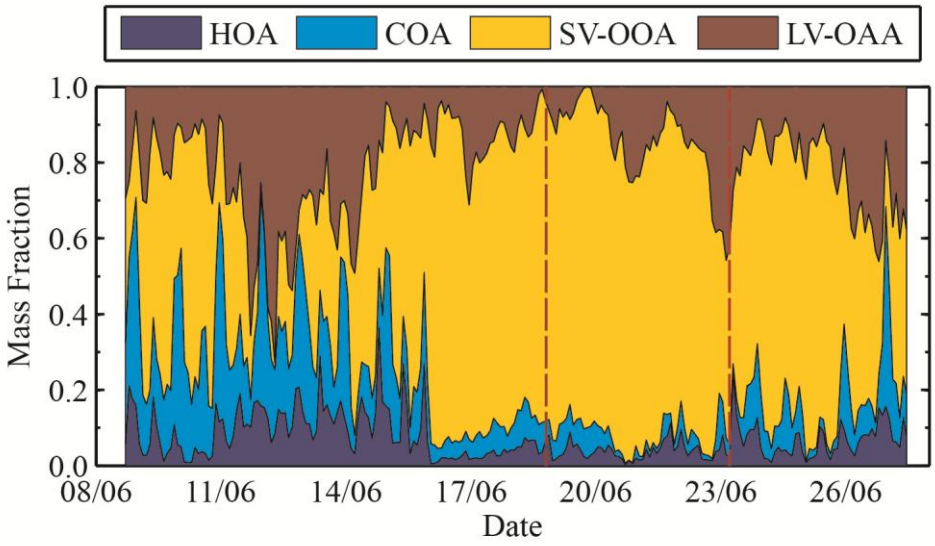

Fig S4. Relative mass fractions of the organic material measured by the HR-ToF-AMS categorized according to the Positive Matrix Factorization (PMF) in Patras. HOA, COA, SV- and LV- OOA stands for hydrocarbon like organic aerosol, cooking organic aerosol, semi-volatile oxygenated organic aerosol and low volatility organic aerosol. Red dashed lines indicate the end of the first and the start of the third sub-period, respectively.

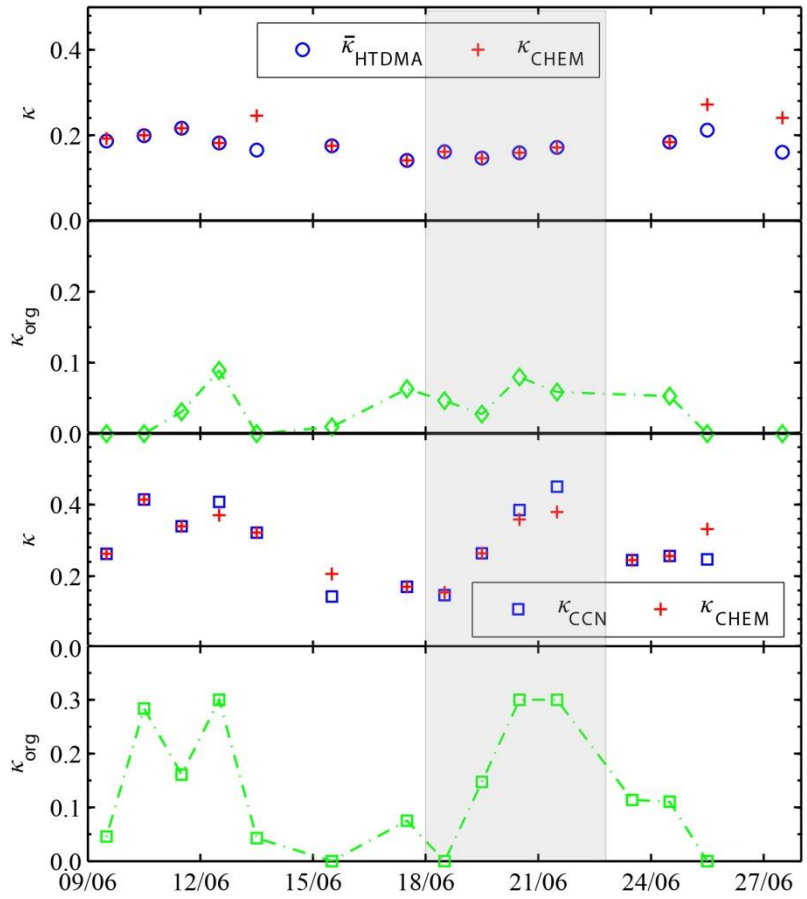

Fig S5. Comparison between predicted κ_{CHEM} determined by the filter samples with measured $\bar{\kappa}_{HTDMA}$ and κ_{CCN} in Patras. κ_{CHEM} was predicted by applying the κ-Köhler theory on the bulk chemical composition of the $PM_{2.5}$ particles. The hygroscopic parameter of the organic fraction (κ_{org}) was estimated by fitting the predicted κ_{CHEM} values to the measurements by varying κ_{org} from 0.0 to 0.3. The grayed area marks the second sub-period.

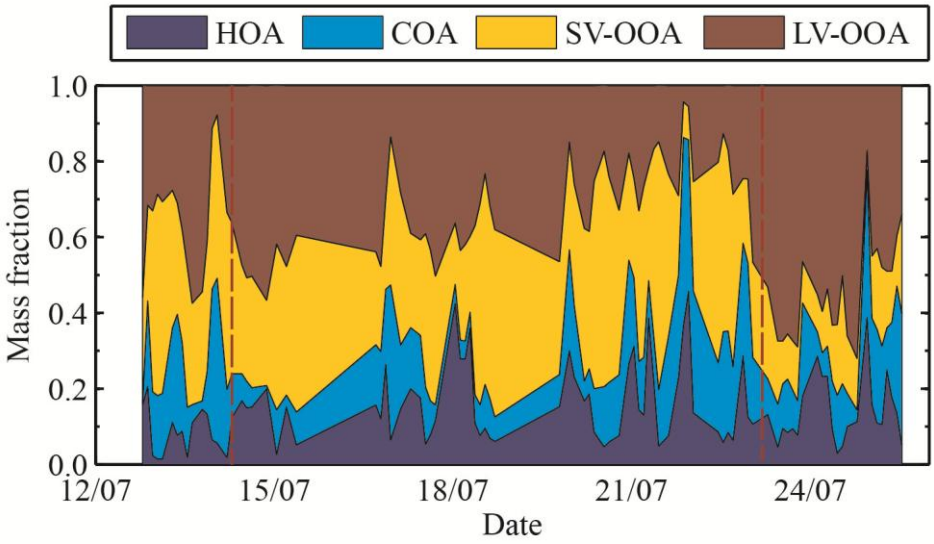

Fig S6. Relative mass fractions of the organic material measured by the HR-ToF-AMS, categorized according to the Positive Matrix Factorization (PMF) in Athens. HOA, COA, SV- and LV- OOA stands for hydrocarbon like organic aerosol, cooking organic aerosol, semi-volatile oxygenated organic aerosol and low volatility organic aerosol. Red dashed lines indicate the end of the third and the start of the fifth sub-period, respectively.

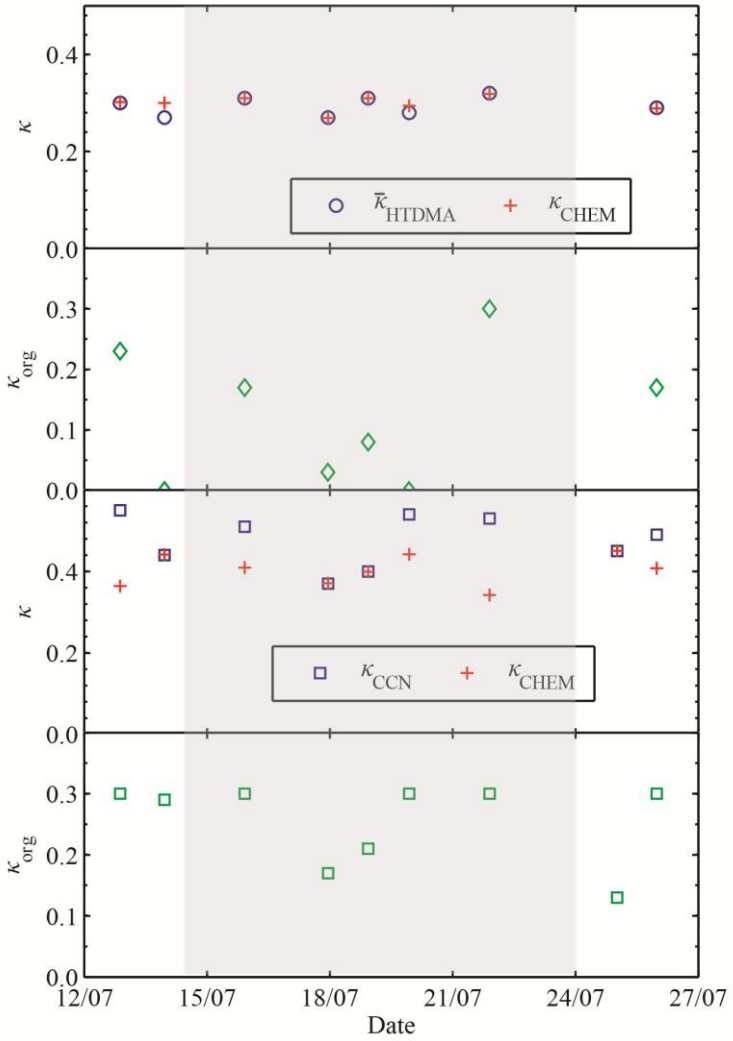

Fig S7. Comparison between predicted κ_{CHEM} determined by the filter samples with measured $\bar{\kappa}_{HTDMA}$and κ_{CCN} in Athens. κ_{CHEM} was predicted by applying the κ-Köhler theory on the bulk chemical composition of the $PM_{2.5}$ particles. The hygroscopic parameter of the organic fraction (κ_{org}) was estimated by fitting the predicted κ_{CHEM} values to the measurements by varying κ_{org} from 0.0 to 0.3. The grayed area marks the fourth sub-period.

Table S1. Median values and range (in brackets) of the estimated aerosol and organic fraction's, hygroscopic parameters (κ_{CHEM} and κ_{org}) at different saturation (*S*) conditions in Patras. For the estimation, κ_{CHEM} was fitted to the measured hygroscopic parameters of particles having dry mobility diameter of 120 nm by varying κ_{org}.

S	Variable	P1	P2	P3
Sub	κ_{CHEM}*	0.19 (0.14-0.25)	0.16 (0.15-0.18)	0.24 (0.18-0.27)
	κ_{org}*	0.02 (0.00-0.09)	0.05 (0.03-0.08)	0.00 (0.00-0.05)
Super	κ_{CHEM}*	0.29 (0.15-0.41)	0.26 (0.15-0.38)	0.29 (0.26-0.33)
	κ_{org}*	0.06 (0.00-0.30)	0.13 (0.00-0.30)	0.05 (0.00-0.11)

*Estimation using off-line chemical composition measurements of $PM_{2.5}$ (24-h filters).

Table S2. Median values and range (in brackets) of the estimated aerosol and organic fraction's, hygroscopic parameters (κ_{CHEM} and κ_{org}) at different saturation (*S*) conditions in Athens. For the estimation, κ_{CHEM} was fitted to the measured hygroscopic parameters of particles having dry mobility diameter of 120 nm by varying κ_{org}.

S	Variable	P3	P4	P5
Sub	κ_{CHEM}*	0.30 (0.30-0.30)	0.31 (0.27-0.32)	0.35 (0.29-0.41)
	κ_{org}*	0.12 (0.00-0.23)	0.08 (0.00-0.30)	0.17 (0.17-0.17)

Super	κ_{CHEM}*	0.40	0.40	0.43
		(0.36-0.44)	(0.34-0.44)	(0.41-0.45)
	κ_{org}*	0.30	0.30	0.22
		(0.29-0.30)	(0.17-0.30)	(0.13-0.30)

*Estimation using off-line chemical composition measurements of $PM_{2.5}$ (24-h filters).

PART II: Development of Techniques for the Improvement of the Methods Used for Determining Aerosol Physicochemical Properties

D. A Cost-Effective Electrostatic Precipitator for Aerosol Nanoparticle Segregation

S. Bezantakos[1,2], L. Huang[3], K. Barmpounis[3], M. Attoui[4],

A. Schmidt-Ott[3] and G. Biskos[1,3,5,6]

[1]*Department of Environment, University of the Aegean, Mytilene 81100, Greece*
[2]*Institute of Nuclear Technology and Radiation Protection, NCSR Demokritos, 15310 Ag. Paraskevi, Attiki, Greece*
[3]*Faculty of Applied Sciences, Delft University of Technology, Delft 2628-BL, The Netherlands*
[4]*University Paris Est Creteil, University Paris-Diderot, LISA, UMR CNRS 7583, France*
[5]*Faculty of Civil Engineering and Geosciences, Delft University of Technology, Delft 2628-CN, The Netherlands*
[6]*Energy Environment and Water Research Center, The Cyprus Institute, Nicosia 1645, Cyprus*

Published: January 2015

Aerosol Research Letter
Aerosol Science and Technology , 49:iv–vi, 2015

1. INTRODUCTION

Measuring the size of aerosol particles having diameters smaller than 100 nm (i.e., nanoparticles) is important for assessing their environmental impacts (McMurry, 2000) and investigating their potential technological applications (Biskos *et al.*, 2008). The most effective way for sizing aerosol nanoparticles is by classifying them based on their electrical mobility using differential mobility analyzers (DMAs; Knutson and Whitby, 1975). Despite that DMAs can classify particles with a high resolution by simply changing the potential difference between their two electrodes, their high cost and bulky size is limiting for widespread applications. Diffusion Batteries (DBs) that distinguish aerosol particles based on their diffusivity, can also be used as particle size classifiers (DeMarcus and Thomas, 1952). Although compact designs of DBs have been proposed, a number of technical limitations (cf. McMurry, 2000) has made them less favorable for particle size measurements compared to electrical mobility classifiers.

In this letter we introduce a simple and cost-effective method for size segregating aerosol nanoparticles by employing tubes composed of Electrostatic Dissipative Materials (EDMs). EDM tubes have surface resistivities that range from 10^5 to 10^{12} Ω/sq. Applying a potential difference along the tube creates an electric field of varying strength that has a radial and an axial component (see the discussion section). This field affects the charged particles passing through the tube in two ways: the axial field decelerates the particles and therefore increases their residence time in the tube and their chance for diffusional deposition to its walls, whereas the radial field removes particles by electrostatic deposition. As a result of these two processes EDM tubes can be viewed as a combination of a DB and an electrostatic precipitator (or a crude DMA), with the advantage of being significantly more simple and inexpensive.

The relative penetration efficiency of the particles passing through an EDM tube (i.e. the ratio of the particle number concentration at the outlet when a potential difference is applied along the tube over that when it is grounded) can be predicted using a modified version of the semi-empirical model employed for diffusion batteries:

$$P_r = \alpha \times \exp(-\beta \times \mu_{\text{diff}} \times \mu_{\text{elec}}) + \gamma \times exp(-\delta \times \mu_{\text{elec}}), \quad (1)$$

Here α, β, γ, and δ are positive empirical constants, whereas μ_{diff} and μ_{elec} are dimensionless parameters accounting for particle deposition by diffusion and electrostatic forces, respectively. For laminar flow conditions μ_{diff} is given by (Hinds, 1999):

$$\mu_{\text{diff}} = \frac{DL}{Q}. \quad (2)$$

Here, D is the diffusion coefficient of the particles, L is the length of the tube, and Q is the aerosol volumetric flow rate. In a similar manner, μ_{elec} can be defined as:

$$\mu_{\text{elec}} = \frac{Z_{\text{p}}V}{Q} f_{\text{g}}, \quad (3)$$

where Z_{p} is the electrical mobility of the particles and f_{g} is a factor accounting for the dependence of the edge effects of the electric field to geometrical parameters, given by:

$$f_{\text{g}} = \frac{\pi d_{\text{tube}}^2}{4L_{\text{HV}}}. \quad (4)$$

Here d_{tube} is the inner diameter of the EDM tube and L_{HV} is the distance between the grounded inlet and the position along the tube where the high voltage is applied. Expressions for the parameters used to calculate D and Z_{p} are given in Section S1 in the supplement (SI).

2. EXPERIMENTAL

The EDM tube (Freelin Wade, Model 1A-405-81) used in our tests had a length of 240 mm and inner diameter of 6.4 mm. Three metallic rings were attached along its length as shown in Figure 1: one at the inlet, one at the outlet, and one at an intermediate point between the inlet and the outlet. The metal rings at the inlet and the outlet were grounded, while the intermediate ring was connected to a positive high-voltage power supply (Fug, Model HCN14-12 500) that can deliver up to 12.5 kV.

The experimental setup for characterizing the classifier consisted of an aerosol Spark Discharger Generator (SDG; Schwyn *et al.*, 1988), a custom-made DMA (Section S2 in the SI) with a closed recirculating system for the sheath flow, the EDM-tube and two Condensation Particle Counters (CPCs; Agarwal and Sem, 1980) as shown in Figure 1. In brief, the SDG was used to produce polydisperse singly-charged silver particles of variable sizes by adjusting the energy per spark and the carrier gas flow as described by Tabrizi *et al.* (2009). Positively-charged, monodisperse particles having electrical mobility diameters from 10 to 55 nm were obtained after classification by the DMA. The monodisperse particles were then passed through the EDM tube before their concentration was measured by an ultrafine CPC (uCPC; TSI Model 3025).

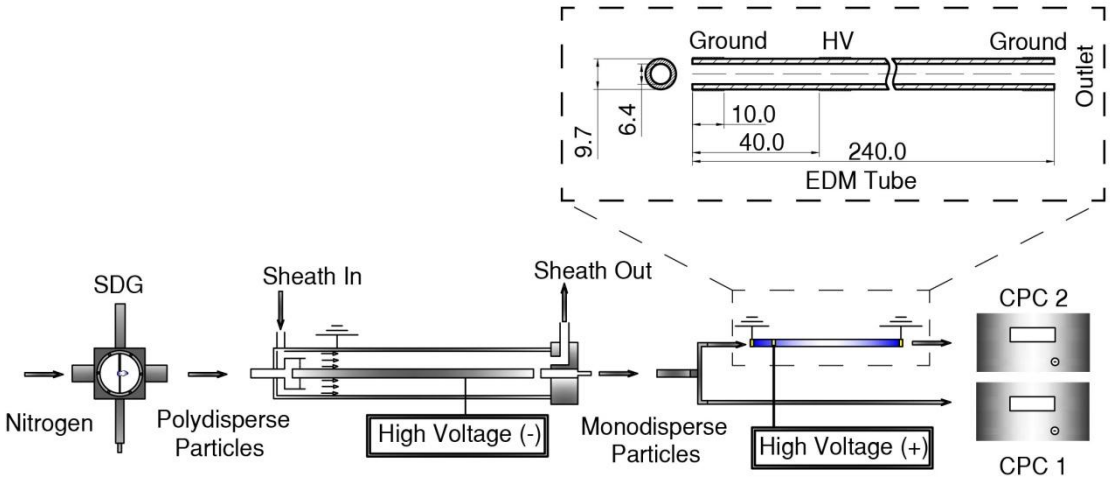

FIG. 1. Schematic diagram of the experimental setup and the EDM-tube classifier (inset). Metal rings are attached to the tube for grounding the inlet and the outlet, and for applying a high voltage at an intermediate point (i.e., 40 mm downstream the inlet) along the tube. A DMA was used to select monodisperse positively charged silver particles produced by a SDG. The monodisperse particles having electrical mobility diameters ranging from 10 to 55 nm were then passed through the EDM tube, which was operated at voltages ranging from zero to 8 kV. The particle number concentration was measured downstream the EDM tube by a uCPC. A CPC was used to check the stability of the number concentration of the monodisperse particles upstream the EDM tube.

The relative penetration efficiency through the EDM-tube when the applied voltage at the intermediate electrode varied from 1 to 8 kV was calculated by:

$$P_r(V) = 1 - \left(\frac{N(0)-N(V)}{N(0)}\right) = \frac{N(V)}{N(0)}. \quad (5)$$

Here $N(0)$ and $N(V)$ are the average particle number concentrations measured over 60 s by the uCPC downstream the EDM tube when zero and V volts were respectively applied at the intermediate electrode. A second CPC (TSI Model 3072) was used to verify that the particle number concentration upstream the EDM tube was stable throughout the measurements.

3. RESULTS AND DISCUSSION

Figure 2 shows the measured and predicted relative penetration efficiency of particles having electrical mobility diameters from 10 to 55 nm that enter the EDM tube. Measurements are shown for two different aerosol flow rates, 0.32 and 0.76 lpm, when 1 to 8 kV were applied on the intermediate electrode of the tube. The semi-empirical model (i.e., Equation 1) was fitted to the measurements using the least squares method, yielding

the following constants: α = 0.65, β = 2668.83, γ = 0.35, and δ = 4.21. For all particle sizes and operating conditions tested, the agreement between predictions and measurements was within 15%, which is in the same range to the uncertainty of our setup.

For a fixed aerosol flow, the larger particles require higher potential differences between the intermediate ring electrode and the two ends of the EDM tube in order to decrease their penetration probability. When the potential difference is also fixed, the relative penetration of the particles increases logarithmically with their size, yielding curves that become steeper as particle size decreases (Figure 2). The size resolving capability of the EDM tube is higher in these steep regions of the curves; a feature that is highly desirable when electrostatic precipitators are used for particle segregation. Another feature of the EDM tubes that makes them attractive classifiers is that in the steep regions of the penetration efficiency curves, the relative size resolution is almost constant. This is verified by the fact that the curves are almost parallel when a logarithmic horizontal axis is used in the plots shown in Figure 2.

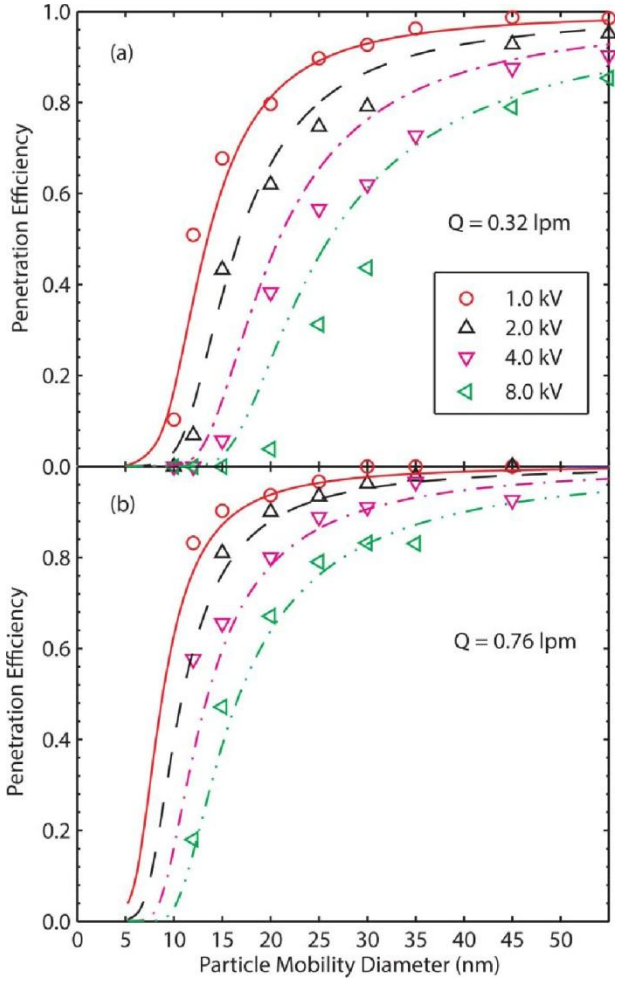

FIG. 2. Relative penetration efficiency of particles passing through the EDM-tube classifier at a flow rate of 0.32 lpm (a) and 0.76 lpm (b). Symbols indicate experimental measurements while lines are produced using the semi-empirical model (i.e., Equation. 1) described in this work.

Interestingly, the relative penetration efficiency curves of the EDM tube are steeper compared to those of classical parallel-plate precipitators having the same cross-sectional area (Section S3 and Figure S1 in the SI), indicating that they would perform much better as classifiers. This characteristic can be attributed by the diffusional deposition of the charged particles, which is enhanced by the axial component of the electric field that can significantly decelerate the smaller charged particles in the EDM tube. To further investigate the role of the electric field on the penetration of the particles through the EMD tube, we used a numerical model to calculate its strength when 1 kV is applied at the intermediate ring electrode (Section S4 and Figure S2 in the SI). The electric field is significantly distorted near the three electrode rings, inducing a radial component that is extremely strong in their vicinity (i.e., the "Hot Spot" regions indicated in Figure S2), but decays fast along the axial and radial dimension. This component of the field attracts the positively charged particles towards the walls right at the edge of the grounded electrode ring at the inlet of the tube (i.e., "Hot Spot 1") thereby increasing the probability of their deposition. At the same time, the mean strength of the axial component of the electric field upstream (Zone 1) and downstream (Zone 2) the high voltage electrode is 30 and 5.5 kV/m, respectively (Figure S2c). For 10-nm singly charged particles, this field can reduce the mean convective particle velocity by 0.07 m/s in Zone 1 and increase it by 0.01 m/s in Zone 2. For typical flow rates used through the EDM tubes (i.e., in the range of an lpm), this can substantially increase the residence time of the particles, if not force them to move opposite to the direction of the flow, in Zone 1 thereby increasing their probability of deposition to the tube walls. This feature is reflected by the relative penetration efficiency curves that are noticeably steeper compared to those of parallel plate precipitators as discussed above.

4. CONCLUSIONS

In this work we demonstrate the ability of EDM tubes to be used as effective and compact electrostatic precipitators that can be employed for size segregation of charged aerosol nanoparticles, and provide a semi-empirical model to predict their performance.

These tubes can be considered a combination of a DB and an electrostatic precipitator. Compared to DBs, where only the flow rate can be adjusted to select particles of different size, EDM tubes offer higher flexibility as they can segregate particles by simply adjusting the potential difference along their inner surface. Compared to classical parallel plate electrostatic precipitators, EDM tubes exhibit steeper cut-off curves. This feature is highly attractive for their potential use in mobility spectrometers or in tandem systems downstream a DMA for measuring size-dependent particle properties such as hygroscopicity and volatility. Considering also their simple design, high portability, and negligible cost, EDM tubes can open up new opportunities in environmental monitoring as discussed above.

REFERENCES

Agarwal, J. K. and Sem, G. J. (1980). Continuous flow, single-particle-counting condensation nucleus counter. *J. Aerosol Sci.*, 11:343–357.

Biskos, G., Vons, V., Yurteri, C. and Andreas, S.-O., (2008). Generation and sizing of particles for Aerosol-based Nanotechnology. *KONA Powder Part J.*, 26, 13–35.

DeMarcus, W. C. and Thomas, J. W. (1952). Theory of a Diffusion Battery. USAEC Report ORNL-1413, Oak Ridge National Laboratory, Oak Ridge, TN.

Hinds, W. C. (1999). Aerosol Technology: Properties, Behavior, and Measurement of Airborne Particles, 2nd Edition. John Willey & Sons, Inc..

Knutson, E.O., Whitby, K.T. (1975). Aerosol Classification by Electric Mobility: Apparatus, Theory, and Applications. *J. Aerosol Sci*., 6: 443-451.

McMurry, P. H. (2000). A review of Atmospheric Aerosol Measurements. *Atmos. Environ*., 34:1959-1999.

Schwyn S., Garwin E., Schmidt-Ott A. (1988). Aerosol Generation by Spark Discharge. *J Aerosol Sci.*, 19(5):639–642.

Tabrizi N. S., Ullmann M., Vons V. A., Lafont U. and Schmidt-Ott A. (2009). Generation of Nanoparticles by Spark Discharge. *J. Nanopart. Res.*, 11:315–332.

SUPPLEMENTARY MATERIAL

S1: Supporting equations for the EDM tube penetration model:

The diffusion coefficient and the electrical mobility of the particles are respectively given by:

$$D = \frac{kTCc}{3\pi\eta d_p}, \quad \text{(S1)}$$

$$Z_p = \frac{neCc}{3\pi\eta d_p}, \quad \text{(S2)}$$

where k is the Boltzmann constant (1.38 x 10^{-23} J/K), T is the absolute temperature (T = 298 K for all the calculations described in the letter), η is the air viscocity (1.81 x 10^{-5} kg/ms), e is the electron charge (1.6 x 10^{-19} C), n is the number of elementary charges on the particles, d_p is the particle diameter and C_c is the Cunningham slip correction factor given by:

$$Cc = 1 + \frac{\lambda}{d_p} \times \left(2.34 + 1.05 \times exp\left(-0.39 \times \frac{d_p}{\lambda}\right)\right). \quad \text{(S3)}$$

Here λ is the air mean free path (66 x 10^{-9} m at atmospheric pressure).

S3: Details of the custom-made DMA used in our experiments:

A cylindrical type DMA having 0.935 and 1.9575 cm inner and outer radii, respectively, and an effective length of 11.47 cm was used in all the measurements. The sheath flow of the DMA was driven by a controlled closed loop system which included a blower, a heat exchanger, a pressure transducer connected to a laminar flow element for measuring the flow, and a PID controller. A 1:10 aerosol-to-sheath-flow ratio was used throughout all the experiments.

S3. Comparison EDM-tube and Parallel-Plate ESPs

Figure S1 compares EDM-tube penetration efficiency curves predicted by Eq. 1 with corresponding curves (i.e., exhibiting the same cut-off diameters at 50% penetration, *d*50) for a parallel plate electrostatic precipitators having the same cross-sectional area as predicted by the modified Deutsch-Anderson equation (Leonard *et al*., 1967).

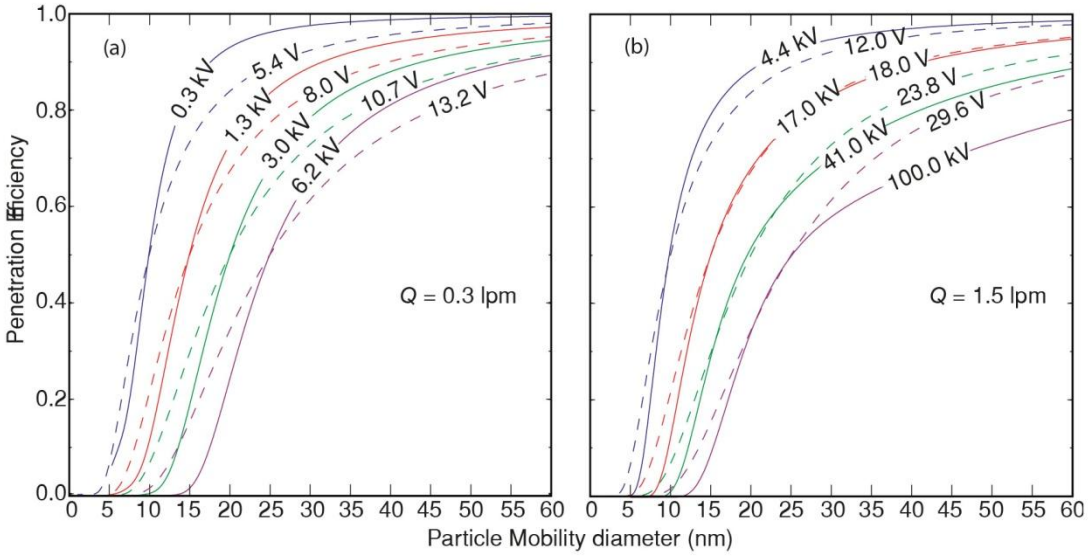

Fig. S1. Comparison between predicted penetration efficiency curves of the EDM tube (solid lines) and of a parallel plate electrostatic precipitator using the modified Deutsch-Anderson equation (dashed lines). For the calculations we assumed that both instruments have the same cross sectional area (i.e., 32.15 mm2) and operate at the same flow rates: (a) 0.3 lpm, and (b) 1.5 lpm. All curves intersect at 50% penetration efficiency. The labels on each curve indicate the potential required to obtain 50% penetration efficiency for particles having dry mobility diameters of 10, 15, 20, and 25 nm.

S2: Numerical Model:

The electric field inside the EDM tube was numerically simulated using version 4.3b COMSOL® multiphysics. More specifically, we developed a 2-dimensional axisymmetric model, with the axis of symmetry being the center of the tube (cf. Figure. S2a). The boundary conditions included the potential on the intermediate electrode *(*i.e., V = 1000 V*)* and the grounded inlet and outlet *(*V = 0 V*)*. The resistivity of the EDM tube material is 4×10^{10} ohm×cm, according to the manufacturer. Since the relative permittivity of the specific material is unknown in the calculations we assumed values that range from 2.0 to 7.0, which are typical for most polyurathanes. Variation of the relative permittivity in this range had a less than 4% influence on the calculated electric field strength. The strength of the electric field within the tube was determined by solving Poisson equation:

$$-\nabla \times (\varepsilon_0 \nabla V - P) = \rho \qquad \text{(S4)}$$

where ε_0 is the permittivity of free space, V is the potential, P the polarization of the medium and ρ is the charge density (ρ = 0 in our calculations). To solve Eq. S.4 we used an extremely fine mesh (ca. 5 x 10^5 elements) and the multifrontal massively parallel sparse direct solver (MUMPS; COMSOL® multiphysics 4.3b reference manual).

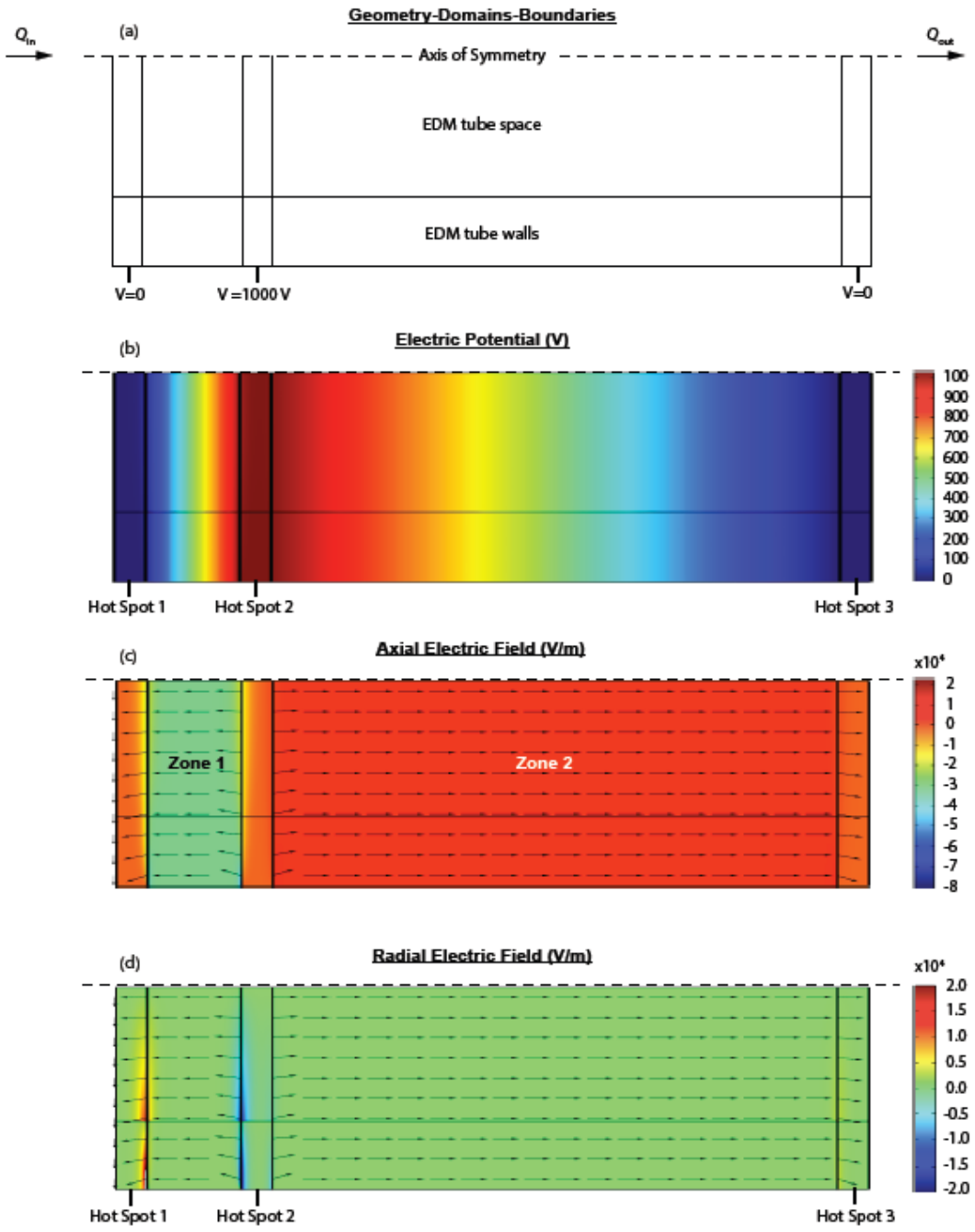

Fig. S2. Predicted electric field strength within the EDM tube when 1 kV is applied on the intermediate electrode. The calculations performed using Comsol multiphysics® show (a) the Geometry, (b) the voltage profile, (c) the axial component *E*z, and (d) the radial component *E*r of the electric field. Zones 1 and 2 respectively denote the region upstream and downstream the intermediate electrode where the high voltage is applied, while the "Hot Spots" indicate locations where *E*r is significantly stronger compared to the rest of the area within the EDM tube. Note: The aspect ratio in all plots is distorted to highlight the above-mentioned features, while the arrows are used to illustrate the electric field direction and not its magnitude.

References

COMSOL® multiphysics version 4.3b. Reference manual. Stockholm, Sweden: COMSOL AB

Hinds, W. C. (1999). Aerosol Technology: Properties, Behavior, and Measurement of Airborne Particles, 2nd Edition. John Willey & Sons, Inc.

Leonard, G., Mitchner, M., & Self, S. (1967). Particle transport in electrostatic precipitators. *Atmos. Environ.*, 14:1289–1299.

Pecht, M. (2000). In "The Electrical Engineering Handbook". Boca Raton: CRC Press LLC.

E. Conclusions

The aim of the first part of this thesis was to study the hygroscopic properties of atmospheric sub micrometer particles at remote and suburban locations of Greece. Particles mixing state was also revealed from the HTDMA measurements and estimations on the hygroscopicity range of particles organic fraction were provided using the particles chemical composition and employing κ-Köhler theory. In the second part we studied the performance of a new method for size-segregating aerosol nanoparticles.

1 Aerosols hygroscopic properties over remote locations

Hygroscopicity measurements that were conducted on the remote location on the island of Lemnos (Northern Aegean Sea) showed that particles sizing from 50 to 170 nm had medium hygroscopicities exhibiting an average growth factor of 1.2. The measurements revealed that particles were internally mixed, which was expected for long-range transported, aged aerosols. At the same period airborne measurements of aerosols physicochemical properties, including their chemical composition, which was derived by an airborne cToF-AMS, were conducted over the Aegean Sea region. During two flights the aircraft performed two missed approaches in the vicinity of the ground station thus allowing a closure study between the measured particle hygroscopicity (i.e. from the ground station HTDMA) and the one predicted by their chemical composition. From this closure study we estimated the hygroscopic parameter κ of the organic fraction, which accounted for ca. 50% of the particles dry volume, in the range of 0.03 and 0.10.

Differences in the origin and path of the air masses arriving in the region were responsible for the variability in particles chemical composition, which was measured during the two flights over the wider area of the Aegean Sea. Most importantly the organic species accounted for almost 50% of the volume of the particles, while their acidity increased with increasing altitude. Using the organics hygroscopic κ values, obtained from the closure study and the airborne measurements of aerosols chemical composition, we estimated the vertical profiles of their hygroscopicity over the wider area of the Aegean Sea. Despite the variability in particle hygroscopicity caused by the different origin and paths of the air masses reaching the region the median values of particle hygroscopicity were similar to the ones of continental aerosol particles.

2 Aerosols hygroscopic properties over suburban locations

Particle hygroscopicity and mixing state was measured at two suburban locations in the vicinity of Patras and Athens, Greece. A combined setup including an HTDMA and a CCNC was employed for conducting simultaneous, size resolved measurements of particles ranging from 60 to 120 nm at both sub- and super-saturation conditions. The hygroscopic parameter of the aerosols organic fraction was estimated using measurements of their chemical composition, conducted by an HR-ToF-AMS.

The particles mixing state was, as expected, influenced by the prevailing winds, resulting in an increase in the fraction of externally mixed particles when the winds were crossing the nearby cities. More specifically, aerosols over Athens were more often externally mixed than those observed over Patras. During periods of increased externally mixed fraction, the population of less hygroscopic particles was also increased, indicating that freshly emitted particles from the cities are less hygroscopic than the aged ones. At both sub- and super-saturated conditions, particles observed over Athens were more hygroscopic than those observed over Patras, with the latter resembling hygroscopicities observed for continental Europe aerosols.

The estimated organic fraction hygroscopicities in Patras indicated that the aerosols organic fraction varied from hydrophobic to less hygroscopic, exhibiting κ values from near zero to 0.2. In Athens however, values higher than 0.3 are needed for a good closure between the measured and chemical composition estimated particle hygroscopicities. This discrepancy leads in either assuming the presence of refractory matter (i.e. not detectable by the AMS) or the presence of highly hygroscopic organic matter. Since our observations cannot lead to conclusive results, we suggest long term, including refractory matter chemical composition, measurements at the same area.

3 Methods and techniques for improving the determination of aerosols physicochemical properties

EDM-tubes have the ability to be used as effective and compact electrostatic precipitators that can be employed for size segregation of charged aerosol nanoparticles. More importantly, their performance can be predicted using a simple semi-empirical model, thus simplifying the procedure of determining the size of particles that pass through the EDM-tube at various condintions. These tubes, which can be considered as a combination of a DB and an electrostatic precipitator, offer higher flexibility than DBs as

they can segregate particles by simply adjusting the potential difference along their inner surface. Compared to classical parallel plate electrostatic precipitators, EDM tubes exhibit steeper cut-off curves, which is a highly attractive feature for their potential use in mobility spectrometers or in tandem systems downstream a DMA for measuring size-dependent particle properties such as hygroscopicity and volatility. While their sizing resolution and accuracy is not better than systems which employ DMAs, their negligible cost and increased portability poses an advantage in certain applications, where quantity leads to increased quality. Such applications could involve an array of instruments for increasing the spatial resolution of environmental monitoring, without the need of increased expenses, or light systems which could be part of a portable network of sensors.